

**STOCHASTIC ANALYSIS OF ANT-BASED ROUTING AND  
PROBABILISTIC MODELING OF MEDIUM ACCESS CONTROL  
IN WIRELESS NETWORKS**

by

Rui Fang

A dissertation submitted to the Faculty of the University of Delaware in partial fulfillment of the requirements for the degree of Doctor of Philosophy in Applied Mathematics

Spring 2015

© 2015 Rui Fang  
All Rights Reserved

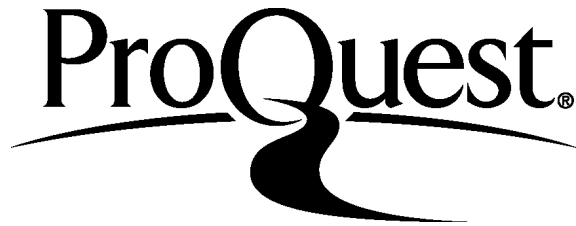
ProQuest Number: 3718332

All rights reserved

INFORMATION TO ALL USERS

The quality of this reproduction is dependent upon the quality of the copy submitted.

In the unlikely event that the author did not send a complete manuscript and there are missing pages, these will be noted. Also, if material had to be removed, a note will indicate the deletion.



ProQuest 3718332

Published by ProQuest LLC (2015). Copyright of the Dissertation is held by the Author.

All rights reserved.

This work is protected against unauthorized copying under Title 17, United States Code  
Microform Edition © ProQuest LLC.

ProQuest LLC.  
789 East Eisenhower Parkway  
P.O. Box 1346  
Ann Arbor, MI 48106 - 1346

STOCHASTIC ANALYSIS OF ANT-BASED ROUTING AND  
PROBABILISTIC MODELING OF MEDIUM ACCESS CONTROL  
IN WIRELESS NETWORKS

by

Rui Fang

Approved: \_\_\_\_\_

Louis F. Rossi, Ph.D.

Chair of the Department of Mathematical Sciences

Approved: \_\_\_\_\_

George H. Watson, Ph.D.

Dean of the College of Arts and Sciences

Approved: \_\_\_\_\_

James G. Richards, Ph.D.

Vice Provost for Graduate and Professional Education

I certify that I have read this dissertation and that in my opinion it meets the academic and professional standard required by the University as a dissertation for the degree of Doctor of Philosophy.

Signed: \_\_\_\_\_

Louis F. Rossi, Ph.D.  
Professor in charge of dissertation

I certify that I have read this dissertation and that in my opinion it meets the academic and professional standard required by the University as a dissertation for the degree of Doctor of Philosophy.

Signed: \_\_\_\_\_

Mokshay Madiman, Ph.D.  
Member of dissertation committee

I certify that I have read this dissertation and that in my opinion it meets the academic and professional standard required by the University as a dissertation for the degree of Doctor of Philosophy.

Signed: \_\_\_\_\_

Gilberto Schleiniger, Ph.D.  
Member of dissertation committee

I certify that I have read this dissertation and that in my opinion it meets the academic and professional standard required by the University as a dissertation for the degree of Doctor of Philosophy.

Signed: \_\_\_\_\_

Chien-Chung Shen, Ph.D.  
Member of dissertation committee

## ACKNOWLEDGEMENTS

First, and most of all, I would like to express my special appreciation to my advisor Professor Louis F. Rossi, for his patience, motivation, enthusiasm, and immense knowledge. His guidance helped me in all the time of research and writing of this thesis. My sincerely thanks also goes to professor Chien-Chung Shen and his team for their continuous support and advise throughout the last four years. I would also like to thank professor Mokshay Madiman, professor Gilberto Schleiniger, for serving as my committee members and their encouragement, insightful comments, and hard questions.

I would like to thank everyone who have helped and enlightened me during my doctoral studies, especially Zequn Huang for many fruitful teamworks and research discussions we had. I am also very grateful to all the professors and staff I have met at University of Delaware for their generous guidance and kindness.

My sincere thank also goes to my parents, Jinyu Zhao and Ran Fang, for giving birth to me at the first place and supporting me spiritually throughout my life. I would also like to thank my beloved fiancée Xiaomei He who spent sleepless nights with me and was always support me in the moments when there was no one to answer my queries.

Last but not the least, I would like to thank the support received for my research by Army SBIR grant A072-074-1669.

## TABLE OF CONTENTS

<b>LIST OF TABLES</b> . . . . .	<b>ix</b>
<b>LIST OF FIGURES</b> . . . . .	<b>xi</b>
<b>ABSTRACT</b> . . . . .	<b>xiv</b>
 <b>Chapter</b>	
<b>1 INTRODUCTION</b> . . . . .	<b>1</b>
1.1 Background and Motivations . . . . .	1
1.2 Related Works . . . . .	4
1.3 Dissertation Outline . . . . .	7
<b>2 DYNAMIC ROUTING EXPONENT STRATEGY FOR ANT-BASED ROUTING PROTOCOL</b> . . . . .	<b>10</b>
2.1 Introduction . . . . .	10
2.2 Preliminaries of Ant-based Routing . . . . .	12
2.3 Dynamic Routing Exponents . . . . .	18
2.3.1 5-node network . . . . .	19
2.3.2 50-node network . . . . .	19
2.3.3 Statistical Comparison and Impact of $\Lambda$ . . . . .	21
2.4 Conclusions . . . . .	23
2.4.1 Summary . . . . .	23
2.4.2 Limitation and Next Step . . . . .	25
<b>3 ANALYSIS OF ANT-BASED ROUTING WITH WIRELESS MEDIUM ACCESS CONTROL PROTOCOL MACA</b> . . . . .	<b>27</b>
3.1 Review of Basic Wireless MAC Protocols . . . . .	27

3.2	Modeling and Case Studies for MACA Protocol . . . . .	32
3.2.1	Two-Sender Scenarios . . . . .	32
3.2.1.1	Model Validation . . . . .	35
3.2.2	Three-sender Scenario with MACA . . . . .	37
3.2.2.1	Approximating Transition Probabilities with Monte Carlo Simulation . . . . .	42
3.3	Modeling and Analysis of BARP with MACA . . . . .	44
3.3.1	Modeling of BARP with Packet Loss . . . . .	44
3.3.2	Evaluation and Validation . . . . .	46
3.4	Evaluation of MACA for Multi-hop Wireless Networks: A Regression Study . . . . .	48
3.4.1	The Complications of Multi-hop Wireless Networks . . . . .	49
3.4.2	A Regression Model . . . . .	50
3.4.3	Evaluations and Predictions . . . . .	51
3.5	Conclusion . . . . .	53
<b>4</b>	<b>PROBABILISTICALLY MODELING OF IEEE 802.11 DISTRIBUTED COORDINATION FUNCTION . . . . .</b>	<b>55</b>
4.1	Review of IEEE 802.11 Distributed Coordination Function (DCF) . . . . .	55
4.1.1	Preliminaries . . . . .	57
4.1.2	Assumptions . . . . .	59
4.2	Modeling the Distributed Coordination Function . . . . .	61
4.2.1	Modeling of Node States . . . . .	61
4.2.2	Modeling of States Transitions . . . . .	64
4.2.2.1	x As a Listener/Receiver . . . . .	64

4.2.2.2	<i>x</i> As a Sender . . . . .	68
4.2.3	Representation of Transition Probabilities . . . . .	71
4.2.3.1	Carrier Sensing while in the Idle or Back-off States . . . . .	73
4.2.3.2	Receiving/overhearing Packets . . . . .	75
4.2.3.3	End of Sending . . . . .	77
4.2.3.4	End of Waiting . . . . .	78
4.2.4	Equilibrium Distribution . . . . .	81
4.2.4.1	System Formulation . . . . .	81
4.2.4.2	System Closure . . . . .	84
4.3	Examples . . . . .	85
4.3.1	QualNet Simulation . . . . .	85
4.3.2	A 2-node Network. . . . .	87
4.3.3	A Triangle Network . . . . .	92
4.3.4	2 Senders and 1 Receiver . . . . .	96
4.4	Conclusion and Future Work . . . . .	101
<b>5</b>	<b>CONCLUSIONS AND FUTURE WORK . . . . .</b>	<b>105</b>
	<b>BIBLIOGRAPHY . . . . .</b>	<b>108</b>
	<b>Appendix</b>	
<b>A</b>	<b>DERIVATION OF EQUATIONS . . . . .</b>	<b>114</b>
<b>B</b>	<b>BALANCE EQUATIONS FOR STATIONARY JOINT STATES . . . . .</b>	<b>116</b>

## LIST OF TABLES

2.1	Table of parameters used in network simulations. . . . .	18
3.1	Parameters used in verification. The values are in microsecond ( $10^{-6}$ s). . . . .	37
3.2	Comparisons of drop, success and fail rate of data packets between model and simulations. . . . .	37
3.3	Parameters used in Monte Carlo Simulations . . . . .	42
3.4	Evidence for the effectiveness of Monte Carlo Method . . . . .	42
3.5	Validation of symmetry with Monte Carlo method . . . . .	44
3.6	BARP parameters used in QualNet simulation . . . . .	47
3.7	At left and right, the pheromone distribution on each path and ants drop rate ( $\times 10^{-4}$ ) comparisons. . . . .	48
4.1	The node statues in terms of antenna, channel, and queue . . . . .	63
4.2	Transition probability function approximations - case 1 . . . . .	85
4.3	Transition probability function approximations - case 2 . . . . .	86
4.4	Transition probability function approximations - case 3 . . . . .	86
4.5	Transition probability function approximations - case 4 . . . . .	87
4.6	Parameters used in QualNet simulation . . . . .	88
4.7	Non-Trivial Transition Probabilities . . . . .	88
4.8	Non-Trivial Transition Probabilities . . . . .	93

4.9	Non-Trivial Transition Probabilities for $x_1$ . . . . .	98
4.10	Non-Trivial Transition Probabilities for $x_2$ . . . . .	98

## LIST OF FIGURES

2.1	Stationary states calculated using the stochastic model. Solutions S1, S5 and S7 were calculated with $\beta = 0.5$ and $\Lambda = 0.3$ . Solution S1p was calculated with $\beta = 2$ and $\Lambda = 0.3$ . . . . .	16
2.2	Continuous dependence of solutions on $\beta$ for the simple 5-node network configuration used in Figure 2.1. Here $\lambda$ is fixed on 0.3. Each curve represents the pheromone values on corresponding link shown by the legends. . . . .	17
2.3	Pheromone values as a function of time using dynamic routing exponents for both Matlab and QualNet simulations. . . . .	20
2.4	Two stationary solutions with $\beta = 0.5$ on the left, $\beta = 2$ on the right, both with $\Lambda = 0.3$ . Node $s$ is shown by red spot and node is shown by green spot. Pheromone values are normalized by the maximum pheromone value over the entire network. . . . .	21
2.5	Distribution of normalized pheromone values at some important moments of simulation. At time 50, a multi-route state is achieved and beta starts to vary. The solution settles down at time 80, when beta stops to vary. . . . .	22
2.6	Evolution of average hop count over time. . . . .	23
2.7	Statistic research of dynamic routing exponent strategy on improving performance of routing protocols. . . . .	24
2.8	Average length of optimal single-route with respect to $\Lambda$ . . . . .	25
3.1	The Hidden Terminal Problem. The sensing ranges of the transmitters 1 and 2 are marked with shaded disks while that of receiver R is denoted by green circle. Both 1 and 2 are exposed to R but hidden from each other, resulting in vulnerable transmissions at R. . . . .	30

3.2	$\sigma$ denotes the propagation delay (time); $T_D$ denotes the transmission delay of RTS or CTS packets; $\lambda_{1,2,3}$ are three critical moments; $CW$ denotes the initial back-off contention window size. . . . .	33
3.3	Directed diagram for the Markov chain: $S$ represents the successful sending of data packet. $F$ corresponds to data packet being corrupted, and $C_i$ 's, $i = 1, 2, 3, \dots$ mean sender is competing with others (if any) by randomly sending RTS packet within period of back-off window size $2^{i-1}CW$ . The states, $(s_1(t), s_2(t))$ , where $s_1, s_2 \in \{S, F, C_1, C_2, C_3, \dots\}$ , show the status of (sender1, sender2) at time $t$ . . . . .	36
3.4	The three-sender scenario with hidden terminals . . . . .	38
3.5	A simple network topology . . . . .	44
3.6	A simple 5 node topology. The circles indicate the transmission ranges of each nodes. There are 10 possible directed transmissions demonstrated by the arrows. . . . .	52
3.7	Three types of prime interactions observed for the target link (red): deeper blue means higher impact. Type 1 relates to the masked node problem, as the interface at node 4 will be occasionally blocked by signal from node 5; Type 2 indicates the typical symmetric hidden terminal problem; Type 3 corresponds to the asymmetric hidden node problem which causes unfairness because receiver 3 will more likely be blocked by 4, but not by 2. . . . .	52
3.8	A comparison between model predictions and QualNet statistics on data delivery. The result on the top corresponds to 6 node ring topology and the bottom corresponds to 8 node ring topology. . . .	53
4.1	Non-persistent CSMA/CA algorithm implemented in 802.11 DCF . . . . .	56
4.2	IEEE 802.11 DCF timeline with RTS/CTS access mechanism . . . . .	59
4.3	Carrier Sense Block at upper layer . . . . .	66
4.4	Carrier Sense Block at base layer . . . . .	69
4.5	RTS/CTS Contention Block . . . . .	70
4.6	A 2-node network scenario without hidden terminals. . . . .	87

4.7	2-node joint state model ( $m = 0$ ) . . . . .	90
4.8	Comparison of steady state probabilities at $x_1$ : the tuples represent (back-off stage, back-off counter); 'W' represents the status of CTS timeout; 'Snt' combines states of sending RTS/ receiving CTS/ sending DATA; 'Rcv' combines states of receiving RTS/ sending CTS/ receiving DATA . . . . .	91
4.9	A 3-node network scenario without hidden terminals. . . . .	92
4.10	Comparison of steady state probabilities at $x_1$ : the tuples represent (back-off stage, back-off counter); 'W' represents the status of CTS timeout; 'U' represents the freezing status due to busy channel; 'Snt' combines states of sending RTS/ receiving CTS/ sending DATA; 'Rcv' combines states of receiving RTS/ sending CTS/ receiving DATA; 'Ovh' denotes overhearing RTS; 'NAV' represents the freezing status due to NAV . . . . .	97
4.11	A 3-node network scenario with hidden terminal. . . . .	98
4.12	Comparison of steady state probabilities at $x_1$ : the tuples denote (back-off stage, back-off counter); 'R' denotes status of sending RTS packets; 'C/A' combines states of sending CTS/ receiving DATA; 'Ovh' denotes overhearing CTS; 'NAV' represents the freezing status due to NAV from CTS . . . . .	102
4.13	Comparison of steady state probabilities at $x_2$ : 'I' represents the idle status; 'U' represents the freezing status due to busy channel; the tuples represent the 1st step or last step of receiving RTS from $x_1$ or $x_3$ ; '(C/A)' combines states of receiving CTS/ sending DATA from/to $x_1$ or $x_3$ . . . . .	103

## ABSTRACT

In computer networks, routing determines how data move across a network from a source to a destination, while medium access control (MAC) defines when and how to transmit data from one node to another. Ant-based routing protocols have successfully provided an effective, if not optimal, solution to the routing problem by using control packets, called “ants”, to explore networks, discover routes and reinforce the best routes. However, the modeling of ant-based routing in the context of wireless local area networks (WLANs) is challenged by the intrinsic complexity of wireless medium access control and its cross-layer interaction. Therefore, this dissertation mainly concerns two problems: improvement of an ant-based algorithm’s performance on routing problem and mathematical characterization of medium access control for wireless local area networks.

Our contributions are threefold. First we introduce a novel strategy for ant-based routing to achieve optimal solutions that have least hop count. Next, we modestly analyze the integrated behaviors of ant-based routing with medium access control based on the case investigations of a practical MAC protocol MACA (Multiple Access with Collision Avoidance). Finally, we develop a detailed Markov model according to the comprehensive descriptions of the Distributed Coordination Functions (DCF) in IEEE 802.11, an international standard that specifies access scheme for WLANs.

This dissertation is organized as follows. Chapter 1 presents the background of routing and medium access control problems in WLANs, and reviews related research efforts on ant-based network routing and the IEEE 802.11 DCF. In Chapter 2, we show that our strategy leverages the previous efforts to model and analyze ant-based routing protocols on wired networks that explained how some critical parameters drive the network into near optimal route configurations. A simulation study of the strategy

on both simple 5-node network and large 50-node network demonstrates a significant improvement on the discovery rate of stable single route solutions with minimum distance from a source to a destination as measured by hop count. In Chapter 3, we start by performing case studies to understand the MACA protocol based on a Markov chain analysis. The findings are incorporated into the previous analytical framework of ant-based routing protocol, and the predicted behaviors of the resulting integration model are validated through realistic simulations. A regression study is also conducted to evaluate MACA performance by packet delivery ratio in multi-hop wireless networks. Finally in Chapter 4, we give the detailed derivation of our new model for the IEEE 802.11 DCF. The validity of our model does not depend on the network parameters and topology. For steady state calculations, we approximate joint probabilities from marginal probabilities using product approximations. By assessing the model in a variety of representative networks, we find excellent agreement of equilibrium node states with realistic simulations of network traffic.

## Chapter 1

### INTRODUCTION

#### 1.1 Background and Motivations

With proliferation of computers and thriving technologies of telecommunication, wireless local area networks (WLANs) play a critical role in modern society. Since its debut at the University of Hawaii laboratory in 1971, WLANs are becoming more ubiquitous than ever. Interactions between computers, mobile phones, tablets, wearable and smart devices all require data communications over shared radio frequencies. The increasing popularity comes with the major benefit of mobility, as users can dynamically access the network, move among different environments, create ad hoc scenarios for a limited time and then leave [41]. On the other hand, the technological limitations in radio transmission such as low bandwidth and vulnerability to signal interference necessitates an optimal network framework with delicate design and efficient implementation in response to typical performance requirements and Quality of Service (QoS) demands. It is often of interest to simulate a wireless LAN to gain insight into its behaviors for the purpose of performance improvement. However, experimentation with the live network is usually disruptive and can be very costly both in terms of software and time [38]. Instead, a detailed and comprehensive model is usually more desired and valuable both qualitatively and quantitatively for apprehending the problems such as performance analysis and optimizations. The most exploited mathematical tools and foundations belongs to the theory of stochastic processes such as Markov chains [36] and queuing systems [33]. The accompanying complexity of developing and investigating these models is such that exact solutions are available only for limited simple cases which are theoretically important but lack practical relevance [61]. The intrinsic

challenges of modeling as well as explosive growth of applications together has made wireless local area networks one of the most important research topics in computer science, and has drawn considerable attentions from the mathematics community as well [5, 9, 20, 24, 31].

Most common WLANs are based on IEEE 802.11 international standards, also known as Wi-Fi [3], which describe two variations of operating mode for WLANs. The first one contains infrastructure such that every device/computers/nodes in the network only communicate to a centralized control unit called Access Point (AP), which also serves as bridges cabled to other local networks or the internet. Sacrificing some flexibility that wireless communications provide, the infrastructure WLANs are simpler to design and can guarantee certain level of QoS for chosen nodes [40]. In contrasts, the infrastructure-less scenarios, also referred to *ad hoc networks*, offers greatest possible flexibility as each node can either directly communicate (peer to peer) or relay message to another (multi-hop forwarding) without any coordination from central administration. However, it also leads to complex issues such as the problem of routing for maximal network utilization. Routing, in essence, is the task of exploring and maintaining the paths from a source to a destination on which a data packet can travel. Such tasks are particularly challenging in the ad hoc setting where the nodes are able to move within the network. This means that the network topology will vary dynamically. Also the data transmissions are unreliable due to broken links. Many routing protocols have appeared in the literature that incorporate certain level of adaptivity and robustness to cope with mobility and loss of information in wireless ad hoc networks. Those classical protocols, such as link state routing algorithms, are called proactive routing, or table-driven routing, as they maintain up-to-date routes information to all nodes, including those to which no packets are being sent [53]. On the other hand, the reactive protocols, or source-initiated on-demand routing, create and maintain routes only on as needed basis, for example, Dynamic Source Routing [29]. Moreover, hybrid routing combines both proactive and reactive components trying to merge the advantages of the two. A specific example of a hybrid algorithm are

ant-based routing protocols, which differ substantially from traditional protocols in terms of the technologies implemented. Inspired by swarm intelligence and Ant Colony Optimization (ACO) [8], ant-based routing naturally provides desired properties of wireless ad hoc networks such as adaptivity and robustness [18]. As the first part of the thesis, we focus on the mathematical analysis and simulation study for a dynamical system that was developed in [59] for basic ant-based routing protocols (BARP). We improve the performance of BARP by showing it is possible to select near-optimal routes as measured by hop count when using a time dependent routing strategy.

Although ant-based routing protocols have been successfully applied to exploit routes in multi-hop wireless networks [16, 17, 18, 43], the rigorous mathematical modeling and analysis of the performance was limited to wired networks because the models did not include particular pathological features of channel access in wireless networks such as the *hidden terminal problem*: data transmissions are vulnerable to interference when transmitting nodes have only partial information about the network topology. The efficiency of wireless communication requires independent nodes to coordinate transmission and reception of data packets over a shared spectrum in a distributed way. The coordination of such communications is accomplished through Medium Access Control (MAC) protocol, a set of rules that defines when and how to transmit data from one node to another. Operating on the data link layer in OSI (Open Systems Interconnection) architecture of modern computer network, the MAC protocols aim for avoiding interference from packets collisions while maximizing spatial reuse. A number of MAC protocols, such as Aloha [4, 47], MACA [30], CSMA/CA, etc., have proven to be effective both generally and in special circumstances [34]. Most studies of MAC protocols are experimental, using either simulated or real network traffic to directly compare performance. MAC protocols themselves are complex and have resisted efforts to create consistent mathematical models that can reproduce detailed network performance timelines. The main bulk of the thesis is therefore to derive and validate a detailed mathematical model for the Carrier-Sensed Multiple Access with Collision Avoidance (CSMA/CA) protocol together with binary exponential backoff,

which form the IEEE 802.11 Distributed Coordination Function (DCF). This detailed model is valuable in and of itself to understand how protocol parameters affect performance, and it is a natural building block for understanding upper layer protocols such as BARP that operate on top of the MAC layer.

## 1.2 Related Works

Inspired by the mechanisms of ant’s pheromone trail laying and following behaviors, ant-based routing protocols deploy control packets to discover routes between pairs of nodes, reinforce optimal routes via pheromone deposition, and discard less-efficient routes through pheromone evaporation. There have been a variety of contributions in the design and mathematical study of ant-based routing algorithms. The pioneering works of Schoonderwoerd et al. [54] in 1997 were the first to consider the applications of ant-based algorithms within the domain of routing in distributed networks. The authors designed an ant-based control system for call-routing in telephone networks. The development of ant-based routing protocols for packet-switched communication networks dates back to 1997-1998 when Di Caro and Dorigo introduced an algorithm called “AntNet” [15]. It was designed to provide adaptive routing solutions in fixed, wired computer networks, and was followed by a number of other ant-based algorithms such as ARA [25], AntHocNet [16], ANSI [43], which were proposed for solving routing problems of wireless mobile ad hoc networks. While the merits of these routing algorithms were experimentally studied using a set of predetermined protocol parameters, other investigators began to apply deep mathematical analysis to understand the complex behaviors of ant-based routing protocols and the impacts of protocol parameters on network performance. Yoo, La and Makowski rigorously studied a simple two router ant-based system with multiple parallel routes [65]. The study rigorously determined the long-time asymptotics for the system. This work was augmented by Punyaslok and Baras [42], who modeled the arrival times of data and control packets along parallel routes between two routers. Following the similar patterns in [59], the extensions map the stochastic problem to a system of ordinary differential equations (ODEs).

The authors identify stationary states and analyze their stability. For larger networks, Bean and Costa developed a framework for studying ant-based systems, connecting equilibrium solutions with Wardrop equilibrium, a special case of Nash equilibrium, from traffic flow theory [6]. Different from [59], Bean and Costa’s routing model follows a succession of unique steady states and assume globally-synchronized clocks at each nodes. Others have augmented empirical studies by modeling different aspects of the protocol. Saleem et al. have developed mathematical frameworks for the analysis and measurement of collision probabilities to routing overhead, route optimality and energy consumption [50, 51, 52]. Along similar lines, Zhahid et al. have developed a mathematical framework for analyzing beehive based protocols [66]. Finally, an analytic framework based on Markov chain analysis is proposed in [48, 49] where the authors analyze and explore a full range of routing exponents (referred to as sensitivity parameter) to optimize network performance.

On the other hand, in the domain of wireless medium access control, many researchers have constructed mathematical models to understand and predict ensemble network behaviors under IEEE 802.11 Distributed Coordination Function (DCF). However, the complexity of this DCF under general network topologies requires that investigators make severe assumptions about potential collisions between nodes. The enormously influential work of Bianchi [7] on fully connected single-hop saturate networks begins by assuming that the collision probability on each node is constant and independent of network topology and node states. As we shall see, this is clearly not the case in general and a Markov model based on this assumption cannot hope to model the DCF. Numerous works have extended this approach to try to capture missing elements of the DCF in a way that is both simpler than a full simulation and valuable as a predictive instrument for studying protocols.

There have been many extensions of Bianchi’s work to model single-hop transmissions where there are no hidden terminals. For instance, the basic model in [7] is adapted to the assumption of freezing backoff counter due to busy medium in [68], which is further polished and strengthened in [19] by introducing the dependence of

consecutive slots, and also in [57] by redefining the discrete time scale given in [7]. Wu et al. [63] augment Bianchi’s model by assuming finite retransmission attempts, which is also adopted in [27]. In [26], the authors propose another model extension for saturation throughput analysis by considering the effect of non-ideal channel conditions, while [14] presents a similar model for unsaturated cases. In addition to throughput analysis, a comprehensive analysis of delay performance is conducted by [67], where the authors modify node state transitions in [7] with signal transfer functions to characterize the probability distribution of MAC layer service time for WLANs in both saturated and non-saturated traffic situations. Others, for instance, [13], model the statistical behaviors of the Head-of-Line packet instead of nodes and perform unified study on both throughput and delay. A great deal of effort has also been made to model and analyze IEEE 802.11 DCF in the presence of hidden terminals, where some prospective senders are not within the sensing range of others. For instance, to model the existence of hidden terminals, [64] employs fix-sized time slots and details the state transition to formalize the channel status considering the interaction between physical and virtual carrier sensing in a discrete time Markov system. However, the authors follow the same assumption that collision probability is constant regardless of retransmission history. In contrast, [28] uses the joint backoff stage of the two stations that are hidden from each other as state in order to account for the interactions between them. Unfortunately, these models are limited to infrastructure scenarios using access points and depend on the network topology.

There has also been some efforts to model and analyze multi-hop transmissions. Guillemin et al. propose a model for CSMA in multi-hop settings based on a random walk on lattice [24]. The underlying assumption in this model is that node behavior is synchronized so that the problem can be parametrized by the queue size on each node. However, nodes in a network undergo random exponential backoffs when there is channel contention so these assumptions are not valid. Efficiency requires that network protocols operate asynchronously with each node acting opportunistically to empty its queue or respond to other node’s requests for it to accept data. Other investigators

rely upon statistical descriptions of transmission nodes combining with channel behaviors to develop a model. Garetto et al. [23] model CSMA for various two contenting flow topologies to study the unfairness problem and further supplement it to predict throughput in arbitrary topology [22]. The authors implement a decoupling model for each individual node with an embedded discrete time renewal process based on the basic assumption that the current channel state is independent of previous state. However, [60] points out that the above assumption is unrealistic with the presence of hidden terminals and the consequent de-synchronization of the nodes. Instead, Tsertou and Laurenson describe the channel by modeling a first-order dependence between consecutive channel state and adjusted Bianchi’s original model using fixed-sized time slot and contention window [60]. Mustapha et al. [37] apply a discrete-time modeling approach that combines a topology model, a channel model and a simplified node state model with only three states for analyzing throughput of multi-hop ad hoc networks. In the similar vein but different methodology, Shi et al. [55] extend Bianchi’s assumptions on backoff-stage dependence of collision probabilities, non-saturate queues, *etc.*, and develop a detailed continuous-time model of CSMA networks where the correlations of nodes are described through a companion channel model of joint backoff states. Unfortunately, the true statistical description that they are attempting to capture depends upon network topology and queue sizes. A more useful model will generate the statistical description given network parameters and topology. This is precisely what we set out to do.

### 1.3 Dissertation Outline

This dissertation is divided into three components to tackle different yet interconnected issues regarding to WLANs. In chapter 2, we start by briefly introducing the ant-based routing protocols and its merits for exploiting the intelligence of swarms to solve a complex problem such as near-optimal path searching. Then we describe a modeling framework in detail that was originally developed by [59] for ant-based routing protocol in ad hoc networks using dynamical systems theory. The rigorous study

of a representative small network by examining stationary solutions and their linear stability suggests we can improve the performance of ant-based routing by dynamically adjusting the routing exponent, a critical parameter that controls the behaviors of the protocol and our model. The contribution of this thesis is novel in that we leverage this technology and validate its effectiveness and efficiency by two specific examples, a 5-node network and a 50-node network, using both theoretically and realistic simulations with Matlab and QualNet respectively. As a concluding remark of this chapter, we point out the limitations of current modeling frameworks for ant-based routing on wireless networks due to the intrinsic complexity of medium access controls (MAC) and its cross-layer interactions.

To investigate the integrated behaviors of ant-based routing algorithm with medium access control (MAC) in wireless networks, Chapter 3 begins with an introductory review of several important wireless MAC protocols, from Aloha to CSMA/CA, which lay the foundation for the modern wireless communication standards. We then explore the operational details of one specific MAC protocol MACA (Multiple Access with Collision Avoidance) in the following sections. MACA is the first one ever designed to address the hidden terminal problem in shared channel networks [30]. We model the behavior of MACA and perform case studies in both two-sender and three-sender network scenarios with a Markov chain analysis. Then we take a modest step by modeling and analyzing the integrated behaviors between ant-based routing protocol and MACA on a simple 6-node topology. The efforts are validated by comparing numerical solutions of steady states with the QualNet simulation of realistic wireless communications. The last section of this chapter discusses the difficulties we have encountered to generalize our MACA modeling framework with Markov chain analysis and an alternative approach where the details of MAC protocol are lumped together with a single linear regression model.

In chapter 4, we focus on the derivation and verification of a stochastic model from the detailed IEEE 802.11 DCF description. Our work starts with making reasonable assumptions, which, distinct from [7] and its many extensions such as [19, 26,

57, 63, 67, 68], does not claim that the packets collision probabilities on each node are constant or independent of network topology. Instead, we have developed a detailed discrete time Markov model of interconnected node states including multiple back-off stages and binary exponential back-off counters to capture the dominant first order effects of nodes responses to contention. For steady state calculations, we approximate joint state densities from marginal probabilities using product approximations. To assess the quality of the model, we compare detailed equilibrium node states with results from realistic QualNet simulations in three representative wireless network configurations. We find a very close correspondence between our model and realistic simulations of network traffic.

## Chapter 2

### DYNAMIC ROUTING EXPONENT STRATEGY FOR ANT-BASED ROUTING PROTOCOL

Ant-based routing originates from the Ant Colony Optimization algorithm within the field of swarm intelligence. With the highly desirable features such as flexibility, robustness, decentralized control and self-organization, ant-based routing protocols has been shown to provide an effective solution in terms of both delay and packet delivery ratio to the routing problem of wireless ad hoc LANs, *i.e.*, mobile Ad Hoc Networks (MANET) [12], where bandwidth is limited and topology is constantly changing. In ant-based routing protocols, the routing exponent controls how ants hop from node to node to discover routes. Previous work has shown that stable multi-route solutions for small routing component values are dynamically connected to stable single-route solutions for large routing component values. Typically, these stable single-route solutions correspond to paths that have or almost have the smallest hop count. In this chapter, we leverage this idea to improve the performance of ant-routing protocols by dynamically adjusting the routing exponent. The results are validated via simulation.

#### 2.1 Introduction

Swarm intelligence is a term that refers to the action of a locally coordinated group of individuals that can achieve a complex objective or behavior. Often the local coordination algorithms are inspired by ecological systems including social insects, self-organizing colonies of single-celled organisms or movements of larger animals such as flocks of birds. Each individual possesses incomplete information about the problem to be solved, and coordination is achieved typically through interaction with a subset of individuals in the swarm. Through these interactions, complex, near-optimal behavior

can emerge [8]. One successful application of swarm intelligence is the use of ant-based protocols to route data through networks.

Ant-based routing protocols use control packets, called “ants”, to explore networks, discover routes and reinforce the best routes. Throughout this thesis, we will use the terms “ant” and “control packet” interchangeably. True ants in the biological world mark foraging trails with chemical pheromone that can be detected by other ants. The pheromone evaporates over time, so that inefficient routes fade from disuse. More efficient popular routes are reinforced as ants deposit more pheromone along them. Similarly, in ant-based protocols, virtual pheromone is stored on the nodes as the ants traverse the network. In short, the key to the routing protocol is a spatially distributed, mathematical model of pheromone deposition and evaporation. Research has shown that ant-based routing protocols provide an effective solution to the routing problem of both wired networks [15] and mobile ad hoc networks [16, 17, 43]. In this chapter, we will use a mathematical framework for studying routing protocol dynamics to improve their performance.

A modeling framework introduced in [59] to describe the evolution of pheromones in ant-based routing protocols using dynamical systems theory correctly predicts stationary states of realistic network protocols. In this study, it was shown that some of the principles gained from rigorous analysis of small networks, transfer to larger networks that are much more difficult to be mathematically analyzed. In particular routing exponents that are much smaller than unity, lead to multi-route solutions and exponents that are much larger than unity lead to single-route solutions. However, not all single-route solutions are optimal in the sense that they require more than the minimum number of hops to travel from a sender node to a receiver node. Also, it was shown that if one treats the routing exponent  $\beta$  as a parameter, stable multi-route solutions were dynamically connected to the optimal single-route solution on small networks. In this chapter, we will leverage this idea to show that on large networks, it is possible to improve the performance of ant-routing protocols by dynamically adjusting the routing exponent.

The rest of the chapter is organized as follows. In Section 2.2, we describe a modeling framework, which is the mathematical foundation of dynamic routing exponent strategy. In Section 2.3, we introduce this strategy by two specific examples, a 5-node network and a 50-node network using Matlab and QualNet simulations, and then validate its effectiveness by statistical comparison. Section 2.4 concludes this part of our work and states the limitations.

## 2.2 Preliminaries of Ant-based Routing

In our modeling framework, a computer network is viewed as a directed graph. Each node represents a computer station or a wireless transmitter and pairs of nodes are neighbors if they are connected either through cable or within the radio coverage range of each other. Each link is weighted by pheromone values, which determine how ants will travel in the network along multi-hop routes. Using pheromone tables on each node, ant-based routing protocols deploy ants to discover possible routes between pairs of nodes, and optimize routing tables to enhance shorter, desirable routes via pheromone deposition and discard longer, less efficient routes via evaporation of pheromone. In our mathematical modeling framework, the behaviors of ant-based routing are characterized by three general rules: route discovery, route reinforcement (deposition) and route decay (evaporation).

Route discovery is accomplished by the random motion of ants through the network as they hop from node to node. Following the notation used in [59], an ant at node  $i$  will move to node  $j$  with probability  $p_{ij}$ ,

$$p_{ij} = \frac{(\tau_{ij})^\beta}{\sum_{h \in N_i} (\tau_{ih})^\beta}, \quad (2.2.0.1)$$

where  $\tau_{ij}$  represents the pheromone values on the link from node  $i$  to node  $j$ ,  $N_i$  is the set of all connected neighbors of nodes  $i$  and  $\beta$  is the routing exponent which controls the behaviors of the protocols. The routing tends toward pure random if  $\beta \rightarrow 0$ , resulting in more options of routes. On the contrary, if  $\beta \rightarrow \infty$ , the routing is deterministic, and the ants will always pick the link with the most pheromone value,

consequentially favoring single-route solution. The protocol uses two different types of ants. Ants traveling from source  $s$ , seeking route to destination  $d$ . are called “forward ants”. If the network consists of  $m$  nodes, we define  $\mathbf{y}^{(n)}$  be the  $m$ -dimensional vector probability density of ants over the network at the  $n^{\text{th}}$  time step, and discrete time scale  $h_3$  be the amount of time for each ant to make one hop between nodes. The forward ants traverse the network following the Markov process according to a transition matrix  $P^{(n)}(\beta) = [p_{ji}]$  at the  $n^{\text{th}}$  time step,

$$\mathbf{y}^{(n+1)} = P^{(n)}(\beta)\mathbf{y}^{(n)}, \quad (2.2.0.2)$$

because both probability density and pheromone values on each link are evolving only dependent on present state by every discrete synchronous step. Here the  $k^{\text{th}}$  component of the density vector  $\mathbf{y}^{(n)}$  is the probability of finding an ant on the  $k^{\text{th}}$  node of the network. This implies that if we have  $N$  ants in the networks, then the expected number of ants at each node is  $N\mathbf{y}^{(n)}$ . Once a forward ant reaches the destination, it becomes a “backward ant”, and will trace back to the source from the destination, reinforcing route by depositing pheromone along the path it takes. On the other hand, route decay (evaporation) follows a global rule regardless of ant activity. Pheromone throughout the networks decays exponentially in the absence of deposition. Overall, the routing protocol defines how the matrix  $P = [p_{ji}]$  evolves from one iteration to the next through pheromone deposition and evaporation. We denote the matrix  $P$  at discrete time step  $n$  as  $P^{(n)}$ . From the previous analysis and implications from 2.2.0.1, we know that the routing exponent  $\beta$  controls whether single-path routes are selected or multi-path routes are selected. For a complete description and analysis of the protocol, see [59]. In this section, we will review the essential features and properties of the protocol.

A full-fledged routing protocol is very difficult to analyze because it has many parameters such as packet size, processing time of ants [11], and features to respond to different contingencies, for instance, network congestion. Instead, we will study and implement a very simple routing protocol and explore it using an analytic framework. Since ant-based routing is a dynamic process, we identify three critical time increments.

The increment  $h_1$  is the amount of time between evaporation events on each node. The increment  $h_2$  is the amount of time between deployment of ants from a source node  $s$ . The increment  $h_3$  is the time required for a control packet to move from one node to the next. For stability issues, we assume that  $h_1 < h_3 \ll h_2$  such that all ants in the networks can finish their tour before a new cohort of ants is released. The routing protocol can be described as follows. Independent of all the ant activity, pheromone

- 1  $N$  ants are released from the source node. The source node resets its clock to  $t = 0$ .
- 2 Each ant moves through the network following (2.2.0.1) and maintaining a node-visited stack until it arrives at the destination node.
- 3 An ant reaching the destination node will retrace its steps back to the source. If the ant's route from source to destination is cycle-free (i.e. no node is visited twice), the ant deposits pheromone along the links it traverses. Otherwise, no pheromone is deposited. Typically, the amount of pheromone deposited on a link is inversely proportional to the hop count of the route traveled between source  $s$  and destination  $d$ .
- 4 When a backward ant arrives at the source, it is destroyed.
- 5 When the source node clock reaches  $t = h_2$ , return to step 1.

**Algorithm 1:** Basic Ant-based Routing Protocol

will decay along all links every  $h_1$  period.

In [59], the reduction of pheromone level on link  $ij$  from discrete time step  $t_n$  to  $t_{n+1}$  (e.g.  $t_{n+1} - t_n = h_1$ ) is described as

$$\tau_{ij}^{(n+1)} = \tau_{ij}^{(n)} - \kappa_1 h_1 \tau_{ij}^{(n)} = (1 - \kappa_1 h_1) \tau_{ij}^{(n)} \quad (2.2.0.3)$$

where  $\kappa_1$  is a constant evaporation rate. If  $h_1 \rightarrow 0$ , (2.2.0.3) is equivalent to  $\tau'_{ij}(t) = -\kappa_1 \tau_{ij}(t)$  which indicates that pheromone will decay exponentially in time:  $\tau_{ij}(t) = \tau_{ij}(0)e^{-\kappa_1 t}$ . The deposition of cohort of  $N$  ants on link  $ij$  is characterized by

$$\tau_{ij}^{(n+1)} = \tau_{ij}^{(n)} + \kappa_1 h_2 N F_{ij}^{(n)} \quad (2.2.0.4)$$

Here, the discrete time interval is  $h_2$ , a sufficient amount of time for all ants to complete their tour to the destination and return (recall  $h_2 \gg h_3$ );  $\kappa_2$  is a constant rate that

controls deposition and  $F_{ij}^{(n)}$  is the deposition function that determines the increment of pheromone value at each step. According to the step 3 in the ant-based routing algorithm, stochastically, the deposition function takes the form:

$$F_{ij}^{(n)} = \frac{1}{N} \sum_{k=1}^{\infty} \frac{1}{k} \tilde{p}_{ij}^{sd}(k) \quad (2.2.0.5)$$

where  $\tilde{p}_{ij}^{sd}(k)$  is the probability of an ant following a  $k$ -hop route from source node  $s$  to destination node  $d$  passing through link  $ij$  without any cycles. The summation is the expected inverse hop count,  $\left\langle \frac{1}{H_{sd}} \right\rangle$  made by a single ant. This is a natural way to reinforce shorter routes more than longer routes because the amount of pheromone deposited along the route is inversely proportional to the path cost. Unfortunately, there is no known close form of probability  $\tilde{p}_{ij}^{sd}(k)$  for a given graph. However, the computation of  $\left\langle \frac{1}{H_{sd}} \right\rangle$  is still possible by construction of a K-cycle-free tree using recursive algorithm [59].

Now, combine (2.2.0.3), (2.2.0.4) and (2.2.0.5), an analytic model for the behavior of this ant-based routing protocol can be derived:

$$\tau_{ij}^{(n+1)} = \underbrace{(1 - h_1 \kappa_1)^{(h_2/h_1)} \tau_{ij}^{(n)}}_{\text{evaporation}} + \underbrace{h_2 \kappa_2 \sum_{k=1}^{\infty} \frac{1}{k^p} \tilde{p}_{ij}^{sd}(k)}_{\text{deposition}}, \quad (2.2.0.6)$$

The link undergoes  $h_2/h_1$  evaporation events between step 1 and step 5 of the routing algorithm, and it is understood that  $h_2/h_3$  transitions of (2.2.0.2) occur for every transition of (2.2.0.6).

If we think of the ant-based protocol as a nonlinear dynamical system, we can understand network performance by examining stationary solutions and their linear stability. A stationary state occurs when (2.2.0.2) and (2.2.0.6) are independent of the time steps  $h_1$ ,  $h_2$  or  $h_3$  by taking the limit to 0 and satisfy the system,

$$\Lambda \tau_{ij}^{(n)} = \sum_{k=1}^{\infty} \frac{1}{k} \tilde{p}_{ij}^{sd}(k) \quad (2.2.0.7)$$

where  $\tau_{ij}^{(n)}$  is an equilibrium pheromone distribution and  $\Lambda = \frac{\kappa_1}{\kappa_2}$  is called pheromone deposition number. For a detailed derivation of (2.2.0.7), see Appendix A. Note that

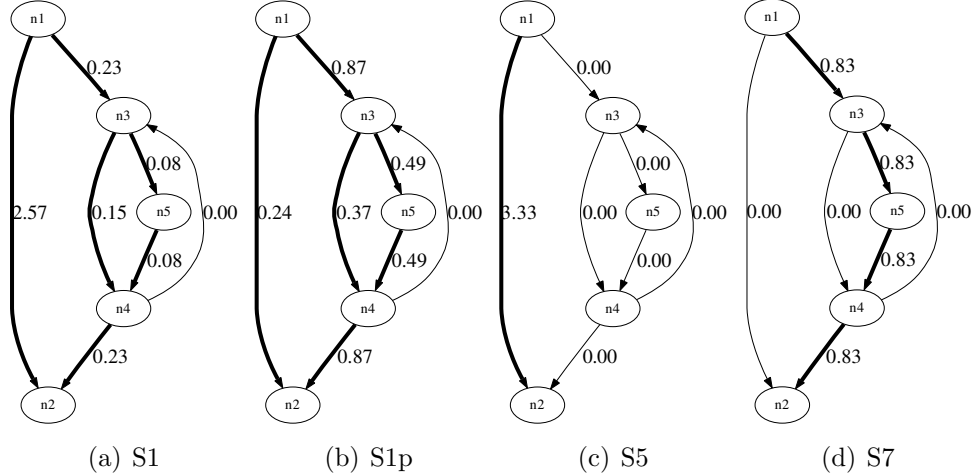


**Figure 2.1:** Stationary states calculated using the stochastic model. Solutions S1, S5 and S7 were calculated with  $\beta = 0.5$  and  $\Lambda = 0.3$ . Solution S1p was calculated with  $\beta = 2$  and  $\Lambda = 0.3$ .

$\tilde{p}_{ij}^{sd}(k)$  depends upon  $\tau_{ij}$ . Since this is a nonlinear system, solutions are not necessarily unique. In fact, a single  $\beta, \Lambda$  pair may have many stationary solutions. The eigenvalues and eigenvectors of the Jacobian of this system reveals whether or not a given stationary solution is stable. Earlier work presented a phase diagram for a representative 5-node network [59].

The previous work shows that some of the principles and features gained from rigorous study of small networks are consistent with larger and more complicated networks that are much more difficult to analyze. In particular, for the simple 5-node network and a larger 50-node network, small routing exponents  $\beta \ll 1$  lead to stable, multi-route solutions whereas large exponents  $\beta \gg 1$  lead to stable single-route solutions. Examples are shown in Figure 2.1 where solution S1 is stable but solutions S1p, S5 and S7 are unstable in the parameter regimes used to generate the solutions. However, solutions with the same qualitative structure as S5 and S7 are stable when  $\beta = 2$ .

Moreover, stable multi-route solutions are dynamically connected to the optimal single route solution on the 5-node network. As shown in Figure 2.2, if we follow the

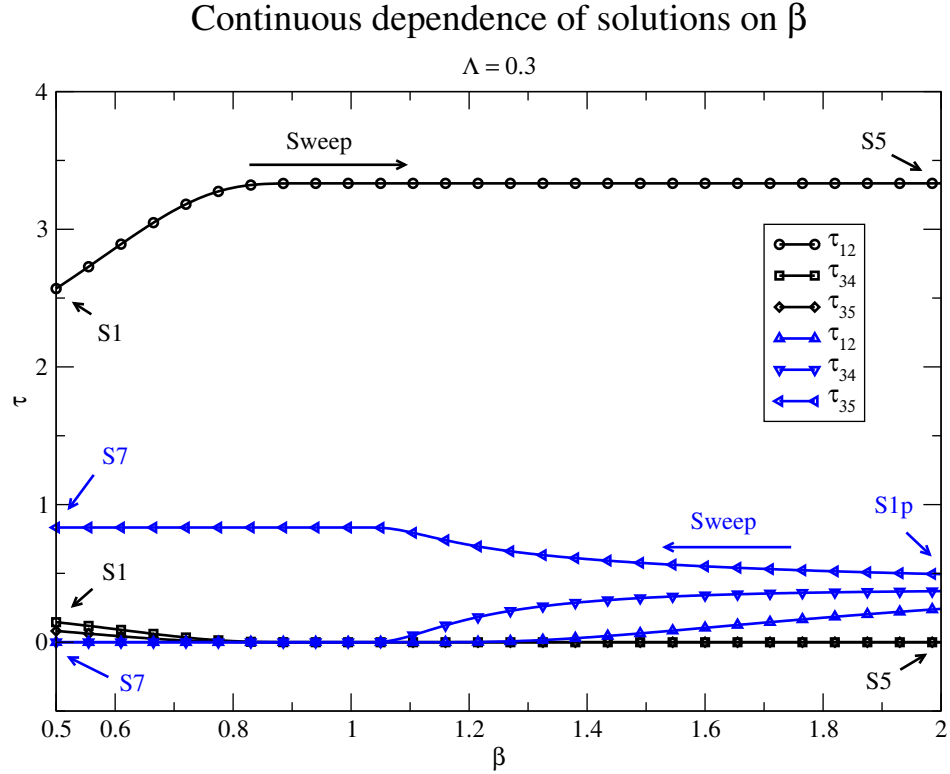


**Figure 2.2:** Continuous dependence of solutions on  $\beta$  for the simple 5-node network configuration used in Figure 2.1. Here  $\lambda$  is fixed on 0.3. Each curve represents the pheromone values on corresponding link shown by the legends.

structure of certain stationary solutions, we see that the stable multiple-route solution S1 is dynamically connected to the optimal single-route solution S5 by sweeping the value of  $\beta$  from 0.5 to 2. On the other hand, the unstable multiple route solution S1p is connected to the suboptimal, unstable single-route solution S7 by a sweep of  $\beta$  from 2 to 0.5. One possible explanation is that shorter routes are reinforced more readily when the system is more deterministic which is the case when  $\beta$  is large.

These results and observations on large networks suggest that we can improve ant-based routing by dynamically adjusting the routing exponent. Large values of  $\beta$  offer the advantage of stability and determinism, but there is no guarantee that the single-route selected will be optimal. The earlier study suggests that the system will

Total time of Simulation	199.99
N	200
$\beta$	0.5 $\rightarrow$ 2
$\kappa_1$	0.3
$\kappa_2$	1
$\Lambda$	0.3
h1	1
h2	1
h3	0.01

**Table 2.1:** Table of parameters used in network simulations.

naturally evolve into the optimal single-route state if we start with a stable multi-route solution with  $\beta$  small and then steadily increase  $\beta$  to a large value.

### 2.3 Dynamic Routing Exponents

In this section, we first validate the efficiency of this technique of dynamically adjusting the routing exponent on a 5-node network. Then, we leverage this idea to show that on large networks, it is also possible to improve the performance of ant-routing protocols. We implement our algorithm in Matlab, without a physical communication model so there are no packet drops, and in QualNet with realistic protocol and communication models. QualNet [2] is a state-of-the-art simulator that contains sets of comprehensive tools for accurate, efficient simulation of large-scale, heterogeneous networks. It provides an exact, high quality, reproduction of external network behavior so that the simulation result is almost the same as on actual systems. Table 2.1 summarizes the parameter settings used by both Matlab and QualNet simulations. In the QualNet simulation, each topology is modeled as a point-to-point mesh network with link bandwidth of 100 Mbps and link propagation delay of 1 millisecond. The ant-based routing protocol operates in the network layer, and encapsulates ants in the IP packets.

### 2.3.1 5-node network

To demonstrate the concept of using dynamic routing exponents, we apply this idea on the 5-node network where the dynamics are well understood. (We note that a phase portrait was calculated in [59]). We initiate simulation with random pheromone values over the network. Rather than using a fixed value in (2.2.0.1),  $\beta$  will be a function of time and slowly vary from 0.5 to 2.0 as follows.

$$\beta(t) = \begin{cases} 0.5, & t < 50 \text{ (allow time for multiroute solution to stabilize)} \\ 0.5 + \frac{t-50}{20}, & 50 \leq t \leq 80 \text{ (move network toward single-route solution)} \\ 2.0, & t > 80 \text{ (proceed with optimal solution)} \end{cases} \quad (2.3.1.1)$$

This function allows the routing protocol to relax into a multiroute solution before slowly moving the system toward an optimal or near-optimal single-route solution. Thus, we expect the network to move toward stable multiroute solution S1 when  $0 < t \leq 50$  and then move toward S5, the optimal single-route that directly connect source and destination. This is precisely what we observe in Figure 2.3, which demonstrates dynamic pheromone distribution on four critical routes of the simple 5-node networks shown in Figure 2.1.

### 2.3.2 50-node network

With the same configurations summarized in Table 2.1, the Matlab simulation for a 50-node network has successfully validated the anticipated result that routing exponent  $\beta = 0.5$  leads to the formation of multiple route solution, while  $\beta = 2$ , on the other hand, corresponds to the existence of the single-route solutions. We consider optimal solutions to be solutions with the minimum possible hop-count. Depending on the initial conditions, single-route stable solutions found with large routing exponents are observed to be close to optimal, but not typically optimal. In Figure 2.4, we see two typical stable solutions. Since the shortest path possible connecting source and

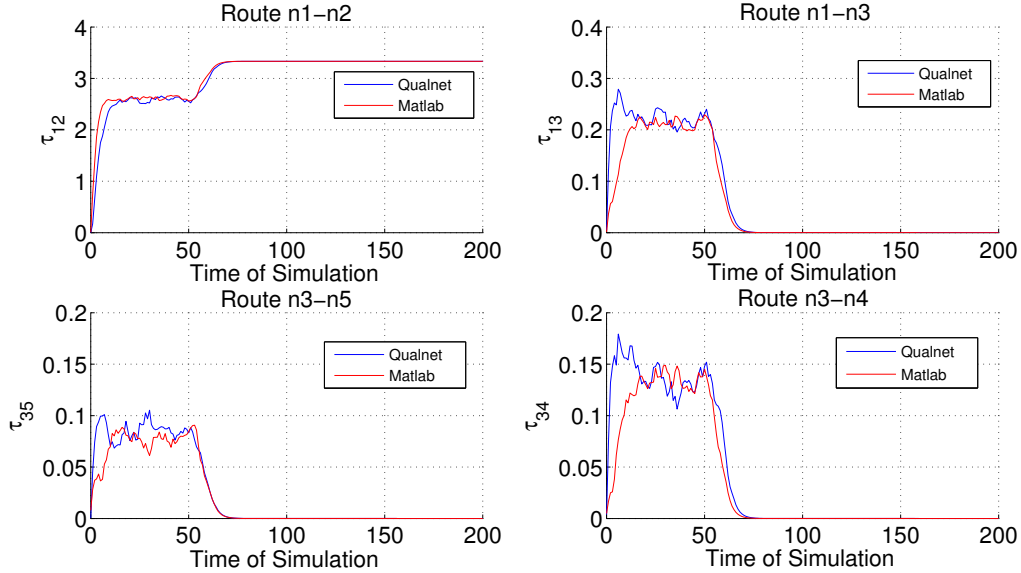


**Figure 2.3:** Pheromone values as a function of time using dynamic routing exponents for both Matlab and QualNet simulations.

destination in this network is 6-hops, the single-route is nearly optimal (7 hops) but not optimal.

Now we will explore our dynamic routing exponent strategy (2.3.1.1) by translating the design principles for the small network to 50-node network settings. Again, the simulations begin with random pheromone values over all links in the network. Along the time of simulation of ant-based routing protocol, we capture several key instants, shown by Figure 2.5, that illustrate the reorganization of pheromone values over the network driven by the dynamic routing exponent  $\beta$ . Similar to the 5-node network case, we see the system initially settles into a multi-route solution as shown in Figure 2.5(a). As  $\beta$  increases, we see the network evolve toward single-route solutions in Figure 2.5(b,c). Beyond this point, the system has settled into a stable, globally optimum, 6-hop solution as shown in Figure 2.5(d). In addition, Figure 2.6 depicts one instance of the evolution of average hop count from the perspective of the control packets over time as  $\beta$  changes linearly from 0.5 to 2 between simulation time instances

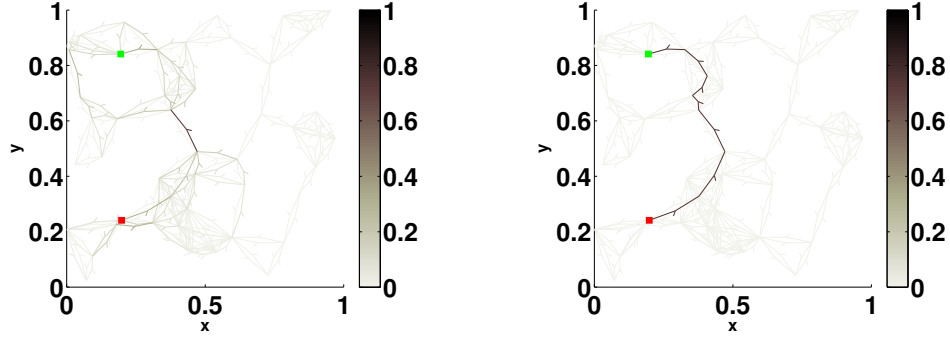


**Figure 2.4:** Two stationary solutions with  $\beta = 0.5$  on the left,  $\beta = 2$  on the right, both with  $\Lambda = 0.3$ . Node  $s$  is shown by red spot and node  $t$  is shown by green spot. Pheromone values are normalized by the maximum pheromone value over the entire network.

50 and 80.

### 2.3.3 Statistical Comparison and Impact of $\Lambda$

We implemented a statistical analysis to quantify how the performance of ant-based routing protocols can be improved by dynamically adjusting routing exponent from a value less than unity to that larger than unity. We performed the same experiment on the 50-node network 100 times using different random initial conditions and compared the performance using  $\beta = 2$  (standard practice for protocols like AntHocNet) to using the dynamic  $\beta$  algorithm. All other network parameters are the same. All the simulations are executed with random initial pheromone distribution and  $\Lambda = 0.3$ . Our simple comparison, shown in Figure 2.7, demonstrates a considerable benefit when using the dynamic  $\beta$  algorithm. The difference between the average length of a single-route solution for the  $\beta = 2$  algorithm compared to the variable  $\beta$  algorithm at the end of simulation is almost 2 hops (mean value:  $8.01 \rightarrow 6.11$ ) for the Matlab simulations and 4 hops (mean value:  $10.2 \rightarrow 6.2$ ) for the QualNet simulations.

Our statistical results indicate that the dynamic  $\beta$  strategy is still somewhat sensitive to initial pheromone levels though not nearly so much as the constant  $\beta$  system. If the system is too far from a stable multi-route solution that includes an optimal

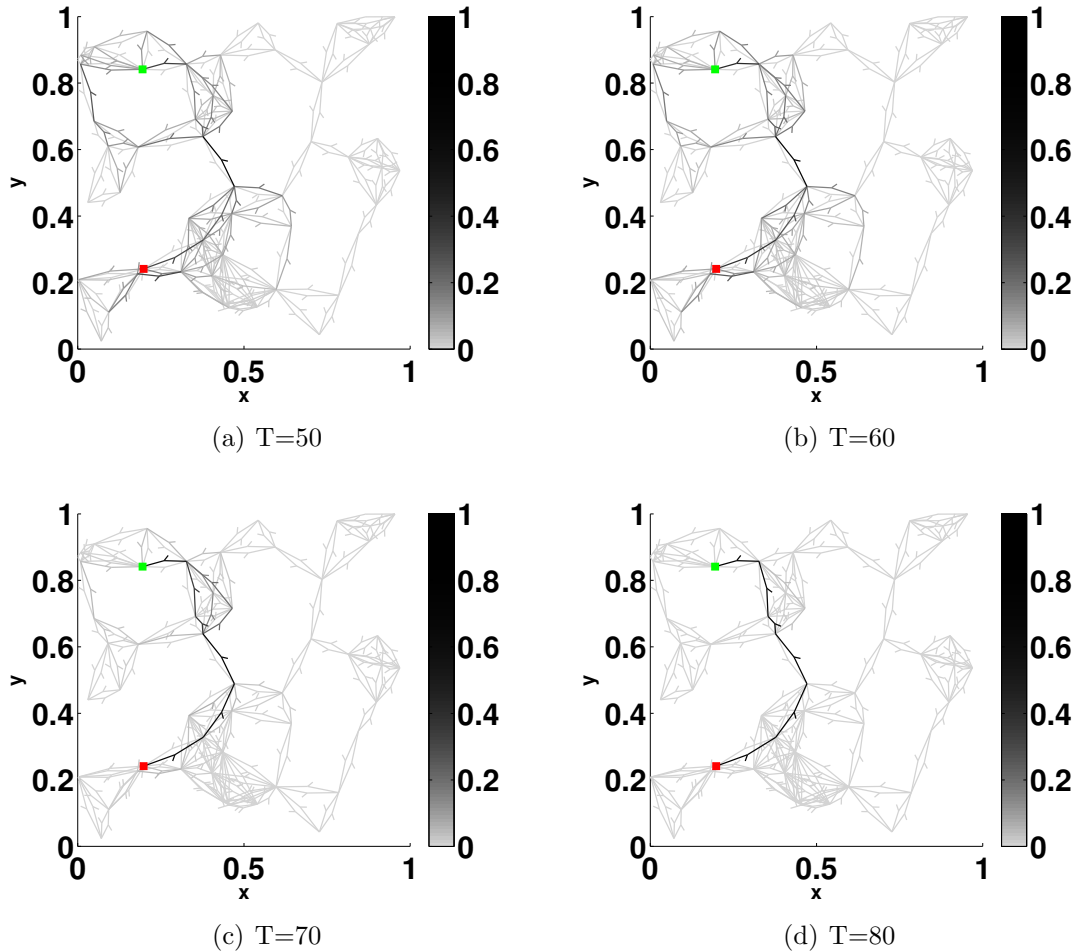


**Figure 2.5:** Distribution of normalized pheromone values at some important moments of simulation. At time 50, a multi-route state is achieved and beta starts to vary. The solution settles down at time 80, when beta stops to vary.

path as an option for ants, the dynamic  $\beta$  algorithm will not be able to smoothly move the network into an optimal configuration. This explains why the optimal route are not always achieved as the mean remains above 6 in the dynamic  $\beta$  trials.

Finally, we test the performance of dynamic routing exponent technique under different values of  $\Lambda$ , the pheromone deposition number (recall  $\Lambda = \frac{\kappa_1}{\kappa_2}$ ), an equally crucial parameter as  $\beta$  in our model. Since  $\kappa_1$  corresponds to the rate of evaporation while  $\kappa_2$  corresponds to the rate of deposition,  $\Lambda$  controls the ratio of evaporation to deposition. We anticipate larger values of  $\Lambda$  to reduce the impact of deposition and

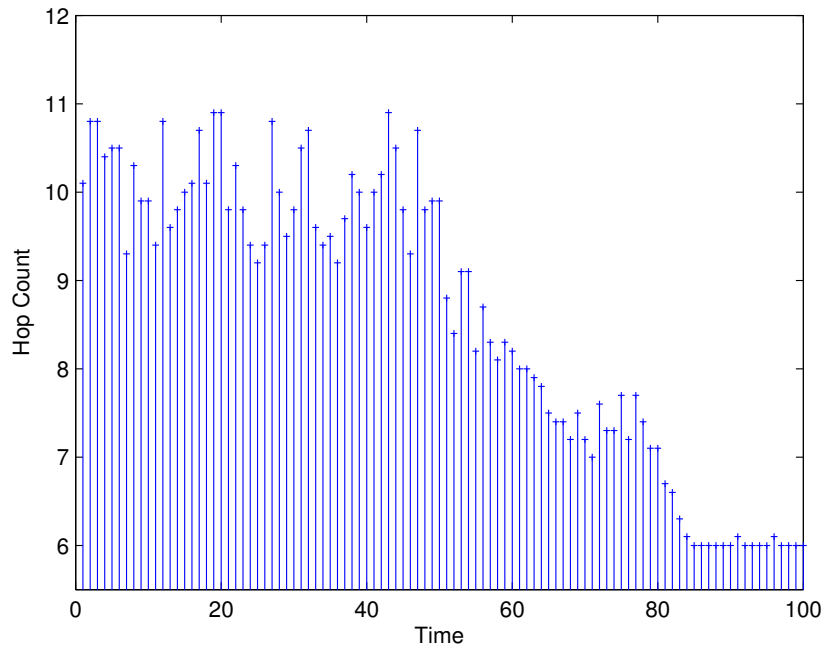


**Figure 2.6:** Evolution of average hop count over time.

so reduce the benefit of the overall technique as we try to drive the system toward an optimal solution. To illustrate this affect, we performed the statistical study on the 50-node network for  $\Lambda = 0.1, 0.2, \dots, 1.0$ . Figure 2.8 shows that when  $\Lambda < 0.5$ , the results are acceptable as the average length of the optimized single-route is roughly 6. However, when  $\Lambda > 0.5$ , the average hop count of the optimized single-routes increases linearly and reach 7.5 when  $\Lambda = 1$ , which is consistent with our expectation.

## 2.4 Conclusions

### 2.4.1 Summary

We have introduced and explored a new algorithm that dynamically adjusts the routing exponent in ant-based protocols. The new algorithm was motivated by an analytic framework that provided a complete description of the nonlinear dynamics of a small network. From this description, we observe that stable multi-route solutions for

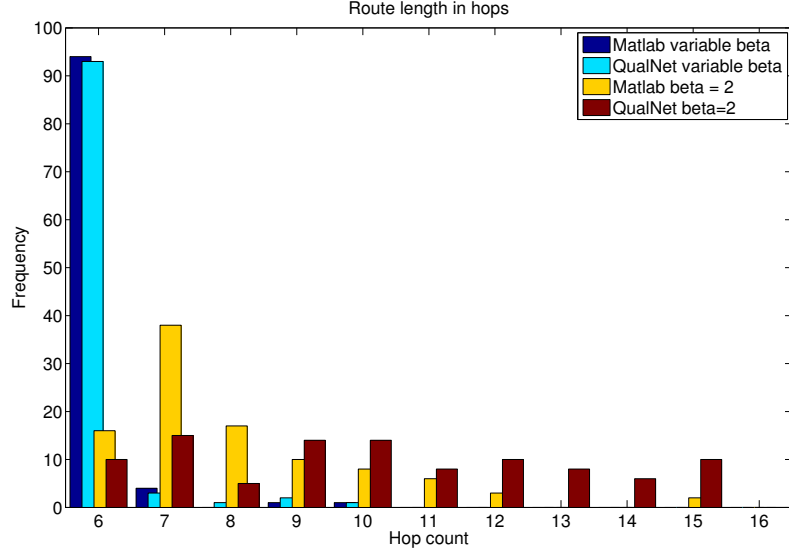


**Figure 2.7:** Statistic research of dynamic routing exponent strategy on improving performance of routing protocols.

small  $\beta$  are dynamically connected to stable single-route solutions for large  $\beta$ . These stable single-route solutions correspond to paths that have the smallest hop count. We give two examples using simulations in both Matlab and QualNet, a simple, 5-node network and a larger 50-node network. For the 5-node network, the results are exactly compatible with the previous rigorous study. For the 50-node network, we leverage principles from the simpler 5-node network and successfully validate them via Matlab and QualNet simulation. In particular, we find the dynamic  $\beta$  protocol performs significantly better than the static  $\beta = 2$  protocol in a large series of tests using random initial pheromone values. Finally, we explore the impact of  $\Lambda$ , the key parameter that determines the relative importance of evaporation and deposition. As expected, we find that the effectiveness of the dynamic  $\beta$  algorithm will be impaired when  $\Lambda$  is large. However, for moderate  $\Lambda$ , our new dynamic  $\beta$  routing protocol finds shorter routes than tradition ant-based routing methods.

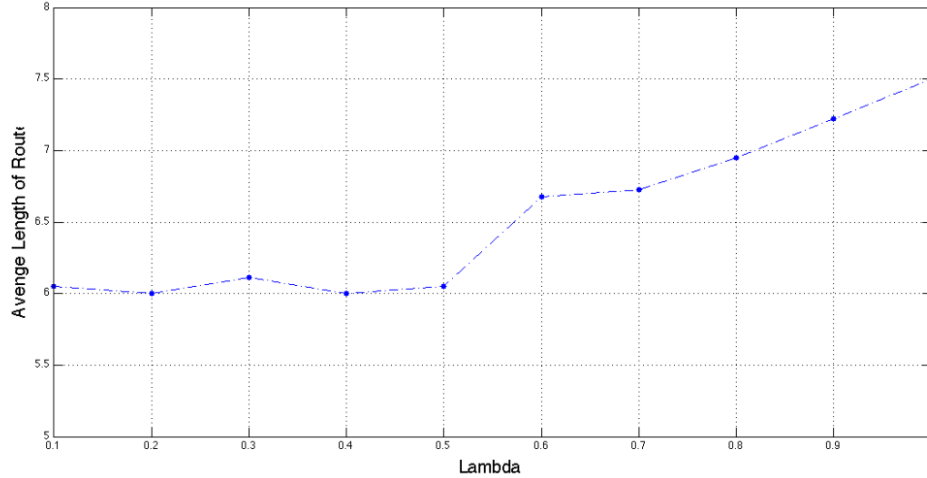


**Figure 2.8:** Average length of optimal single-route with respect to  $\Lambda$ .

### 2.4.2 Limitation and Next Step

Given superior features of adaptability and robustness, ant-based routing algorithms are naturally suitable for ad hoc networks and have been shown empirically to outperform many reference routing algorithms in the field such as AODV [39] in multi-hop WLANs. However, our mathematical modeling and analysis were confined to wired networks because the dynamic model did not incorporate particular pathological features of wireless networks such as *the hidden terminal problem* which may lead to severe losses of information and waste of bandwidth due to packet collisions when two or more frames arrive at the receiver's interface simultaneously. For instance, if we assume wireless communications over the 5-node network in (2.1),  $n_1$  and  $n_4$  will not detect the presence of each other due to the limited signal transmission power. Thus, both nodes are highly vulnerable to transmission failures caused by packet collisions and we observed a considerable amount of ant lost from simulations. In computer networking, such issues are dealt with by medium access control (MAC) protocols, a set of rules that essentially allow multiple independent devices coordinate transmissions and receptions of data packets over shared spectrum so as to mitigate collision.

In the next chapter, we will present case studies for understanding the operational details of wireless MAC protocol MACA (Multiple Access with Collision Avoidance) [30], one of the pioneering schemes designed to handle the hidden terminal problem on shared medium. In particular, MACA introduces a distributed virtual sensing mechanism that has been recognized as a critical part of the modern WLANs standards [3]. Based on the studies, we take a modest step by modeling and analyzing the integrated behavior of Ant-based routing with medium access control of MACA on a simple wireless topology.

## Chapter 3

### ANALYSIS OF ANT-BASED ROUTING WITH WIRELESS MEDIUM ACCESS CONTROL PROTOCOL MACA

As a first step to rigorously characterize the behaviors of ant-based routing algorithm in wireless local area networks, in this chapter we start by investigating the delicate maneuvers of a practical wireless MAC protocol MACA in coordinating independent network traffic over shared spectrum. In particular, a Markov chain analysis of the MAC protocol is presented to reproduce the timeline of channel behaviors and network performance in representative settings. We incorporate the findings into the previous analytic framework of BARP and solve for the equilibrium distribution of ant packets and pheromone level over a simple wireless topology. The results are validated via QualNet simulation using realistic protocol and channel conditions. Finally, we point out the difficulties of model extensions into general wireless networks and adopt an alternative regression approach to identify the problems.

#### 3.1 Review of Basic Wireless MAC Protocols

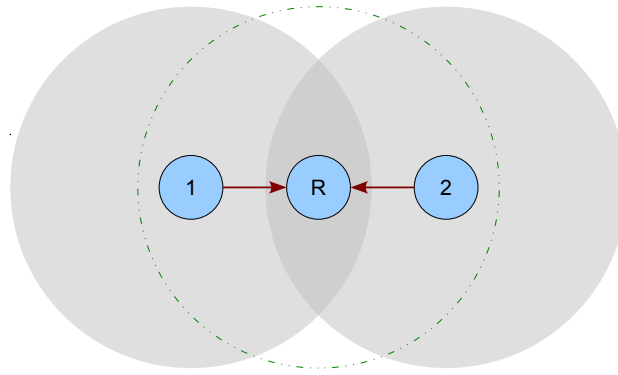
In this section, we will review some fundamental MAC protocols available for wireless LANs. The literature on these protocols and their many variants is huge and is still expanding. We therefore do not intend to provide a detailed account on every aspect of these protocols and contributions to their development. Instead we provide a general background and some key features in which we are particularly interested for further study and in depth analysis.

In wireless computer networks, an effective channel access method allows multiple network devices or nodes to transmit data packets over the same physical transmission medium (*i.e.* air) and share its capacity. The simplest design is called random access. With this scheme, all network devices may transmit whenever they want without considering others' conditions. The ALOHA protocol [4], developed along the pioneering computer network system ALOHAnet in 1970s, was the forerunner of modern wireless MAC technologies that implement a contention based random access mechanism over shared medium for client transmissions without centralized controls. Based on the pure ALOHA protocol (the original one implemented in ALOHAnet), a user transmits whenever a data packet is ready to be sent irrespective of whether the channel is occupied by other users. Despite the simplicity and convenience of this design, random access leads to packet collisions when two or more devices decide to transmit within the same transmission period. The resulting mingling of signals will corrupt both data packets thus packet collisions cause the loss of information and waste channel bandwidth. ALOHA requires that all failed packets be retransmitted at a later time. The moment is randomly chosen following certain prior selected probability distribution in order to shrink the possibility of future interruptions. One implement was slotted version of ALOHA protocol where time is divided into uniform time intervals. In this scheme, each device only transmits at the beginning of the next time slot. The collision problem is relieved because there are no overlapping transmissions compared to pure ALOHA. Any two packets either collide completely or not at all. The performance of both pure and slotted ALOHA protocol has been rigorously modeled and analyzed by assuming independent Poisson traffic source with constant packet generation rate [4, 47].

Successful implementations of the ALOHA system led to the development of the Carrier Sense Multiple Access (CSMA) protocol. Within the same vein, CSMA protocol is especially reinforced to protect the payloads from being destroyed by packet collisions. In its essence, CSMA requires all stations monitor the channel first before the initiation of every transmissions (including the retransmissions). Only when the

channel is sensed idle will a station be permitted to transmit. The Carrier Sensing (CS), known as CCA (Clear Channel Assessment), is accomplished through physical measurement of the energy level received on the station's radio interface. If that value is above a pre-selected threshold, the sensing node determines that another node is currently transmitting, i.e. the channel is occupied. The CSMA protocol operates in two types. The first one is called  $p$ -persistent. Under this mode, a sender transmits the packet with probability  $p$  if the channel is determined idle. Otherwise, the sender waits persistently until the channel goes idle, then attempts to send again with probability  $p$ . If the sender chooses not to transmit (with probability  $1 - p$ ), then it repeats the described procedures at the next available time slot. As a special case when  $p = 1$ , nodes will aggressively transmit whenever the channel becomes available. The 1-persistent mode has been widely implemented in wired network system such as Ethernet which uses CSMA/CD (with Collision Detection) protocol [1]. The second type of CSMA protocol aims to limit the interference among packets by always rescheduling transmissions after a randomly distributed back-off (waiting) time when a busy channel is detected. Therefore this is known as a non-persistent algorithm, which has been shown to have overall superior performance compared to 1-persistent (or  $p$ -persistent if  $p$  is not carefully determined) CSMA in terms of the network throughput, an important measure that represents the rate of all successful transmissions over the channel [32].

Although CSMA protocols greatly reduce the chance of signal interference and offer large advantages as compared to ALOHA protocol [32], the physical CS mechanism has not completely eliminated the possibility of collisions. For instance, two stations may decide to transmit at the exact same time so neither will find the channel is busy prior to their transmissions. Moreover, despite the sensing efforts, in a general wireless setting collisions can still be unconfined at the receiver in the presence of two (or more) concurrent transmitters who can not detect the traffic from each other. In other words, a lack of a carrier does not necessarily mean it is always safe to transmit. The latter is referred to as the hidden terminal problem or hidden node problem. This problem is usually illustrated through a typical topology given by Figure 3.1. Due to



A Two-Sender Scenario

**Figure 3.1:** The Hidden Terminal Problem. The sensing ranges of the transmitters 1 and 2 are marked with shaded disks while that of receiver R is denoted by green circle. Both 1 and 2 are exposed to R but hidden from each other, resulting in vulnerable transmissions at  $R$ .

the effect of path attenuation in wireless communications, i.e. the reduction in power density of a radio wave as it propagates through medium, a node can only determine the channel conditions accurately within a certain range. This pathological feature of the radio communications has been shown to badly degrade the performance of CSMA in wireless LANs [32, 58].

To address the hidden terminal issues, a *virtual carrier sensing* scheme has been widely recognized and implemented to improve the original CSMA protocols. The augmented scheme, known as Carrier Sense Multiple Access with Collision Avoidance, or simply CSMA/CA, has not only been shown beneficial to WLANs in the presence of hidden terminals, but used in various wired network architectures as well. According to the virtual sensing scheme, a sender and a receiver handshake via short and expendable RTS (Request To Send)/ CTS (Clear To Send) control packets before transmitting the long and valuable data packets. Both RTS and CTS packets are transmitted with a duration field, an indicator called Network Allocation Vector (NAV), in which the

sender explicitly specifies the least amount of time required by the transmission immediately following the current packet that contains the NAV. Therefore, a neighboring node overhearing the broadcasted RTS or CTS packets addressed to other nodes will defer its own transmission long enough for the addressed communication to finish. After a successful RTS/CTS handshake, the sender can transmit its data packet without frequently incurring collisions with neighboring and hidden nodes.

The virtual carrier sensing algorithm using RTS/CTS handshakes was first proposed by the MAC protocol Multiple Access with Collision Avoidance (MACA) [30] on single wireless channel. MACA was inspired from the collision avoidance method that was used by the legacy Apple Localtalk network system in which a RTS / CTS dialogue was introduced. Simplified from the traditional CSMA protocols, MACA replaces the physical carrier sensing method by exclusive RTS/CTS exchanges to address the hidden terminal problem and detect collisions at the receiver. Although collisions may frequently occur between RTS packets especially without the CS step before transmitting, MACA can reduce the chance of collisions between data packets as long as RTS packets are significantly shorter than the data packets. However, data packets can still collide with RTS packets. For instance, in Figure 3.1, if 2 fails to overhear the CTS packet that  $R$  responds to its sender 1 (for some reasons that will be discussed later), then the RTS packet from 2 and a data packet from 1 may collide at  $R$ . To study and rigorously characterize the complex behaviors of medium access control on wireless LANs, we first explore the operational details of the MACA protocol. The objective is to understand how MACA manages packet collisions.

The remaining chapter is organized as follows. In Section 3.2, we propose a Markov chain analysis to evaluate MACA performance for a 2-sender network, then discuss the generalization for 3-sender case. In Section 3.3, we analyze the cross-layer interactions between stochastic routing using BARP with medium access control under MACA. In Section 3.4, we implement a regression approach to evaluate MACA performance in wireless multi-hop local area networks. Section 3.5 concludes the efforts and limitations.

## 3.2 Modeling and Case Studies for MACA Protocol

In this section, we perform a case study to understand the complex interactions in the exchange of RTS/CTS packet pairs together with data transmissions. Specifically we model the behavior of MACA protocol in both two-sender and three-sender scenarios with hidden terminals. The model is validated through comparisons between numerical calculations using Matlab and realistic network simulations using QualNet.

### 3.2.1 Two-Sender Scenarios

We start by analyzing the operations of MACA protocol under the classic two-sender topology shown by Figure 3.1 with following assumptions: (i) Senders are positioned symmetrically about the receiver and hidden from each other. (ii) Senders have identical configurations and are synchronized at the beginning. i.e. they intend to transmit at the exact same time. (iii) RTS and CTS packets have the same size and are both significantly shorter than DATA packets. (iv) The channel is in perfect condition without path loss and packet loss during the propagation.

Figure 3.2 illustrates the MACA timeline associated with a typical communication between sender 1 and receiver R. Before a data packet can be transmitted, a successful RTS/CTS handshake between sender and receiver is required:

- 1 *Sender 1 randomly chooses a time  $t_1$  (e.g.  $t_1 = \lambda_1$  in the timeline) between 0 and CW to send a RTS packet  $RTS_1$  by broadcasting.*
- 2 *After a delay of  $\sigma + T_D$ , receiver obtains  $RTS_1$ , then replies with a CTS packet  $CTS_1$  by broadcasting immediately.*
- 3 *When sender 1 receives  $CTS_1$  after another delay of  $\sigma + T_D$ , it begins to transmit data packet by broadcasting immediately.*
- 4 *When sender 2 overhears  $CTS_1$  at the moment  $t_1 + 2T_D + 2\sigma$  (e.g.  $\lambda_3$  in the timeline), it freezes and sets its NAV counter equal to the transmission delay of  $DATA_1$  immediately.*

If the RTS/CTS handshake fails, another RTS will be scheduled by the sender at a later time. Specifically, the retransmission of an RTS follows a random back-off scheme where the moment of retry is uniformly chosen between 0 and the back-off

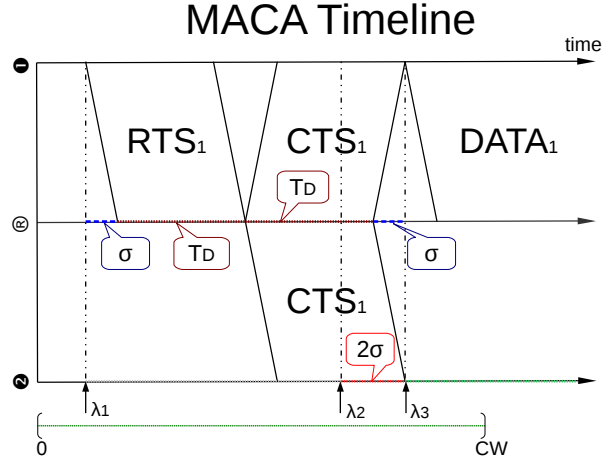


**Figure 3.2:**  $\sigma$  denotes the propagation delay (time);  $T_D$  denotes the transmission delay of RTS or CTS packets;  $\lambda_{1,2,3}$  are three critical moments;  $CW$  denotes the initial back-off contention window size.

*contention window (CW)* size. We require that the back-off window size doubles for each RTS retry. When a RTS retry limit is reached, the data packet will be dropped.

Based on the results of QualNet simulation using realistic communication models, we make three key observations:

- #1. If one terminal is receiving a packet while another packet arrives, then both packets will be corrupted.
- #2. If one terminal is sending a packet while another packet arrives, then both packets will be dropped (inward packet is ignored, the signal of outward packet is weakened).
- #3. In the PHY layer, sending has a higher priority than receiving [21].

Here the first observation corresponds to the packet collision. The PHY (physical) layer in observation #3 is defined in the seven-layer OSI framework of computer networking. It specifies the methods of transmitting raw bits over a real link.

Thus, given the second sender also randomly choosing a time  $t_2$  (assume  $t_2 > t_1$  here) between 0 and  $CW$  to send a RTS packet  $RTS_2$ , we can conclude three possibilities:

- 1) If  $t_2 < \lambda_2 = \lambda_1 + 2T_D$ ,  $RTS_2$  either collides with  $RTS_1$ , according to observation #1, or interrupts the sending of  $CTS_1$ , based on the observation #2. No data packet will be sent, and both senders will resend RTS packet following the rules of the back-off mechanism (back-off window size doubles) after a constant period called RTS timeout.
- 2) If  $\lambda_2 < t_2 < \lambda_2 + 2\sigma = \lambda_3$ ,  $CTS_1$  will successfully arrive at sender 1 but not at sender 2 according to the observation #3. Sender 1 then sends the data packet which will collide with  $RTS_2$  provided the size of the data packet  $\gg$  the size of RTS packet.
- 3) If  $t_2 > \lambda_3$ , both senders will successfully receive  $CTS_1$ . Then sender 2 will become quiet and sender 1 successfully sends the data packet.

For the case of  $t_2 < t_1$ , by the symmetry assumption, the analysis is the same. In general, we define the time that the  $j$ -th sender sends RTS packets with back-off window size  $2^{n-1}CW$  as

$$T_j^{(n)} = (n-1)\tilde{T} + \sum_{k=1}^n t_j^{(k)}, \quad T_j^{(0)} = 0 \quad (3.2.1.1)$$

where  $\tilde{T}$  is the length of RTS timeout, and  $\forall j$ ,

$$\begin{cases} t_j^{(0)} = 0 \\ t_j^{(n)} \sim U(0, 2^{n-1}CW) \quad i.i.d \quad \forall n > 0 \end{cases}$$

From the analysis above, we develop a stochastic model for the two-senders system, of which the behaviors at time  $t$  are characterized with the joint statuses of the two senders. Figure 3.3 demonstrates the directed diagram of the states. In particular, the transition possibilities are given by the aggregating behaviors of the RTS-competing

process. All the other transition probabilities unlabeled in the figure are equal to 1 because there are only two competitors in this scenario such that whoever first finishes the data transmission, the other always succeed.

$$P1, n = P\left(T_2^{(n)} - T_1^{(n)} > 2(T_D + \sigma) \middle| |T_2^{(m)} - T_1^{(m)}| < 2T_D, m = 0, 1, 2, \dots, n-1\right) \quad (3.2.1.2)$$

$$P2, n = P\left(T_2^{(n)} - T_1^{(n)} < -2(T_D + \sigma) \middle| |T_2^{(m)} - T_1^{(m)}| < 2T_D, m = 0, 1, 2, \dots, n-1\right) \quad (3.2.1.3)$$

$$P3, n = P\left(|T_2^{(n)} - T_1^{(n)}| < 2T_D \middle| |T_2^{(m)} - T_1^{(m)}| < 2T_D, m = 0, 1, 2, \dots, n-1\right) \quad (3.2.1.4)$$

$$P4, n = P\left(-2(T_D + \sigma) < T_2^{(n)} - T_1^{(n)} < -2T_D \middle| |T_2^{(m)} - T_1^{(m)}| < 2T_D, m = 0, 1, 2, \dots, n-1\right) \quad (3.2.1.5)$$

$$P5, n = P\left(2T_D < T_2^{(n)} - T_1^{(n)} < 2(T_D + \sigma) \middle| |T_2^{(m)} - T_1^{(m)}| < 2T_D, m = 0, 1, 2, \dots, n-1\right) \quad (3.2.1.6)$$

### 3.2.1.1 Model Validation

If we set the RTS retransmission limit as  $L$ , then we can verify the two-sender model by evaluating the success, failure and drop rates of data packets for any sender and comparing the results with QualNet simulations. In particular, we only focus on the results of sender 1. Let  $P_D$  denote the probability that sender 1 drops the data packet,  $P_S$  be the chance that sender 1 succeed in delivering the data packet and  $P_F$  represent the probability that sender 1 fails to send the data packet due to collision,

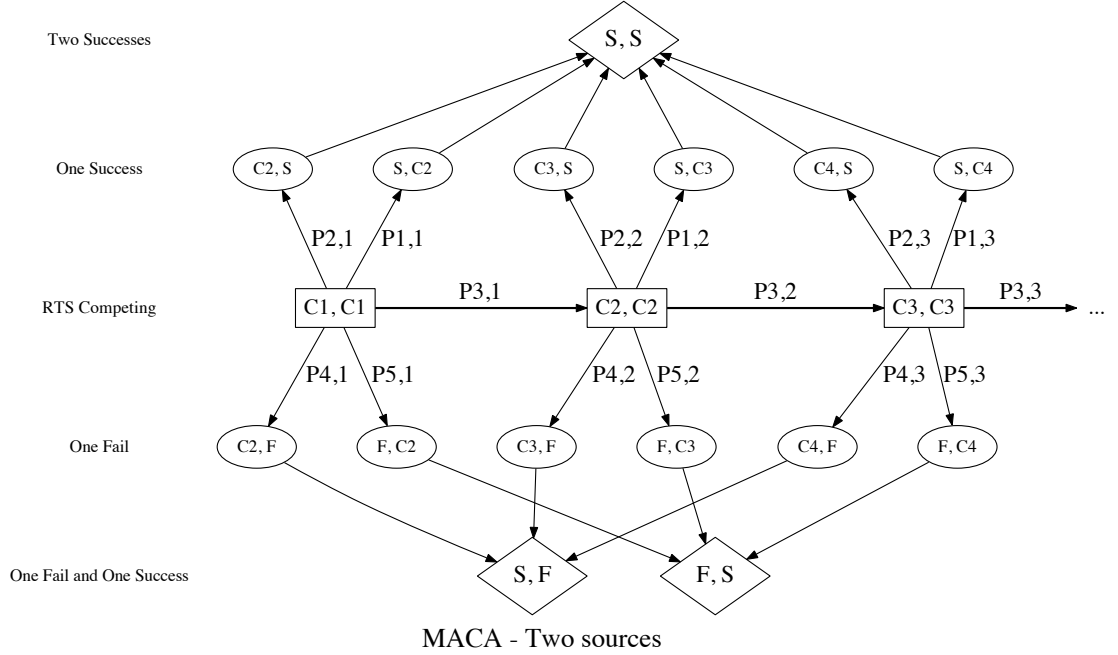


**Figure 3.3:** Directed diagram for the Markov chain:  $S$  represents the successful sending of data packet.  $F$  corresponds to data packet being corrupted, and  $C_i$ 's,  $i = 1, 2, 3, \dots$  mean sender is competing with others (if any) by randomly sending RTS packet within period of back-off window size  $2^{i-1}CW$ . The states,  $(s_1(t), s_2(t))$ , where  $s_1, s_2 \in \{S, F, C_1, C_2, C_3, \dots\}$ , show the status of (sender1, sender2) at time  $t$ .

based on the diagram 3.3 and define  $P_{3,0} := 1$ , we conclude

$$P_D = \prod_{i=0}^{L-1} (P_{3,i})(P_{4,L}) + \prod_{i=1}^L (P_{3,i}) \quad (3.2.1.7)$$

$$P_S = \sum_{n=1}^L \prod_{i < n} (P_{3,i})((P_{1,n}) + (P_{2,n})) + \sum_{n=1}^{L-1} \prod_{i < n} (P_{3,i})(P_{4,n}) \quad (3.2.1.8)$$

$$P_F = \sum_{n=1}^L \prod_{i < n} (P_{3,i})(P_{5,n}) \quad (3.2.1.9)$$

Notice that sender 1 will drop the data packet in the case of sender 2 encountering a collision with RTS packet from sender 1 associated with the probability  $(P_{4,L})$ , as the RTS retransmission limit  $L$  has been reached.

The transition probabilities (3.2.1.2) - (3.2.1.6) are calculated in Mathematica using the parameters shown in Table 3.1. The results are plugged into the equations

$T_D$	290.583
$CW$	600
$\sigma$	3.75

**Table 3.1:** Parameters used in verification. The values are in microsecond ( $10^{-6}$ s).

(3.2.1.7) - (3.2.1.9). On the other hand, for the QualNet trials, both senders compete in separated and synchronized sessions and in total each forwards one million data packets. In the end, we summarize the frequency of the data packets delivered, collided or dropped for sender 1. We repeat the experiments 3 times using distinct retransmission threshold for RTS packets. e.g.  $L = 1, 2, 3$ . The results are given in Table 3.2 where the relative error between two probabilities  $p$  and  $q$  is computed by  $\frac{|p-q|}{|p|}$ .

**Table 3.2:** Comparisons of drop, success and fail rate of data packets between model and simulations.

RTS limit 1	$P_D$	$P_S$	$P_F$
Model	0.999329	0.000357	0.000314
QualNet	0.999347	0.000322	0.000331
Relative error	0.00002	0.097	0.052
RTS limit 2	$P_D$	$P_S$	$P_F$
Model	0.695105	0.301066	0.003515
QualNet	0.695335	0.300747	0.003918
Relative error	0.00032	0.001	0.114
RTS limit 3	$P_D$	$P_S$	$P_F$
Model	0.287799	0.707052	0.005150
QualNet	0.287638	0.706752	0.005611
Relative error	0.00056	0.00042	0.089

### 3.2.2 Three-sender Scenario with MACA

We also consider a generalization of the mathematical model for MACA protocol to a scenario with three senders and one receiver, illustrated by Figure 3.4. We follow a similar set of assumptions as described above. Again a form of 3-tuple

$$(s_1(t), s_2(t), s_3(t)), \quad s_1, s_2, s_3 \in \{S, F, N, C_1, C_2, C_3, \dots\}$$

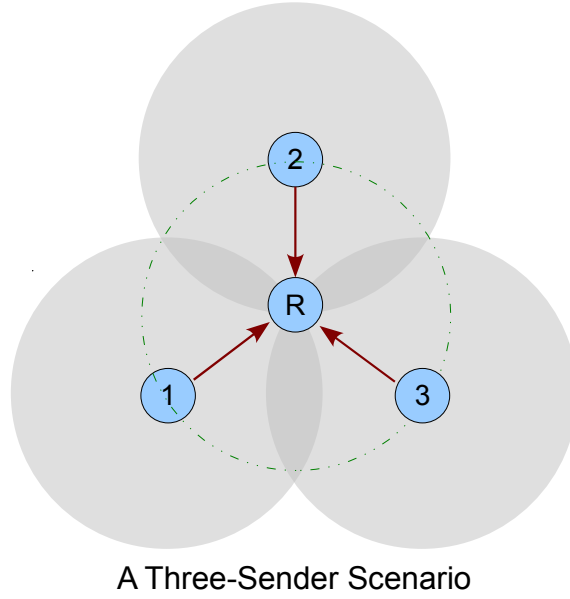


**Figure 3.4:** The three-sender scenario with hidden terminals

is used to represent the states of (sender1, sender2, sender3) at time  $t$ . Here a new status  $N$  is added, which represents that a sender receives CTS packet destined for another node so that it freezes for a specific amount of time governed by NAV.

The Markov process of the system with three senders is much more complicated. In fact, the joint state space of three senders tends to expand exponentially. Starting from any state

$$(C_{n_1}, C_{n_2}, C_{n_3}), \quad \forall n_1, n_2, n_3 = 1, 2, 3, \dots$$

in one transition, there are eight new possible states if we focus on node 1. The descriptions are presented below. Notice that the associated conditions for transmission time of RTS are given regardless of the state transition history.

1.  $(C_{n_1+1}, C_{n_2+1}, C_{n_3+1})$ : No data packets will be sent due to the collision of RTS

packets, or failing to receive a CTS. The corresponding RTS transmission moments satisfy,

$$0 < T_{\alpha(2)}^{(n_{\alpha(2)})} - T_{\alpha(1)}^{(n_{\alpha(1)})} < 2T_D, \quad 0 < T_{\alpha(3)}^{(n_{\alpha(3)})} - T_{\alpha(2)}^{(n_{\alpha(2)})} < T_D, \quad \forall \alpha \in S_3. \quad (3.2.2.1)$$

2.  $(C_{n_1}, C_{n_2+1}, C_{n_3+1})$ : Senders 2 and 3 send RTS packets which collide while sender 1 is still backing off. The corresponding RTS transmission moments satisfy,

$$0 < T_{\alpha'(2)}^{(n_{\alpha'(2)})} - T_{\alpha'(3)}^{(n_{\alpha'(3)})} < 2T_D, \quad T_1^{(n_1)} - T_{\alpha'(2)}^{(n_{\alpha'(2)})} > T_D, \quad \forall \alpha' \in S_3 \text{ s.t. } \alpha'(1) \equiv 1. \quad (3.2.2.2)$$

3.  $(C_{n_1+1}, C_{n_2}, C_{n_3+1})$ : Senders 1 and 3 send RTS packets which collide while sender 2 is still backing off. The corresponding RTS transmission moments satisfy,

$$0 < T_{\alpha''(1)}^{(n_{\alpha''(1)})} - T_{\alpha''(3)}^{(n_{\alpha''(3)})} < 2T_D, \quad T_2^{(n_2)} - T_{\alpha''(1)}^{(n_{\alpha''(1)})} > T_D, \quad \forall \alpha'' \in S_3 \text{ s.t. } \alpha''(2) \equiv 2 \quad (3.2.2.3)$$

4.  $(C_{n_1+1}, C_{n_2+1}, C_{n_3})$ : Senders 1 and 2 send RTS packets which collide while sender 3 is still backing off. The corresponding RTS transmission moments satisfy,

$$0 < T_{\alpha'''(1)}^{(n_{\alpha'''(1)})} - T_{\alpha'''(2)}^{(n_{\alpha'''(2)})} < 2T_D, \quad T_3^{(n_3)} - T_{\alpha'''(1)}^{(n_{\alpha'''(1)})} > T_D, \quad \forall \alpha''' \in S_3 \text{ s.t. } \alpha'''(3) \equiv 3 \quad (3.2.2.4)$$

5.  $(S, N, N)$ : Sender 1 delivers the packet successfully while the other two freeze by NAV. The corresponding RTS transmission moments satisfy,

$$T_2^{(n_2)} - T_1^{(n_1)} > 2T_D + 2\sigma, \quad T_3^{(n_3)} - T_1^{(n_1)} > 2T_D + 2\sigma. \quad (3.2.2.5)$$

6.  $(F, C_{n_2+1}, N)$ : The RTS packet from sender 2 collides with the data packet from sender 1 and sender 3 freezes by NAV. The corresponding RTS transmission moments satisfy,

$$2T_D < T_2^{(n_2)} - T_1^{(n_1)} < 2T_D + 2\sigma, \quad T_3^{(n_3)} - T_1^{(n_1)} > 2T_D + 2\sigma. \quad (3.2.2.6)$$

7.  $(F, N, C_{n_3+1})$ : The RTS packet from sender 3 collides with the data packet from sender 1 and sender 2 freezes by NAV. The corresponding RTS transmission moments satisfy,

$$T_2^{(n_2)} - T_1^{(n_1)} > 2T_D + 2\sigma, \quad 2T_D < T_3^{(n_3)} - T_1^{(n_1)} < 2T_D + 2\sigma. \quad (3.2.2.7)$$

8.  $(F, C_{n_2+1}, C_{n_3+1})$ : Both RTS packets from sender 2 and 3 collide with the data packet from sender 1. The corresponding RTS transmission moments satisfy,

$$2T_D < T_2^{(n_2)} - T_1^{(n_1)} < 2T_D + 2\sigma, \quad 2T_D < T_3^{(n_3)} - T_1^{(n_1)} < 2T_D + 2\sigma. \quad (3.2.2.8)$$

Here  $S_3$  represents the set of all permutations of  $\{1, 2, 3\}$ , RTS transmission time is defined in (3.2.1.1) and the constraints, (3.2.2.1) - (3.2.2.8), are conditioned on the history of state transitions. In particular, we conclude that  $\forall i_x \in \{1, 2, \dots, n_x - 1\}, x \in \{1, 2, 3\}$ , there exists  $i_y \in \{1, 2, \dots, n_y - 1\}, y \in \{1, 2, 3\} \setminus x$ , such that

$$|T_x^{(i_x)} - T_y^{(i_y)}| < 2T_D \quad (3.2.2.9)$$

(3.2.2.9) ensures the existence of a path which links the current state  $(C_{n_1}, C_{n_2}, C_{n_3})$  and the initiate state  $(C_1, C_1, C_1)$ .

Notice that once sender 1 gets to the states  $S$  or  $F$ , we go back to the two-sender case. Although it is unlikely that we will find a regular repeating structure like Figure 3.3 with a linear growth state space as in the two-sender case, it is still possible to find a truncated approximation of the complete state space with recurrent configuration given some proper settings of network parameters. More specifically, the truncated chain should satisfy the following property:

$$|n_x - n_y| \leq 1, \quad \forall x, y \in \{1, 2, 3\}$$

For example, we can assume that the branching term  $(C_{n_1}, C_{n_2+1}, C_{n_3+1})$  will always transit to  $(S, N, N)$  as long as the RTS timeout,  $\tilde{T}$ , is sufficiently longer than the  $n_1$ -th back-off window size at node 1. In this case, node 1 will successfully occupy the channel before node 2 and node 3 resume.

Under this assumption, given current backoff window size as  $2^{n-1}CW$ , let  $P_{cc}^{(n)}$  be the probabilities that all three RTS packets collide, and  $P_{ci}^{(n)}$  represents that two RTS packets collide while the last one from sender  $i$  has not been sent yet.  $P_{si}^{(n)}$  represents the chance that sender  $i$  successfully delivers the data packet and  $P_{fi}^{(n)}$  represents the probability that data packet from sender  $i$  is corrupted, we have,

$$P_{cc}^{(n)} = \sum_{\alpha \in S_3} P\left(0 < T_{\alpha(2)}^{(n)} - T_{\alpha(1)}^{(n)} < 2T_D, \quad 0 < T_{\alpha(3)}^{(n)} - T_{\alpha(2)}^{(n)} < T_D \mid \right. \\ \left. 0 < T_{\alpha(2)}^{(m)} - T_{\alpha(1)}^{(m)} < 2T_D, \quad 0 < T_{\alpha(3)}^{(m)} - T_{\alpha(2)}^{(m)} < T_D, \forall \alpha \in S_3, m = 0, 1, 2, \dots, n-1\right). \quad (3.2.2.10)$$

$$P_{c1}^{(n)} = \sum_{\substack{\alpha' \in S_3 \\ \alpha'(1)=1}} P\left(0 < T_{\alpha'(3)}^{(n)} - T_{\alpha'(2)}^{(n)} < 2T_D, \quad T_{\alpha'(3)}^{(n)} - T_1^{(n)} > T_D \mid \right. \\ \left. 0 < T_{\alpha(2)}^{(m)} - T_{\alpha(1)}^{(m)} < 2T_D, \quad 0 < T_{\alpha(3)}^{(m)} - T_{\alpha(2)}^{(m)} < T_D, \forall \alpha \in S_3, m = 0, 1, 2, \dots, n-1\right). \quad (3.2.2.11)$$

$$P_{s1}^{(n)} = P\left(T_2^{(n)} - T_1^{(n)} > 2T_D + 2\sigma, \quad T_3^{(n)} - T_1^{(n)} > 2T_D + 2\sigma \mid \right. \\ \left. 0 < T_{\alpha(2)}^{(m)} - T_{\alpha(1)}^{(m)} < 2T_D, \quad 0 < T_{\alpha(3)}^{(m)} - T_{\alpha(2)}^{(m)} < T_D, \forall \alpha \in S_3, m = 0, 1, 2, \dots, n-1\right). \quad (3.2.2.12)$$

$$P_{f1}^{(n)} = P\left(2T_D < T_2^{(n)} - T_1^{(n)} < 2T_D + 2\sigma \quad \text{OR} \quad 2T_D < T_3^{(n)} - T_1^{(n)} < 2T_D + 2\sigma \mid \right. \\ \left. 0 < T_{\alpha(2)}^{(m)} - T_{\alpha(1)}^{(m)} < 2T_D, \quad 0 < T_{\alpha(3)}^{(m)} - T_{\alpha(2)}^{(m)} < T_D, \forall \alpha \in S_3, m = 0, 1, 2, \dots, n-1\right). \quad (3.2.2.13)$$

The representations of  $P_{c2}^{(n)}, P_{s2}^{(n)}, P_{f2}^{(n)}, P_{c3}^{(n)}, P_{s3}^{(n)}, P_{f3}^{(n)}$  are similarly defined. We point out that the direct computing of probabilities (3.2.2.10) - (3.2.2.13) becomes increasingly hard as  $n$  goes up. In fact, a crude effort with Mathematica fails to provide effective results when  $n = 2$ .

### 3.2.2.1 Approximating Transition Probabilities with Monte Carlo Simulation

In this section, we implement a Monte Carlo method to approximate the transition probabilities. The detailed description for the 3-sender scenario with focus on node 1 is given by Algorithm 2. The same method applied for all senders. To check the accuracy of this algorithm, we first compute the relative error by comparing the simulated data with the theoretical value achieved through Mathematica when RTS retry limit  $L = 1$ . The parameters used and the results are shown by Table 3.3 and 3.4 respectively. The realistic simulation of QualNet with  $L = 1$  also validate the ef-

**Table 3.3:** Parameters used in Monte Carlo Simulations

$T_D$	293
$CW$	600
$\sigma$	1.333
M	$10^6$

**Table 3.4:** Evidence for the effectiveness of Monte Carlo Method

RTS limit 1	$P_{cc}$	$P_{c1}$	$P_{s1}$	$P_{f1}$
Theory	0.866032	0.044652	$2.24646 * 10^{-6}$	$1.98811 * 10^{-6}$
Monte Carlo	0.866382	0.044535	$1.6 * 10^{-6}$	$1.7 * 10^{-6}$
Relative error	$4.0414^{-4}$	0.0026	0.2857	0.1414
QualNet	0.866765	0.044623	$2 * 10^{-6}$	$2.7 * 10^{-6}$

forts. Note that the three-sender model accurately captures the behaviors of the system transitions on the first phase of RTS competition  $(C_1, C_1, C_1)$ . For the second phase of RTS competition and above, Mathematica fails to work, however the Monte Carlo method still provide us reasonable results. In particular, since all the transmitters are symmetrically positioned and independent, the probabilities  $P_{ci}^{(n)}$ ,  $P_{si}^{(n)}$ ,  $P_{fi}^{(n)}$  for each sender should be the same in theory. This is confirmed by the simulation solutions summarized in Table 3.5 with  $L = 2$ .

**Input:** A matrix  $\mathcal{T}$  of size  $M \times K \times N$ . Here  $M$  is the number of trials,  $K$  is the number of sender ( $K=3$ ), and  $N$  is the number of times RTS packets have been resent.

**Output:**  $P_{cc}^{(N)}, P_{c1}^{(N)}, P_{s1}^{(N)}, P_{f1}^{(N)}$ .

1 Generate matrix  $\mathcal{T} = [\tau_{mkn}]$ , whose elements are given by  $\sum_{i=1}^n t_k^{(i)}(m)$ , where

$$t_k^{(i)}(m) \sim U(0, 2^{i-1}CW) \text{ i.i.d}$$

2 Initialize the following counters to 0.

$n_{valid}$  : Number of trials that are valid – satisfying (3.2.2.1) for all  $n \leq N - 1$ .

$n_{cc}$  : Number of valid trials that satisfy (3.2.2.1) for  $n = N$ .

$n_{c1}$  : Number of valid trials that satisfy (3.2.2.2) for  $n = N$ .

$n_{s1}$  : Number of valid trials that satisfy (3.2.2.5) for  $n = N$ .

$n_{f1}$  : Number of valid trials that satisfy (3.2.2.6), (3.2.2.7) or (3.2.2.8) for  $n = N$ .

3 **for**  $m = 1$  **to**  $M$  **do**

4     **for**  $n = 0$  **to**  $N - 1$  **do**

5         **if**  $\tau_{m1n}, \tau_{m2n}, \tau_{m3n}$  do not satisfy (3.2.2.1) **then**

6             **goto** step 3

7         **end**

8     **end**

9      $n_{valid} = n_{valid} + 1$ ;

10    **if**  $\tau_{m1N}, \tau_{m2N}, \tau_{m3N}$  satisfy (3.2.2.1) **then**

11         $n_{cc} = n_{cc} + 1$ ;

12    **else if**  $\tau_{m1N}, \tau_{m2N}, \tau_{m3N}$  satisfy (3.2.2.2) **then**

13         $n_{c1} = n_{c1} + 1$ ;

14    **else if**  $\tau_{m1N}, \tau_{m2N}, \tau_{m3N}$  satisfy (3.2.2.5) **then**

15         $n_{s1} = n_{s1} + 1$ ;

16    **else if**  $\tau_{m1N}, \tau_{m2N}, \tau_{m3N}$  satisfy (3.2.2.6), (3.2.2.7) or (3.2.2.8) **then**

17         $n_{f1} = n_{f1} + 1$ ;

18    **end**

19 **end**

20 Evaluate  $P_{cc}^{(N)} = \frac{n_{cc}}{n_{valid}}, P_{c1}^{(N)} = \frac{n_{c1}}{n_{valid}}, P_{s1}^{(N)} = \frac{n_{s1}}{n_{valid}}, P_{f1}^{(N)} = \frac{n_{f1}}{n_{valid}}$ .

**Algorithm 2:** Monte Carlo Method for approximating transition probabilities on node 1 in the three-sender scenario

**Table 3.5:** Validation of symmetry with Monte Carlo method

Monte Carlo - RTS limit 2	$P_{ci}$	$P_{si}$	$\overline{P_{fi}}$
sender 1	0.121810	0.047302	575
sender 2	0.122600	0.048001	488
sender 3	0.121802	0.047245	505

### 3.3 Modeling and Analysis of BARP with MACA

As we briefly discussed in Section 2.4.2, the modeling of ant-based routing in the context of multi-hop wireless networks is challenged by the intrinsic complexity of wireless medium access control and its cross-layer interaction. Leveraging our previous work of modeling and analyzing ant-based routing protocols on wired networks, in this section we investigate the integration of such model with the mathematical modeling framework of MACA proposed in Section 3.2.

#### 3.3.1 Modeling of BARP with Packet Loss

Our modest step of modeling and analyzing the integrated behaviors between wireless MAC and ant-based routing starts on a simple six-node topology shown in Figure 3.5. Node 1 is the source ( $s$ ), node 5 is the destination ( $d$ ), and there exist exactly two paths,  $1 \rightarrow 2 \rightarrow 3 \rightarrow 4 \rightarrow 5$  and  $1 \rightarrow 6 \rightarrow 5$ .

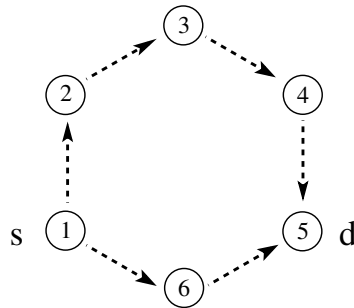


**Figure 3.5:** A simple network topology

Since the maximum number of neighbors for each node is two, we only consider the MACA model for the two-sender scenario. Also, we assume that the probability of a sender successfully sending data packet (ants) only depends on whether other nodes, in the communicating range of the receiver, have data packet (ants) to send. Thus, we define a new component,  $y_D^{(n)}$  which represents the probability of finding an ant dropped at the  $n$ -th time step in the network, to the original density vector of ants  $\mathbf{y}^{(n)}$  in BARP. One can think there exists a virtual node  $D$  that collects all the dropped ant packets. Here, ants are dropped either due to collision at the receiver or RTS retry limit reached at the sender. Also, based on the MACA modeling and the representations of  $P_D$  and  $P_F$ , (3.2.1.7) and (3.2.1.9) in Section 3.2.1, if we set the RTS retransmission limit as  $L$  times and let  $\delta$  be the probability that sender 1 fails to deliver data packet, then

$$\delta = P_F + P_D \approx \sum_{n=1}^L \prod_{i < n} (P3, i)(P5, n) + \prod_{i=1}^L (P3, i), \quad P3, 0 := 0$$

This approximation is accurate in general when  $L > 5$ . Recall the basic ant-based routing procedure described by Algorithm 1 in Section 2.2. The corresponding transition matrix in (2.2.0.2) for the forward ants now also relates to distributions of the ants over the network and becomes

$$\bar{P}^{(n)}(\beta, \mathbf{y}^{(n)}) = [p_{ji}^{(n)} * S_i(y_l^{(n)})], \quad l \in N_i \setminus j$$

where  $N_i$  represents the set of neighboring nodes of  $i$  and

$$S_i(y_l^{(n)}) = \begin{cases} 1 - \delta y_l^{(n)}, & l \neq d \\ 1, & \text{otherwise.} \end{cases}$$

By the definition of  $y_D^{(n)}$ , we get:

$$y_D^{(n)} = \sum_{i,j} y_j^{(n)} (1 - p_{ji}^{(n)} S_i(y_l^{(n)})).$$

We exclude the destination  $d$  in the definition of  $S_i(y_l^{(n)})$  because once a forward ant arrives at  $d$ , it becomes a backward ant which proceeds on a different channel thus

won't interfere with other ongoing forward transmissions. For modeling the backward ants and the existence of equilibrium solution, we add one link from  $d$  back to  $s$  and one link from  $D$  back to  $s$  both with transition probability of 1, that is,

$$y_s^{(n+1)} = y_d^{(n)} + y_D^{(n)}.$$

To complete the system, we also have the normalization condition:

$$\mathbf{y}^{(n)} \cdot \mathbf{1} + y_D^{(n)} = 1.$$

Finally, together with the equilibrium equation of pheromone (recall equation (2.2.0.7)), our stationary solutions for both pheromone and density of ants as  $n \rightarrow \infty$  should satisfy the following non-linear system:

$$\Lambda \tau_{ij} = \sum_{k=1}^{\infty} \frac{1}{k} \bar{P}_{ij}^{sd}(k) \quad (3.3.1.1)$$

$$\mathbf{y} = \bar{P}(\beta, \mathbf{y}) \mathbf{y} \quad (3.3.1.2)$$

$$y_D = \sum_{i,j} y_i (1 - p_{ji} S_i(y_l)) \quad (3.3.1.3)$$

$$y_s = y_d + y_D \quad (3.3.1.4)$$

$$1 = \mathbf{y} \cdot \mathbf{1} + y_D \quad (3.3.1.5)$$

### 3.3.2 Evaluation and Validation

We validate the developed model by comparing the Matlab numerical results of solving its steady state solution with the QualNet simulation results of executing MACA and BARP protocols with realistic wireless communications, using the six-node topology of Figure 3.5.

By using Matlab's **fsolve** subroutine, we compute the steady state solution for both the pheromone distribution ( $\tau_{ij}$  on the link from node  $i$  to node  $j$ ) and the ant drop rate ( $y_D$ ). The initial value of pheromone on each link is 1, and the starting probability density vector of ants is  $(1, 0, 0, 0, 0, 0)$ .

The QualNet simulation uses the parameters summarized in Table 3.6. The initial contention window size is set to 1200 microsecond and RTS retransmission limit

(a) QualNet parameter

Terrain size	1500×1500 m <sup>2</sup>
Number of nodes	6
Mobility	0
Radio range	up to 500 m
PHY protocol	802.11b
Bandwidth	2 Mbps
MAC protocol	MACA

(b) BARP parameter

Ant interval	2 second
Decay interval	2 second
$\beta$	0, 0.5, 2
$h_1$	1
$k_1$	0.3
$h_2$	1
$k_2$	1

**Table 3.6:** BARP parameters used in QualNet simulation

is 6. The channel model implemented is two-ray ground-reflection without fading [44]. Along the two paths (1→2→3→4→5 and 1→6→5) from the source to the destination, forward ants sent from nodes 4 and 6 will collide at the destination node 5. The source originates one forward ant every two seconds. In the simulation, after receiving an ant, a node does not forward the ant until the next integer second. For instance, if a node receives an ant at time 2.123S, it will forward it at 3.000S. By adopting this mechanism, we ensure that node 4 and node 6 compete for sending ants to the destination at exactly the same time, which corresponds to the modeled two-sender scenario. Also notice that the proposed analysis only models the behavior of forward ants. To accommodate this feature in QualNet simulation, backward ants trace its steps back to the source through a ‘wired’ interface at each hop to avoid colliding with forward ants sent wirelessly.

We perform Matlab numerical computation and QualNet simulation with different  $\beta$  values, as they affect pheromone distribution and ant drop rate. When  $\beta$  is

Path \ $\beta$	1→2→3→4→5	1→6→5
0	$\frac{0.178177}{0.137059}$	$\frac{0.356880}{0.297402}$
0.5	$\frac{0.118665}{0.117521}$	$\frac{0.476191}{0.470853}$
2	$\frac{0}{0}$	$\frac{0.714286}{0.713762}$

$\beta$	0	0.5	2
Matlab	3.68	2.92	0.00
QualNet	5.12	3.01	0.00

**Table 3.7:** At left and right, the pheromone distribution on each path and ants drop rate ( $\times 10^{-4}$ ) comparisons.

0, a path is randomly selected independently of pheromone values. As  $\beta$  increases, the path with higher pheromone concentration is favored.

Both Matlab numerical results and QualNet simulation results of pheromone distribution ( $\tau_{ij}$  on the link from node  $i$  to node  $j$ ) are presented together in Table 3.7 (left). Each entry has the format  $\frac{x}{y}$  where  $x$  denotes the Matlab result and  $y$  denotes the QualNet result. As evidenced, they show comparable values.

Table 3.7 (right) compares the Matlab and the QualNet results of ant drop rate with different  $\beta$  values. We observe that the ant drop rate decreases as  $\beta$  increases. When  $\beta = 0$ , ants choose the two paths with equal probability, which then results in more collisions at the destination and drops over the network. As  $\beta$  increases, more ants favor the shorter path 1→6→5 with higher pheromone concentration, which leads to less collisions at the destination. When  $\beta$  is 2, all the ants choose the path 1→6→5 without causing any collision at the destination. Again, we observe comparable results.

### 3.4 Evaluation of MACA for Multi-hop Wireless Networks: A Regression Study

Up to this point, our modeling and analysis efforts of the virtual carrier sensing mechanism for wireless MAC are bound to symmetric single-hop network scenarios where all sources can directly communicate with the destination. Under the symmetry assumption, the detailed timeline of RTS/CTS handshake can be understood by

concentrating on one sender only. Furthermore, with the restriction of single-hop distance, it is also reasonable to assume that the packet collision or delivery rate of a specific sender-receiver pair solely depends on the decisions of other competing nodes within the receiver’s vicinity. The generalization of the Markovian framework presented in Section 3.2, however, is very difficult, especially for the case of wireless multi-hop networks. Instead, in this section we adopt an alternative approach for the purpose of understanding the cross interaction and interference patterns among various traffic flows in a typical setup of wireless multi-hop networks. In particular, we perform a linear regression study of the packet delivery ratio on each directed link by lumping together all the MACA protocol details into the regression coefficients.

### 3.4.1 The Complications of Multi-hop Wireless Networks

In a multi-hop wireless network, e.g. ad hoc WLANs, data traffic flows from source to destination through a series of intermediate nodes whose function is to relay information from one device to another. The previous modeling assumptions on the topology features such as symmetry and one-hop range of interference are therefore insufficient if multiple data frames traverse through the network contemporaneously. For instance, consider the simple yet practical linear network topology in Figure 3.5. Two data flows such as  $1 \rightarrow 2$  and  $3 \rightarrow 4$  might compete for channel access at the same time, resulting in a problematic asymmetric configuration that leads to severe unfairness at all time scales and starvation of the upstream flow [22, 23], since the handshakes between 1 and 2 may be interrupted by the hidden node 3 but not vice versa (no contention at 4). Moreover, the collision/delivery rate of the data stream  $1 \rightarrow 2$  is not exclusively influenced by node 3 as a direct neighbor of the receiver 2, but the actions of two-hop neighbor, 4, as well. The complication is that the transmissions from node 4, either RTS or DATA packet, may collide with the CTS packet broadcasted by 2 at node 3, who then won’t be aware of the succeeding data transmission on  $1 \rightarrow 2$  and may potentially cause a collision. This problem is referred to as the *masked node problem* in the literature [45, 46, 56]. Here node 3 is called “masked” if it is receiving

two or more signals simultaneously. As a consequence, none of the ongoing transmissions, nor the new packets that arrive within the masked period, will be decoded correctly. The masked node problem has been shown to severely limit the effectiveness of the RTS/CTS mechanism in preventing performance degradation in wireless ad hoc networks [62].

### 3.4.2 A Regression Model

In this section, we describe a linear regression model with coefficients calibrated from the QualNet simulations. We intend to capture and evaluate the impacts of asymmetric configurations and masked nodes on the packet delivery ratio for any directed routes. Here, the packet delivery ratio measures the percentage of packets that has been successfully transmitted. Now, given a network topology with  $n$  directed links (*i.e.* there are potentially 12 directed routes for the topology in Figure 3.5), we assume the delivery ratio over a specific link  $m$  is determined by the following:

$$d_m(\mathbf{p}) = c_0 + c_i^{(m)} \sum_{i=1}^n p_i + \sum_{i=1}^n \sum_{j \notin N_i} c_{i,j}^{(m)} p_i p_j \quad (3.4.2.1)$$

Here  $d_m(\mathbf{p})$  is the deliver ratio of data packets on route  $m$  given  $\mathbf{p} = (p_1, p_2, \dots, p_n)$  where  $p_i$  is the probability that link  $i$  is “active” and  $N_i$  is the set of directed links that originate from the same sender as route  $i$ . The interaction terms  $p_i p_j$  are included to capture the effects of cross-inference among every pair of concurrent transmissions on the network. Notice that one sender cannot initiate two transmissions simultaneously, hence the interactions do not exist if  $j \in N_i$ .

Naturally, no packets will be delivered on route  $m$  if it has never been activated, that is,  $d_m = 0$  if  $p_m = 0$ , the model then can be reduced to,

$$\tilde{d}_m(\mathbf{p}) = \tilde{c}^{(m)} p_m + \sum_{j \notin N_m} \tilde{c}_j^{(m)} p_m p_j. \quad (3.4.2.2)$$

The coefficients will be calibrated using the QualNet simulator operated on MACA protocol. The experiments are conducted as follows. Each QualNet trial is comprised

of  $M$  (a sufficient large number) transmission sessions with a chosen  $\mathbf{p}$ : given any link  $m$ ,  $p_m$  is uniformly chosen between 0 and 1 such that

$$\sum_{j \in N_m \cup \{m\}} p_j < 1 \quad (3.4.2.3)$$

(3.4.2.3) implies that at the beginning of each transmission session, a node may decide not to send the head-of-line packet (which then will be dropped). After a trial is done, the delivery ratio,  $\tilde{d}_m(\mathbf{p})$ , are calculated by

$$d_m(\mathbf{p}) = \frac{\# \text{ of packets delivered on } m}{M} \quad (3.4.2.4)$$

Based on the data tuples  $(d_m(\mathbf{p}), \mathbf{p})$  obtained from a sufficient large number ( $\gg 2n$ ) of QualNet trials, we perform a multilinear regression of the observations in  $d_m(\mathbf{p}), \forall m$ , on the predictors in  $\mathbf{p}$  with Matlab diagnostic function.

### 3.4.3 Evaluations and Predictions

We start by solving the regression model (3.4.2.2) on a simple 5-node ring topology shown by Figure 3.6. In particular, we execute the QualNet trials 1000 times with arbitrary combinations of  $\mathbf{p}$  that satisfy the condition (3.4.2.3). The significant coefficients concluded from Matlab statistical test reveal three types of dominant 2-link interactions. Figure 3.7 demonstrated the interactions for a specific link. Since the corresponding coefficients are negative, the regression model confirms and quantifies the adverse influence of masked nodes (interaction type 1) and asymmetric hidden contentions (interaction type 3) on the performance of MACA protocol (measured by packet delivery ratio) in representative wireless multi-hop networks. In particular, the masked node problem impacts performance the most, then the hidden node problem in symmetry, and finally the unbalanced contentions.

Next, we leverage the existing linear model of the 5-node ring topology by only including the above three types of interaction. For any link  $i$ , let  $I_{ij}$  denote the link that interacts with  $i$  in the fashion of type  $j$ . Due to symmetry, all links should be

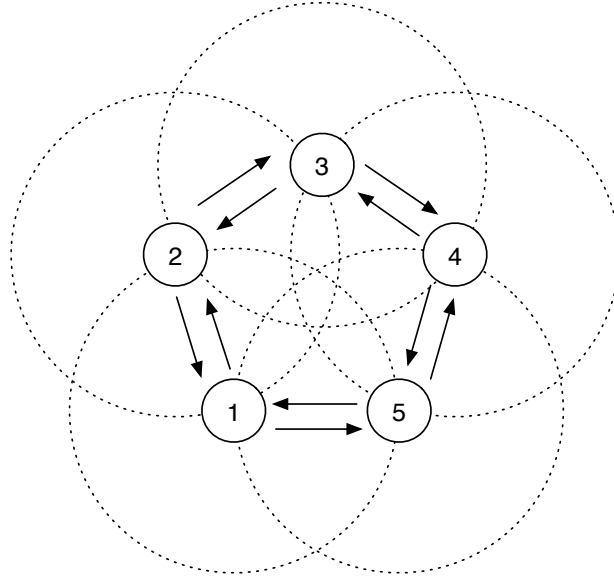


**Figure 3.6:** A simple 5 node topology. The circles indicate the transmission ranges of each nodes. There are 10 possible directed transmissions demonstrated by the arrows.

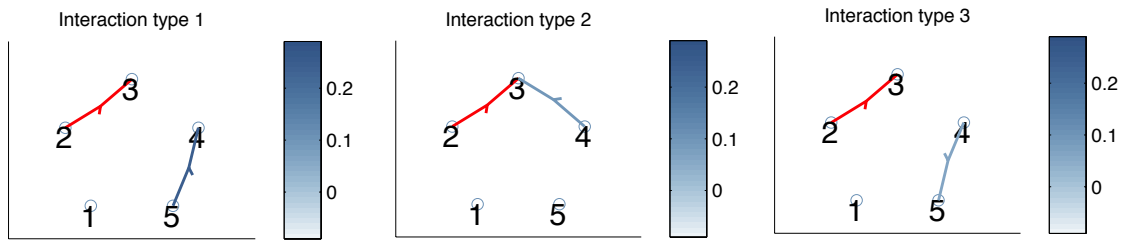


**Figure 3.7:** Three types of prime interactions observed for the target link (red): deeper blue means higher impact. Type 1 relates to the masked node problem, as the interface at node 4 will be occasionally blocked by signal from node 5; Type 2 indicates the typical symmetric hidden terminal problem; Type 3 corresponds to the asymmetric hidden node problem which causes unfairness because receiver 3 will more likely be blocked by 4, but not by 2.

identical. Thus we average the coefficients with respect to directed routes and rewrite

the reduced model for general ring topology as

$$\begin{aligned} \tilde{d}_m(\mathbf{p}) &= \left(\frac{1}{10} \sum_{i=1}^{10} \tilde{c}^{(i)}\right)p_m + \sum_{j=1}^3 \left(\frac{1}{10} \sum_{i=1}^{10} \tilde{c}_{I_{ij}}^{(i)}\right)p_m p_{I_{mj}} \\ &:= C_0 p_m + \sum_{j=1}^3 C_j p_m p_{I_{mj}} \end{aligned} \quad (3.4.3.1)$$

where  $\tilde{c}^{(i)}$  and  $\tilde{c}_{I_{ij}}^{(i)}$ ,  $\forall i$  are known from the solution of 5-node ring topology.

With the new model (3.4.3.1), we achieve good predictions of packet delivery ratio on both ring topologies with 6 nodes and 8 nodes respectively. Focus on one link, Figure 3.8 compares the numerical results  $d_{pred}$  with data  $d$  from 100 QualNet trials using randomly generated transmission probabilities  $\mathbf{p}$ . The relative error,  $\frac{\|d_{pred}-d\|_2}{\|d\|_2}$ , indicates a 4.89% deviation for 6-node scenario and 4.46% for 8-node.

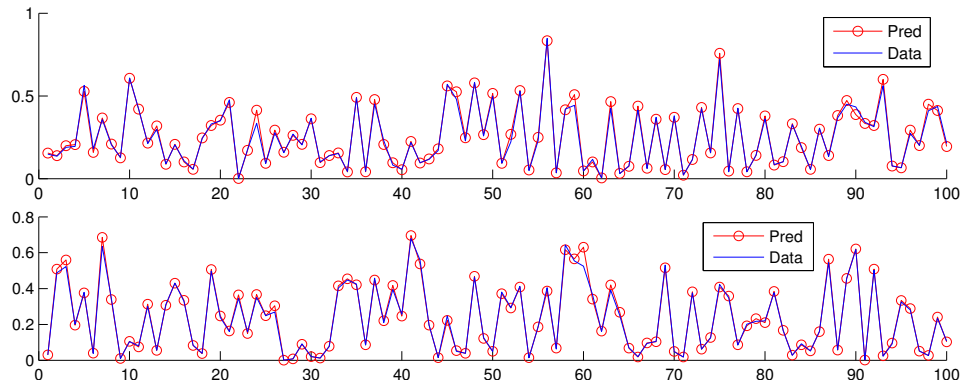


**Figure 3.8:** A comparison between model predictions and QualNet statistics on data delivery. The result on the top corresponds to 6 node ring topology and the bottom corresponds to 8 node ring topology.

### 3.5 Conclusion

In this chapter, we have briefly reviewed several pivotal wireless medium access control protocols and their primary design for managing effective packets switching over a shared radio spectrum. Specifically, we have explored the functional details of MACA, a practical MAC protocol proposed to address the hidden terminal problem, and introduced a Markovian modeling framework to characterize the behaviors of the

RTS/CTS mechanism implemented by MACA protocol on representative single-hop network scenarios. On top of the proposed mathematical analysis of MACA, we revisit the rigorous model of BARP to investigate the cross-layer interactions between wireless medium access control and ant-based routing on a simple network topology. The efforts were validated by comparable results from the numerical analysis of the equilibrium solution to the integration model and QualNet simulations with realistic implementations of wireless communication protocols. Finally, given the difficulties of generalizing the MACA analysis for wireless multi-hop networks, we have implemented an alternative approach with multilinear regression on a simple multi-hop ring topology of size 5 to reveal the problematic asymmetric configurations and the masked node problem. The reduced model using significant coefficients and corresponding interaction terms predicts packet delivery ratios accurately on larger ring topologies.

The modeling efforts and analysis using Markov processes and linear regression have been validated to correctly characterize MACA and network performance on representative infrastructure and ad hoc topologies respectively. However, both approaches are inapplicable to general network scenarios with arbitrary topology and parameters. The Markov model is likely to contain irregular transition structure and rapidly expanded state space unless certain requirements about network parameters are met. For the regression model, it will be difficult to establish an elegant experimental design for universal network scenarios similar to the ring configuration for linear topologies such that all transmissions are equivalent due to perfect symmetry. In the next chapter, we introduce a more useful Markov model with a discrete fixed time scale to generate the statistical description of node behavior and status given network parameters and topology.

## Chapter 4

### PROBABILISTICALLY MODELING OF IEEE 802.11 DISTRIBUTED COORDINATION FUNCTION

In this chapter, we will introduce and analyze a new Markov model of the IEEE 802.11 Distributed Coordination Function (DCF) for wireless LANs. The new model is derived from a detailed DCF description where transition probabilities are determined by precise estimates of collision probabilities based on network topology and node states. For steady state calculations, we approximate joint probabilities from marginal probabilities using product approximations. To assess the quality of the model, we compare detailed equilibrium node states with results from realistic simulations of wireless networks. We find very close correspondence between the model and the simulations in a variety of representative network topologies.

#### 4.1 Review of IEEE 802.11 Distributed Coordination Function (DCF)

IEEE 802.11 [3], the international standard designed for WLANs, provides a detailed MAC layer specification in which the fundamental mechanism for network devices to access the channel without any centralized control is called Distributed Coordination Function (DCF). This is a contention based random access scheme, implementing the non-persistent Carrier Sense Multiple Access with Collision Avoidance (CSMA/CA) protocols. Recall Section 3.1, carrier sense is the ability of a network device to determine if the transmission medium is idle. In general, wireless carrier sense is composed of two distinct techniques: 1) CCA (Clear Channel Assessment), which is performed through physical evaluation of the signal energy on the station's radio interface, and 2) NAV (Network Allocation Vector), a virtual carrier sense mechanism,

which is a data segment that indicates the amount of time required for the transmission immediately following the current packet that contains the NAV. The collision avoidance feature of CSMA/CA requires that a station transmits only when the channel is sensed to be idle. Unfortunately, collisions may still occur when two stations determine an idle channel at the same instant and subsequently transmit. To reduce the chance of repeated collisions of retransmitted packets, CSMA/CA protocols apply a binary exponential back-off (BEB) algorithm, by which every station selects a random back-off time before each retransmission. The name binary exponential originates from the fact that at each retransmission attempt, the longest possible back-off time (contention window size) doubles. Hence it is less likely for two stations to retransmit at the same moment. Diagram 4.1 summarizes the procedures of CSMA/CA protocols implemented by 802.11 DCF. Notice that we implement the same back off rules when

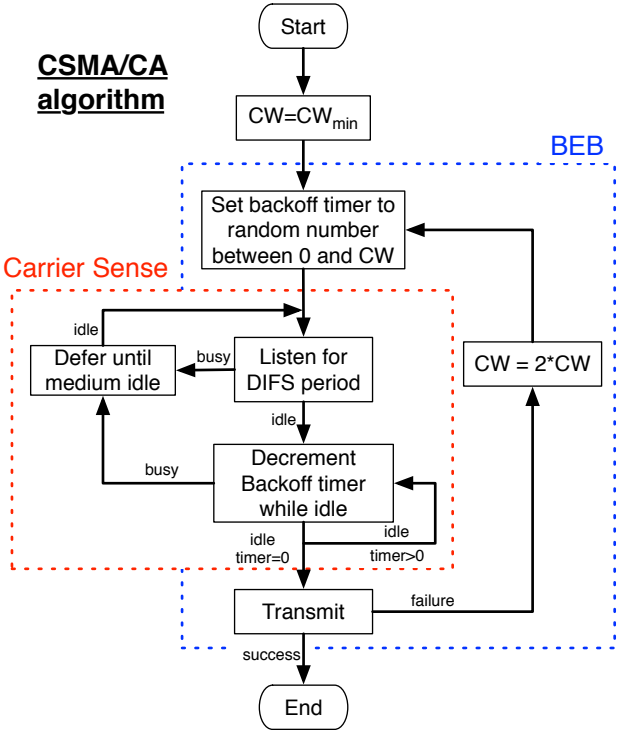


**Figure 4.1:** Non-persistent CSMA/CA algorithm implemented in 802.11 DCF

exploring MACA protocol in Section 3.2.

DCF specifies two approaches for packet transmission. The default scheme is called Basic Access mechanism. Provided the channel is sensed idle, a sender transmits the data packet after a random back-off time interval. A receiver, following the successful reception of a data packet, replies a positive acknowledgment frame. The communication is complete whenever the sender receives an acknowledgment that it anticipates. However, a packet collision may still occur at the receiver node in the presence of other concurrent transmitters who are hidden from the sender. To address this issue, DCF provides an optional technique similar to MACA protocol, known as a Request-to-Send/Clear-to-Send (RTS/CTS) mechanism. Recall that instead of broadcasting a long and valuable data packet directly, a sender/receiver pair operated in RTS/CTS mode reserves the channel by handshaking via RTS and CTS short packets. In particular, since NAV is transmitted along both RTS and CTS packets, a node in immediate vicinity when overhearing either RTS or CTS packets will defer its own transmission long enough for the addressed communication to finish. Although collisions may still occur among RTS or CTS frames, this virtual sensing scheme can diminish the chance of collisions between data packets and improve network throughput as long as RTS/CTS packets are significantly shorter than the data payloads. A complete and comprehensive description of 802.11 DCF can be found in the standard [3].

The remainder of the chapter is organized as follows. In Section 4.1.1 and 4.1.2 we examine the RTS/CTS operations of IEEE 802.11 DCF and introduce assumptions used for model derivation. In Section 4.2 we formulate and discuss the model in details. In Section 4.3 we apply the model in three representative network configurations and examine the results. Section 4.4 concludes the modeling efforts.

#### 4.1.1 Preliminaries

In a wireless local area networks, not all nodes are necessarily within the sensing range of each other, creating hidden terminals. To address this, the 802.11 DCF adopts

an RTS/CTS/DATA/ACK four way handshaking scheme, shown in Figure 4.2 and described as follows:

A sender,  $x$ , will constantly monitor the channel activity by carrier sensing.  $x$  will not attempt to transmit RTS unless the channel is sensed idle for a period of time called the Distributed InterFrame Space (DIFS). On the other hand,  $x$  accesses the channel following the BEB algorithm: at each transmission of RTS packet, the back-off counter is uniformly chosen between 0 and the current Contention Window size. Here the contention window determine the longest possible back-off time a node can choose. The back-off counter is decremented to zero unless  $x$  senses a busy channel. This will suspend the counter until the channel is sensed idle again after a DIFS. Broadcasting of RTS starts when the timer reaches zero. If the receiver  $y$  successfully captures the RTS packet, it will reply to  $x$  by broadcasting a CTS packet after a short period of time interval called the Short InterFrame Space (SIFS). The contention window will be reset to an initial value only when  $x$  correctly receives the CTS from  $y$ . However, CTS reception can be disrupted by a transmission from another node anywhere within range of  $x$ . If the CTS is not received, the contention window doubles, and  $x$  retransmits RTS according to the new contention window after waiting a specified time period of  $T_{out}$ , called RTS Timeout. Thus, at each failed RTS/CTS handshaking attempt,  $w$  is doubled up to a maximum value. Then the window size remains at that threshold until it is reset. If the maximum transmission failure limit (Retry Limit) is reached,  $x$  will discard the data packet and the window size returns to an initial value. The RTS/CTS exchange improves the chances that two nodes will be able to reserve the channel and exchange data after another SIFS in a complex environment. At the end of the successful reception of the data packet from  $x$ ,  $y$  immediately responds with a positive acknowledgement (ACK) after a SIFS. The RTS/CTS/DATA/ACK four way handshaking is complete whenever an ACK is correctly received by  $x$ . If not,  $x$  will reschedule the data packet transmission.

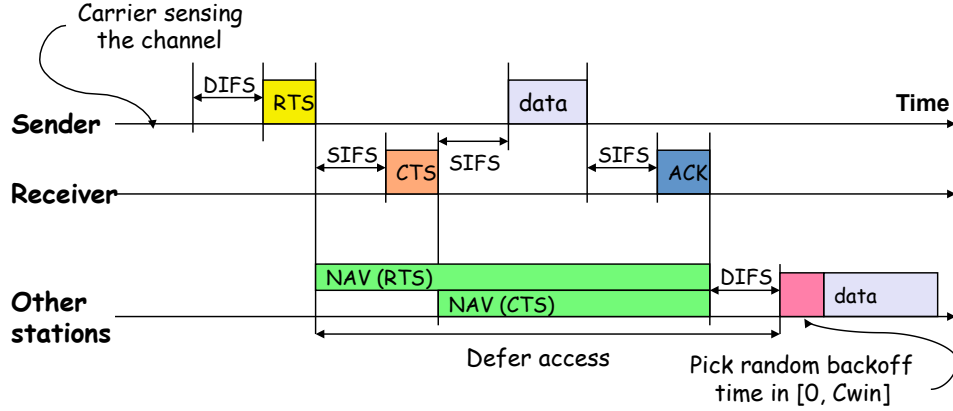


**Figure 4.2:** IEEE 802.11 DCF timeline with RTS/CTS access mechanism

#### 4.1.2 Assumptions

In this section, to systematically develop a predictive model of 802.11 DCF, we introduce the following notation and assumptions.

**Network :** We assume ideal channel conditions. This means there will be no noise, capture effect, etc., and the propagation delay is ignored. Each node operates under homogeneous configurations. All nodes have the same sensing range  $R_s$  and transmission range  $R$ , where  $R < R_s$ .

**Timescale :** Distinct from [7] and its many extensions, we adopt a constant timescale of least duration,  $\sigma$ , which is equal to the time needed at any node to detect the transmission of a packet from any other node. Because  $\sigma$  is very small, we shall assume that any node can immediately detect the transmission of a packet from any other node inside its sensing range  $R_s$ . All the time parameters in the model, i.e, transmission time of RTS, DATA, etc, are assumed to be multiples  $\sigma$ .

**MAC protocol :** For simplification of modeling, we use a modified version of IEEE 802.11 DCF implementing the RTS/CTS mechanism: DIFS is set to be one time unit and SIFS is assumed to be negligible. RTS and CTS packets have the

same size, hence their transmission delays, denoted as  $T_{RTS}$  and  $T_{CTS}$ , are equal. The protocol still adopt the BEB algorithm and the back-off counter is chosen uniformly between 1 and the contention window size. Furthermore, we set the retry limit of the RTS is the number of times that a contention window is allowed to double. Hence if the contention window achieves its threshold, we assume the data packet being sent is dropped.

**Data :** There is no retransmission of data packets. A data frame is dropped either because there is a collision at the receiver or retry limit of RTS reached. Also, we assume the acknowledgment packet (ACK) following a successful data packet transmission has fixed size (2 slots) and always succeeds. Hence the transmission time  $T_{DATA}$  includes the sending/receiving period of data plus ACK.

**Carrier sense :**

1. **CAA - Clear Channel Assessment:** Since the signals from different neighboring nodes can overlap, the busy period a node physically senses in general will not be constant and will most likely depend on the number of active neighbors.
2. **Network Allocation Vector (NAV):** It is included in both RTS and CTS packets indicating how long the channel will be occupied. In the standard, the value of NAV is  $T_{NAV_r} = T_{CTS} + T_{DATA} + T_{ACK}$  if contained in RTS, or  $T_{NAV_c} = T_{DATA} + T_{ACK}$  if contained in CTS. When a node freezes through NAV, it will ignore arriving packets until the NAV period ends. On the other hand, a node will update the freezing period of NAV with the information overheard from either a CTS or RTS packet if a new NAV value is greater than the current NAV value. For simplicity, we employ fixed-size NAV period, and assume a node freezes at the end of NAV if the channel is busy.

**CTS Timeout :** Within the period of CTS timeout,  $T_{out} = T_{CTS} + \sigma$ , any incoming packets arrived from the physical medium, valid or not, will be ignored. At the

end of CTS timeout, we assume a node freezes if the channel is occupied, and resumes back-off/idle if otherwise.

## 4.2 Modeling the Distributed Coordination Function

In a single-hop network (*i.e.* a fully connected graph), every node can sense each other and consequently experiences the same level of contention. However, in a WLAN, the competition among stations for channel access can be biased: a station with more nodes hidden from it may back off longer or encounter more packet collisions than the others which have fewer undetectable contenders. As a result, the performance of the DCF will vary for each node in the network.

### 4.2.1 Modeling of Node States

We model each node  $x$  in the network as a multi-dimensional stochastic process, denoted by

$$\mathcal{H}_x(t) := (s_x(t), b_x(t), a_x(t), v_x(t), \vec{Q}_x(t))$$

with the discrete-time Markov chain, in which the uniform integer time scale,  $\sigma$ , is adopted:  $t_n$  and  $t_{n+1}$  correspond to the beginning of two consecutive slots. ( $t_n := n\sigma$ .)

$s_x(t)$  : **Back-off stage** ( $0, 1, 2, \dots, m$ ) of node  $x$  at time  $t$ , where  $m$  is the maximum back-off stage. By the exponential back-off scheme described in Section 4.1,  $s_x(t) = i$  implies that the contention window size at time  $t = w_i = 2^i w$ .  $w$  is the initial window size.

$b_x(t)$  : **Back-off counter** of node  $x$  at time  $t$ . At the beginning of any back-off stage  $i$ , the counter will randomly choose a value among  $(1, \dots, w_i)$  based on the assumptions of protocol. Then for each following time step  $t_n$ , the back-off counter either decrements or freezes with respect to carrier sense.

$a_x(t)$  : **Action/Status** of node  $x$  at time  $t$ :

$$\left\{ \begin{array}{l} I, \quad x \text{ is idle} \\ B, \quad x \text{ is back-off counting} \\ U, \quad x \text{ is waiting due to unidentified signals sensed} \\ R_{\vec{z}}, \quad x \text{ is sending RTS to } z \\ R_{\overleftarrow{z}}, \quad x \text{ is receiving an uncorrupted RTS from } z \\ R_{\bar{z}}, \quad x \text{ is overhearing an uncorrupted RTS from } z \\ C_{\vec{z}}, \quad x \text{ is sending a CTS to } z \\ C_{\overleftarrow{z}}, \quad x \text{ is receiving an uncorrupted CTS from } z \\ C_{\bar{z}}, \quad x \text{ is overhearing an uncorrupted CTS from } z \\ A_{\vec{z}}, \quad x \text{ is sending DATA to } z \\ A_{\overleftarrow{z}}, \quad x \text{ is receiving an uncorrupted DATA from } z \\ D_z, \quad x \text{ is waiting due to NAV triggered by RTS/CTS from } z \\ W, \quad x \text{ is waiting for a responding CTS} \end{array} \right.$$

Here  $z \in N_x$  where  $N_x$  denotes the set of neighboring nodes of  $x$ . Remark on  $W$ :  $a_x(t) = W$  implies that either the previous RTS packet has been dropped at the receiver so there will be no responding CTS, or the CTS has become unidentified due to collisions at  $x$ .

Table 4.1 characterizes the actions/statuses of  $x$  by the behaviors of  $x$ 's antenna, the channel conditions, and the status of  $x$ 's queue. For instance, if  $a_x(t) = I$ ,  $x$  has nothing to send in the buffer and there is no signal in the medium. Hence its antenna keeps quiet, the channel is sensed free, and its queue is empty. If  $a_x(t) = D_z$ ,  $x$  will be frozen because of NAV, which means the antenna is quiet, the channel can be either busy or free depending on the other nodes' actions, and  $x$ 's queue can be either empty or occupied. The other actions can be described similarly as above.

$v_x(t)$  : **Virtual timer** associated with  $a_x(t)$ . It will start ( $t = t_0$ ) at one of the following values and decrement to 0 at the beginning of each time slot. Otherwise

**Table 4.1:** The node statuses in terms of antenna, channel, and queue

$a_x(t)$	Antenna (Quiet/Sending)	Channel (Busy/Free)	Queue (Empty/Occupied)
$I$	Quiet	Free	Empty
$B$	Quiet	Free	Occupied
$D_z$	Quiet	Busy/Free	Empty/Occupied
$W$	Quiet	Busy/Free	Occupied
$U/R_{\bar{z}}/A_{\bar{z}}/R_{\bar{z}}/C_{\bar{z}}$	Quiet	Busy	Empty/Occupied
$C_{\bar{z}}$	Quiet	Busy	Occupied
$C_{\bar{z}}$	Sending	Busy	Empty/Occupied
$R_{\bar{z}}/A_{\bar{z}}$	Sending	Busy	Occupied

the timer stays at 0.

$$v_x(t_0) = \begin{cases} t_{RTS}, & \text{if } a_x(t_0) \in \{R_{\bar{z}}, R_{\bar{z}}, R_{\bar{z}}\} \\ t_{out}, & \text{if } a_x(t_0) = W \\ t_{CTS}, & \text{if } a_x(t_0) \in \{C_{\bar{z}}, C_{\bar{z}}, C_{\bar{z}}\} \\ t_{DATA}, & \text{if } a_x(t_0) \in \{A_{\bar{z}}, A_{\bar{z}}\} \\ t_{NAVr}/t_{NAVc}, & \text{if } a_x(t_0) = D_z \end{cases}$$

where  $t_0$  is the initial start time. Here,  $t_{RTS} := \lceil T_{RTS}/\sigma \rceil - 1$  (similarly defined for other time parameters).

$\vec{Q}_x(t)$  : **Queue status vector** of node  $x$  at time  $t$ . Here,  $\vec{Q}_x(t) = \langle Y, L \rangle$ , where  $Y$  is the receiver of the Head of Line (HoL) packet that being sent by node  $x$ . The second entry,  $L$ , represents the length of the queue (including the HoL packet) at node  $x$ . If there is no packet in the queue, we say  $\vec{Q}_x(t) = \vec{0} = \langle \emptyset, 0 \rangle$ . Furthermore, we say node  $x$  is on  $l$ -th layer at time  $t$  if  $L = l$ . Whenever the node  $x$  successfully receives a packet during the back-off counting,  $L$  is increased by 1. If node  $x$  finishes transmitting a packet (either success or failure),  $L$  is dropped by 1, and  $Y$  will be updated based on the receiver of the next packet in the queue.

## 4.2.2 Modeling of States Transitions

In this section, we investigate and model the state transitions at each node using notation introduced above. Notice that we do not characterize network performance by thoroughly examining the joint node states and their transitions, even though the joint distribution, once found, can be considered as the most universal form of expressing knowledge [69]. As we shall see an example in Section 4.3.2, the joint state model correctly produce a complete probabilistic description of the network behaviors, however, the full distribution is difficult to model and analyze because it grows exponentially with both the size of network and the cardinality of node state space.

### 4.2.2.1 $x$ As a Listener/Receiver

A node  $x$  is a listener when it is in back-off counting (with occupied queue) or idle (with empty queue). It consistently monitors the channel by both physical and virtual carrier sense. Upon the successful reception of a RTS packet,  $x$  becomes a receiver by completing the RTS/CTS/DATA/ACK handshake. Diagram 4.3 and 4.4 represent the states' transitions for  $x$  based on the description of 802.11 DCF and the assumptions in Section 4.1. Both diagrams share a similar structure, called **Carrier Sense Block** (CSB), which repeatedly appears in our model for every pair of back-off stage and back-off counter.

For Figure 4.3, suppose that at time step  $t_n$  where  $n = 0, 1, 2, \dots$ , node  $x$  is at the  $k$ th step of the  $i$ th backoff stage for receiver  $y$  with  $l$  packets in the queue. At the next time step there are five possible state transitions on node  $x$ , associated with the following probabilities respectively:

$$\textcircled{1}_a = \text{Prob}\{(i, k-1, B, 0, \langle y, l \rangle)_{n+1} | (i, k, B, 0, \langle y, l \rangle)_n\} \quad (4.2.2.1)$$

$$\textcircled{1}_b = \text{Prob}\{(i, k, R_{\bar{z}}, t_{RTS}, \langle y, l \rangle)_{n+1} | (i, k, B, 0, \langle y, l \rangle)_n\} \quad (4.2.2.2)$$

$$\textcircled{1}_c = \text{Prob}\{(i, k, R_{\bar{z}}, t_{RTS}, \langle y, l \rangle)_{n+1} | (i, k, B, 0, \langle y, l \rangle)_n\} \quad (4.2.2.3)$$

$$\textcircled{1}_d = \text{Prob}\{(i, k, C_{\bar{z}}, t_{CTS}, \langle y, l \rangle)_{n+1} | (i, k, B, 0, \langle y, l \rangle)_n\} \quad (4.2.2.4)$$

$$\textcircled{1}_e = \text{Prob}\{(i, k, U, 0, \langle y, l \rangle)_{n+1} | (i, k, B, 0, \langle y, l \rangle)_n\} \quad (4.2.2.5)$$

Here we adopt the short notation:

$$\begin{aligned} & P\{(z_1, z_2, z_3, z_4, z_5)_{n+1} | (z'_1, z'_2, z'_3, z'_4, z'_5)_n\} \\ = & P\{\mathcal{H}_x(t_{n+1}) = (z_1, z_2, z_3, z_4, z_5) | \mathcal{H}_x(t_n) = (z'_1, z'_2, z'_3, z'_4, z'_5)\} \end{aligned}$$

Transition  $\textcircled{1}_a$  occurs when  $x$  detects a quiet channel, that is, currently no neighbors of  $x$  are broadcasting or beginning to transmit any signals. As a result, the back off counter decrements by 1. Transition  $\textcircled{1}_b$  accounts for the fact that, one of  $x$ 's neighbor,  $z$ , begins to send a RTS packet for  $x$  while others neighboring nodes stay quiet. In this case, node  $x$  takes the first step of receiving the RTS packet, so that  $a_x(t_{n+1}) = R_{\overline{z}}, v_x(t_{n+1}) = t_{RTS}$ . Transition  $\textcircled{1}_c$  or  $\textcircled{1}_d$  takes place provided that only  $z$  starts to broadcast a RTS packet or a CTS packet not for  $x$ . In those scenarios,  $a_x(t_{n+1}) = R_{\overline{z}}, v_x(t_{n+1}) = t_{RTS}$  or  $a_x(t_{n+1}) = C_{\overline{z}}, v_x(t_{n+1}) = t_{CTS}$ . The transition  $\textcircled{1}_e$ ,  $a_x(t_{n+1}) = U$ , happens when  $x$  detects disordered signals in the channel, caused by either corrupted or partial packets from  $x$ 's neighbors.

During the receiving (overhearing) of RTS or CTS from a neighbor  $z$ , node  $x$  may observe packet collisions when the hidden nodes of  $z$  initiate transmissions to  $x$ . Thus, given the  $j$ -th step of receiving ( $v_x(t_n) = j$ ), we have the following probabilities associated with the transitions  $\textcircled{2}_b$ ,  $\textcircled{3}_b$  and  $\textcircled{4}_b$ :

$$\textcircled{2}_b = \text{Prob}\{(i, k, U, 0, \langle y, l \rangle)_{n+1} | (i, k, R_{\overline{z}}, j, \langle y, l \rangle)_n\} \quad (4.2.2.6)$$

$$\textcircled{3}_b = \text{Prob}\{(i, k, U, 0, \langle y, l \rangle)_{n+1} | (i, k, R_{\overline{z}}, j, \langle y, l \rangle)_n\} \quad (4.2.2.7)$$

$$\textcircled{4}_b = \text{Prob}\{(i, k, U, 0, \langle y, l \rangle)_{n+1} | (i, k, C_{\overline{z}}, j, \langle y, l \rangle)_n\} \quad (4.2.2.8)$$

Otherwise,  $x$  keeps receiving and the virtual counter  $v_x(t)$  decreases by 1 at each time step with the probabilities:

$$\textcircled{2}_a = \text{Prob}\{(i, k, R_{\overline{z}}, j-1, 0, \langle y, l \rangle)_{n+1} | (i, k, R_{\overline{z}}, j, \langle y, l \rangle)_n\} \quad (4.2.2.9)$$

$$\textcircled{3}_a = \text{Prob}\{(i, k, R_{\overline{z}}, j-1, 0, \langle y, l \rangle)_{n+1} | (i, k, R_{\overline{z}}, j, \langle y, l \rangle)_n\} \quad (4.2.2.10)$$

$$\textcircled{4}_a = \text{Prob}\{(i, k, C_{\overline{z}}, j-1, 0, \langle y, l \rangle)_{n+1} | (i, k, C_{\overline{z}}, j, \langle y, l \rangle)_n\} \quad (4.2.2.11)$$

If a RTS is successfully received, that is,  $a_x(t_n) = R_{\overline{z}}, v_x(t_n) = 0$ ,  $x$  will start to respond with a CTS to  $z$ , shown by  $a_x(t_{n+1}) = C_{\overline{z}}, v_x(t_{n+1}) = t_{CTS}$ . The transmission

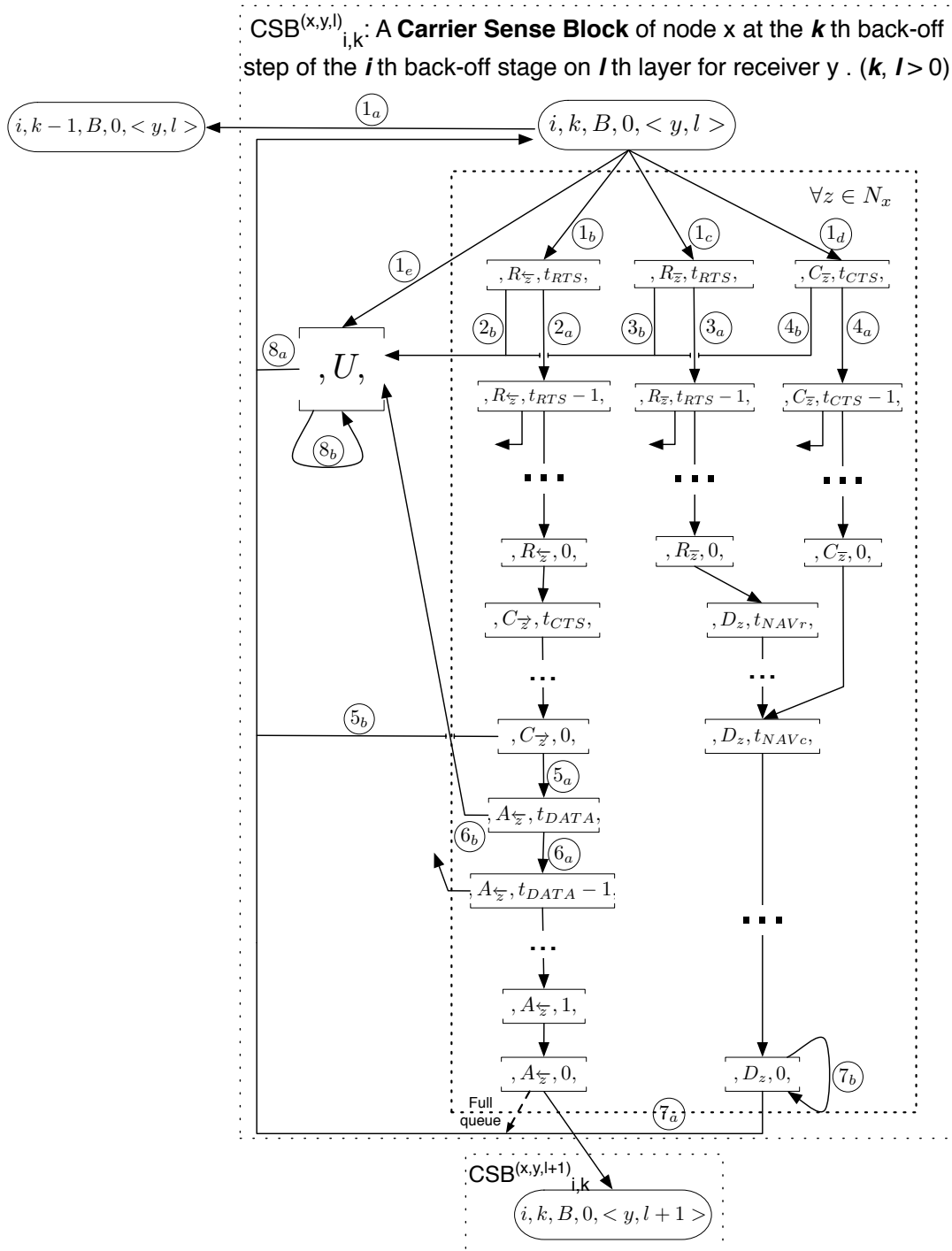


**Figure 4.3:** Carrier Sense Block at upper layer

of the CTS takes  $t_{CTS}$  steps and if successful,  $x$  should begin to receive a data packet from  $z$ . Otherwise, no data will be sent, and  $x$  resumes carrier sensing. Thus we have the following transition probabilities:

$$\textcircled{5}_a = \text{Prob}\{(i, k, A_{\overline{z}}, t_{DATA}, \langle y, l \rangle)_{n+1} | (i, k, C_{\overline{z}}, 0, \langle y, l \rangle)_n\} \quad (4.2.2.12)$$

$$\textcircled{5}_b = \text{Prob}\{(i, k, B, 0, \langle y, l \rangle)_{n+1} | (i, k, C_{\overline{z}}, 0, \langle y, l \rangle)_n\} \quad (4.2.2.13)$$

At each step of receiving DATA, there are two possible transitions:

$$\textcircled{6}_a = \text{Prob}\{(i, k, A_{\overline{z}}, j-1, \langle y, l \rangle)_{n+1} | (i, k, A_{\overline{z}}, j, \langle y, l \rangle)_n\} \quad (4.2.2.14)$$

$$\textcircled{6}_b = \text{Prob}\{(i, k, U, 0, \langle y, l \rangle)_{n+1} | (i, k, A_{\overline{z}}, j, \langle y, l \rangle)_n\} \quad (4.2.2.15)$$

For the first transition,  $x$  correctly receives the next piece of data so  $v_x(t)$  decrease by 1. Otherwise,  $x$  detects a collision, which implies the signal is corrupted, shown by  $a_x(t_{n+1}) = U$ . When  $v_x(t) = 1$ , the receiving of data is complete and  $x$  shall reply with an ACK packet. When  $v_x(t)$  decreases to 0, that is, the DATA/ACK handshake is successful,  $x$  will resume back off counting on the next layer and the queue size increases by 1. If the queue is full, as shown by the dashed arrow in diagram 4.3, the data received will be dropped and  $x$  will resume back-off counting on the same layer.

If  $x$  successfully overhears a RTS, then with probability 1 it will go to silent mode  $D_z$  and update  $v_x(t)$  to  $t_{NAV_r}$ . Similarly, if a CTS is overheard,  $v_x(t)$  changes to  $t_{NAV_c}$ . Upon  $v_x(t)$  reaches 0, the behavior of  $x$  at the next time step depends on the channel status. With probability  $\textcircled{7}_a$ ,  $x$  resumes back-off counting because it senses a quiet channel, or with probability  $\textcircled{7}_b$ ,  $x$  detects a busy channel and waits.

$$\textcircled{7}_a = \text{Prob}\{(i, k, B, 0, \langle y, l \rangle)_{n+1} | (i, k, D_z, 0, \langle y, l \rangle)_n\} \quad (4.2.2.16)$$

$$\textcircled{7}_b = \text{Prob}\{(i, k, D_z, 0, \langle y, l \rangle)_{n+1} | (i, k, D_z, 0, \langle y, l \rangle)_n\} \quad (4.2.2.17)$$

Finally, if  $x$  senses jumbled signals in the channel at time step  $t_n$  ( $a_x(t_n) = U$ ), then after one discrete time step  $x$  either senses the channel is clear and resumes back-off counting ( $a_x(t_{n+1}) = B$ ), or detects a busy channel ( $a_x(t_{n+1}) = U$ ) and waits, with

the following probabilities:

$$\textcircled{8}_a = \text{Prob}\{(i, k, B, 0, \langle y, l \rangle)_{n+1} | (i, k, U, 0, \langle y, l \rangle)_n\} \quad (4.2.2.18)$$

$$\textcircled{8}_b = \text{Prob}\{(i, k, U, 0, \langle y, l \rangle)_{n+1} | (i, k, U, 0, \langle y, l \rangle)_n\} \quad (4.2.2.19)$$

For Figure 4.4 where  $x$  has empty queue, the state transitions are similar except with probability  $\textcircled{1}_a$   $x$  stays idle and keeps monitoring the channel. After a data packet is received, if  $x$  is a relay node, it will randomly or deterministically choose a receiver in  $N_x$  and set a back-off counter between 1 and the initial contention window size  $w$ .

#### 4.2.2.2 $x$ As a Sender

At the end of counting ( $b_x(t) = 0$ ) at any back-off stage,  $x$  becomes a sender by immediately initiating a RTS transmission. The state transitions of  $x$  as a sender are shown in Figure 4.5. A structure, called a **RTS/CTS Contention Block** (RCB) emerges in the model whenever  $x$  attempts a RTS/CTS handshake.

Suppose node  $x$  transmits a RTS packet to  $y$  during  $i$ th backoff stage with  $l$  packets in the queue. After a time period of  $t_{RTS}$ , the RTS transmission either succeeds and begins to receive a CTS from  $y$  with probability

$$\textcircled{9}_a = \text{Prob}\{(i, 0, C_{\overleftarrow{y}}, t_{CTS}, \langle y, l \rangle)_{n+1} | (i, 0, R_{\overrightarrow{y}}, 0, \langle y, l \rangle)_n\} \quad (4.2.2.20)$$

or fails with probability

$$\textcircled{9}_b = \text{Prob}\{(i, 0, W, t_{out}, \langle y, l \rangle)_{n+1} | (i, 0, R_{\overrightarrow{y}}, 0, \langle y, l \rangle)_n\} \quad (4.2.2.21)$$

In this case, there will be no reply so that  $x$  waits until the virtual counter  $v_x(t)$  reaches 0.

At each step of receiving a CTS, depending on whether there is a collision at  $x$ , we have the following transition probabilities:

$$\textcircled{10}_a = \text{Prob}\{(i, 0, C_{\overleftarrow{y}}, j-1, \langle y, l \rangle)_{n+1} | (i, 0, C_{\overleftarrow{y}}, j, \langle y, l \rangle)_n\}$$

$$\textcircled{10}_b = \text{Prob}\{(i, 0, W, t_{out} - j, \langle y, l \rangle)_{n+1} | (i, 0, C_{\overleftarrow{y}}, j, \langle y, l \rangle)_n\}$$

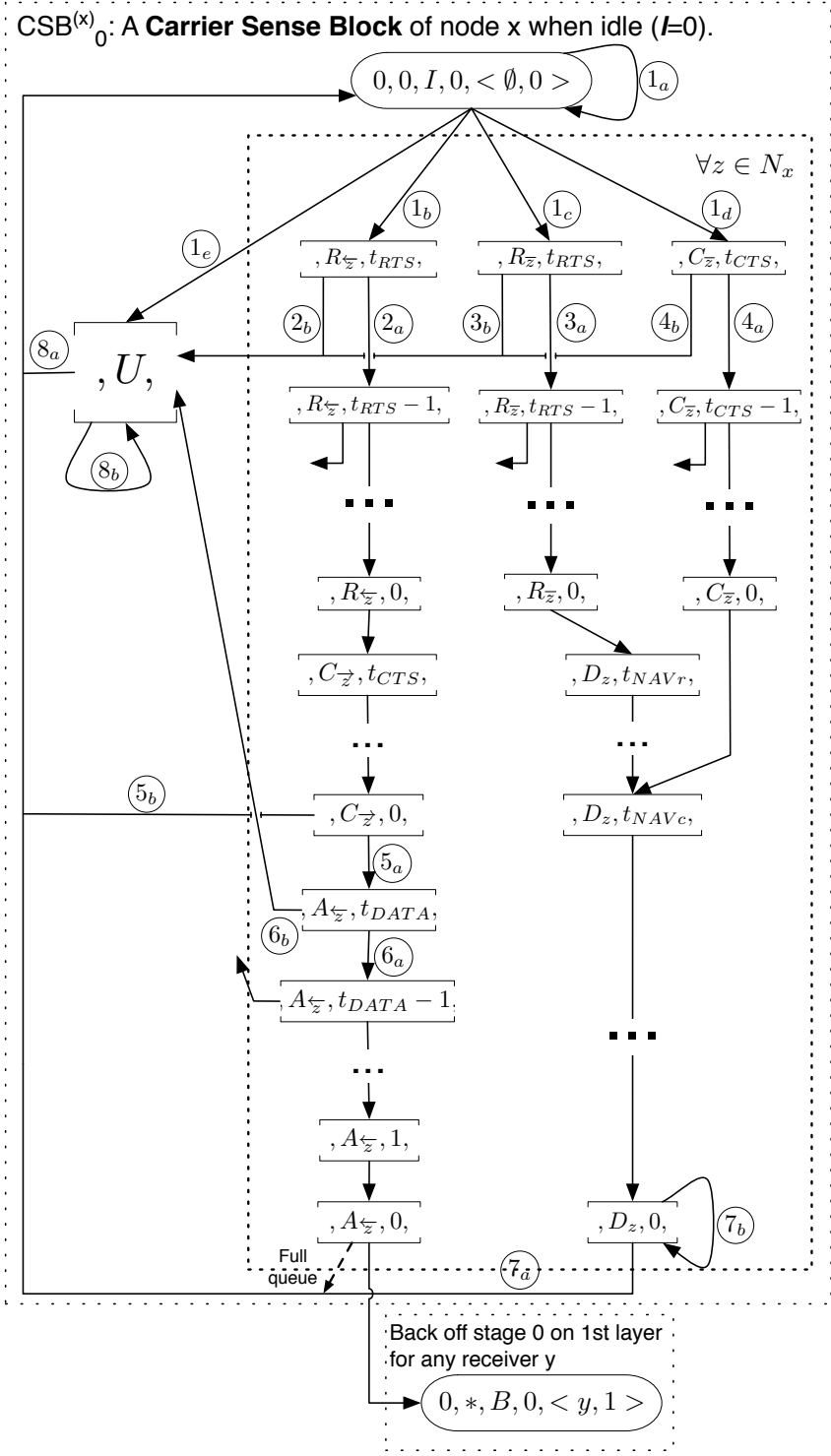


Figure 4.4: Carrier Sense Block at base layer

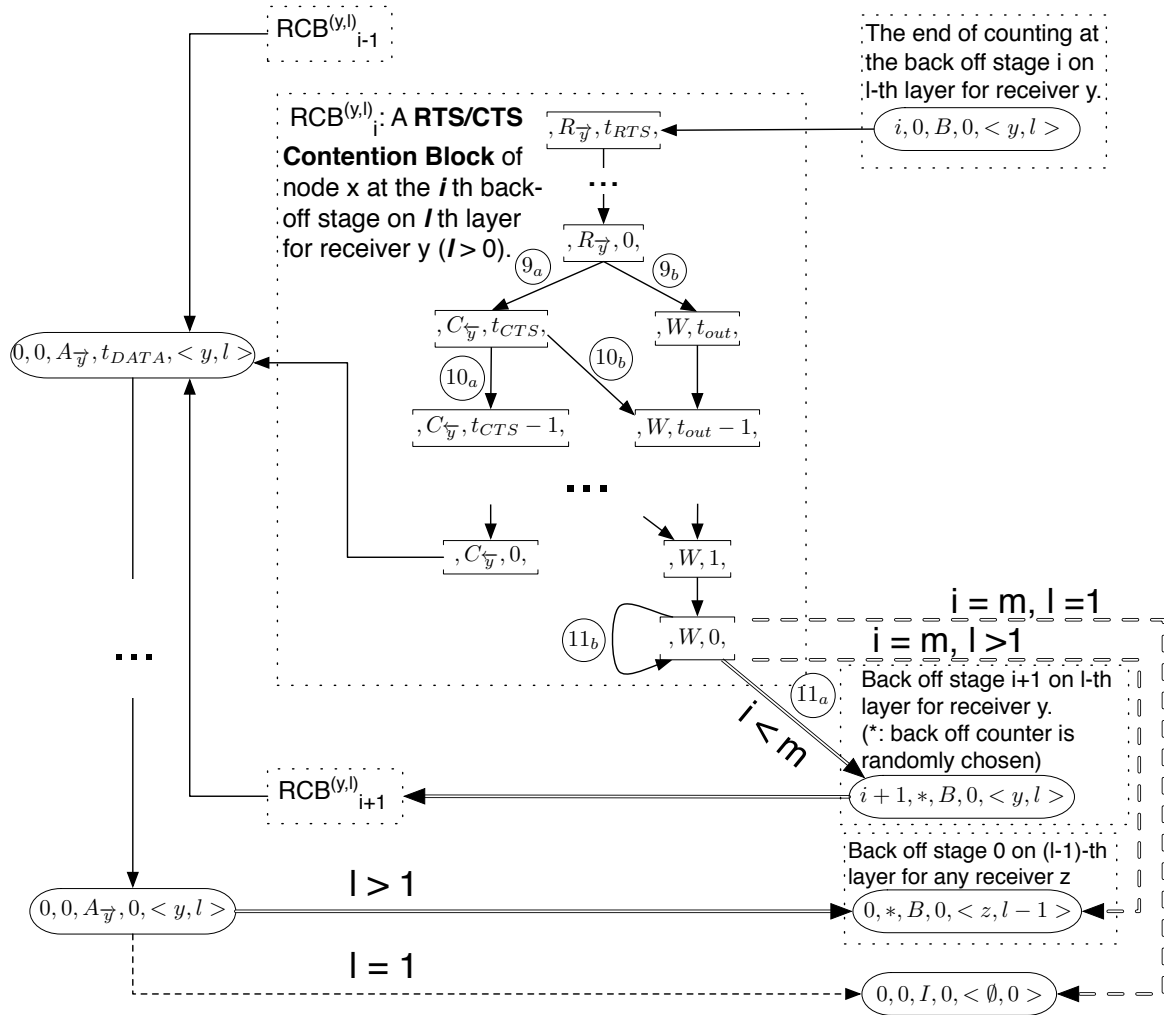


Figure 4.5: RTS/CTS Contention Block

When the receiving of the CTS is complete,  $x$  will initiate an DATA/ACK handshake, which lasts  $t_{DATA}$  time steps. In the end, if  $l = 1$ , *i.e.* the queue is empty,  $x$  becomes idle, otherwise  $x$  restarts the back-off procedure for the next HoL packet and the queue size decreases by 1.

Finally, suppose the RTS/CTS handshake fails,  $x$  senses the channel at the end of the CTS timeout. Given no transmitting neighbors, if the current back-off stage is less than the maximum stage allowed ( $i < m$ ),  $x$  will reset the back off counter between 1 and the doubled contention window size, then resume counting procedure at the back off stage  $i + 1$ . The associated probability function is:

$$(11_a) = \sum_k \text{Prob}\{(i + 1, k, B, 0, \langle y, l \rangle)_{n+1} | (i, 0, W, 0, \langle y, l \rangle)_n\}$$

However, if the maximum stage is reached, then the data packet will be dropped. Based on the current queue size,  $x$  can either restart back-off procedure ( $l > 1$ ) or become idle ( $l = 1$ ):

$$(11_a) = \sum_k \text{Prob}\{(0, k, B, 0, \langle y, l - 1 \rangle)_{n+1} | (m, 0, W, 0, \langle y, l \rangle)_n\}$$

$$(11_a) = \text{Prob}\{(0, 0, I, 0, \langle \emptyset, 0 \rangle)_{n+1} | (m, 0, W, 0, \langle y, 1 \rangle)_n\}$$

For the case that a busy channel is sensed,  $x$  will freeze, as shown by,

$$(11_b) = \text{Prob}\{(i, 0, W, 0, \langle y, l \rangle)_{n+1} | (i, 0, W, 0, \langle y, l \rangle)_n\}$$

### 4.2.3 Representation of Transition Probabilities

In this section, we address the formulations of transition probability functions in detail. For simplicity, we first denote the probability density function for any node  $x$  in the network at time step  $t_n$  by

$$P^{(n)}([\chi_{i,k,j}^{\langle y,l \rangle}]_x) := \text{Prob}\{\mathcal{H}_x(t_n) = \mathbf{h}_x\} = \text{Prob}\{\mathcal{H}_x(t_n) = (i, k, \chi, j, \langle y, l \rangle)\}$$

Here  $i \in [0, m]$ ,  $k \in [0, 2^i w]$ ,  $\chi \in \{I, B, U, R_{\not{z}/\not{z}/\bar{z}}, C_{\not{z}/\not{z}/\bar{z}}, A_{\not{z}/\not{z}}, D_z, W\}$ ,  $j \in [0, t_{NAV_r}]$ ,  $y, z \in N_x$  and  $l \in [0, L_x]$  where  $N_x$  is the set that contains  $x$ 's neighbors

(and  $\emptyset$ ), and  $L_x$  represents the maximum queue size of  $x$ . The joint probability density functions are similarly defined and symmetric:

$$P^{(n)}([\chi_{i,k,j}^{\langle y,l \rangle}]_x, [\bar{\chi}_{i',k',j'}^{\langle y',l' \rangle}]_{x'}, \dots) = P^{(n)}([\chi_{i,k,j}^{\langle y,l \rangle}]_{x'}, [\bar{\chi}_{i',k',j'}^{\langle y',l' \rangle}]_x, \dots)$$

The probability density function of node  $x$  can be obtained by marginalizing out other nodes in the joint state probability density function, *i.e.*

$$\begin{aligned} \text{Prob}(\mathcal{H}_x(t_n) = \mathbf{h}_x) &= \text{Prob}(\mathcal{H}_x(t_n) = \mathbf{h}_x, \bullet) \\ &= \sum_{(\mathbf{h}_{x'}, \dots) \in \Omega(\mathbf{h}_x; x', \dots)} \text{Prob}(\mathcal{H}_x(t_n) = \mathbf{h}_x, \mathcal{H}_x(t_n) = \mathbf{h}_{x'}, \dots) \end{aligned}$$

where  $\Omega(\mathbf{h}_x; x', \dots)$  represents the sub state space of nodes  $\{x', \dots\}$  such that,

$$\text{Prob}(\mathcal{H}_x(t_n) = \mathbf{h}_x, \mathcal{H}_{x'}(t_n) = \mathbf{h}_{x'}, \dots) \neq 0$$

$$\forall (\mathbf{h}_{x'}, \dots) \in \Omega(\mathbf{h}_x; x', \dots)$$

On the other hand, given a set of marginal densities, the joint distribution in general cannot be uniquely determined unless the random variables are independent. This brings forward the main challenge in our modeling framework since for each node, all the critical state transitions mentioned in the last section are dependent on the concurrent states of its neighboring nodes. To be precise, suppose  $N_x = \{x_1, x_2, \dots, x_r\}$  and expanding the marginal probability density function of  $x$  on  $\Omega(\mathbf{h}_x; x_1, \dots, x_r)$ , we have

$$\begin{aligned} &\text{Prob}\{\mathcal{H}_x(t_{n+1}) = \mathbf{h}'_x | \mathcal{H}_x(t_n) = \mathbf{h}_x\} \\ &= \sum_{(\mathbf{h}_{x_1}, \dots, \mathbf{h}_{x_r}) \in \Omega_{\mathcal{A}}(\mathbf{h}_x; x_1, \dots, x_r)} \frac{\text{Prob}\{\mathcal{H}_x(t_n) = \mathbf{h}_x, \mathcal{H}_{x_1}(t_n) = \mathbf{h}_{x_1}, \dots, \mathcal{H}_{x_r}(t_n) = \mathbf{h}_{x_r}\}}{\text{Prob}\{\mathcal{H}_x(t_n) = \mathbf{h}_x\}} \\ &= \frac{\sum_{\Omega_{\mathcal{A}}([\chi_{i,k,j}^{\langle y,l \rangle}]_x; x_1, \dots, x_r)} P^{(n)}([\chi_{i,k,j}^{\langle y,l \rangle}]_x, [\chi_{i,k,j}^{\langle y,l \rangle}]_{x_1}, \dots, [\chi_{i,k,j}^{\langle y,l \rangle}]_{x_r})}{\sum_{\Omega([\chi_{i,k,j}^{\langle y,l \rangle}]_x; x_1, \dots, x_r)} P^{(n)}([\chi_{i,k,j}^{\langle y,l \rangle}]_x, [\chi_{i,k,j}^{\langle y,l \rangle}]_{x_1}, \dots, [\chi_{i,k,j}^{\langle y,l \rangle}]_{x_r})} := \frac{\mathcal{F}_{\Omega_{\mathcal{A}}}([\chi_{i,k,j}^{\langle y,l \rangle}]_x)}{\mathcal{F}_{\Omega}([\chi_{i,k,j}^{\langle y,l \rangle}]_x)} \end{aligned}$$

where  $\Omega_{\mathcal{A}}(\mathbf{h}_x; x_1, \dots, x_r) \subseteq \Omega(\mathbf{h}_x; x_1, \dots, x_r)$  and

$$\begin{aligned} &\text{Prob}\{\mathcal{H}_x(t_{n+1}) = \mathbf{h}'_x | \mathcal{H}_x(t_n) = \mathbf{h}_x, \mathcal{H}_{x_1}(t_n) = \mathbf{h}_{x_1}, \dots, \mathcal{H}_{x_r}(t_n) = \mathbf{h}_{x_r}\} \\ &= \begin{cases} 1, & \text{if } (\mathbf{h}_{x_1}, \dots, \mathbf{h}_{x_r}) \in \Omega_{\mathcal{A}}(\mathbf{h}_x; x_1, \dots, x_r) \\ 0, & \text{otherwise} \end{cases} \end{aligned}$$

For the purpose of evaluating the transition probability functions introduced in Section 4.2.2, we shall establish their connections (shown by functions  $\mathcal{F}_\Omega$  and  $\mathcal{F}_{\Omega_A}$ ) to the probability density functions of joint states with the neighboring nodes. The joint state spaces  $\Omega$  and  $\Omega_A$  will be discussed based on four categories of actions  $\mathcal{A}$  that  $x$  takes.

#### 4.2.3.1 Carrier Sensing while in the Idle or Back-off States

Let us suppose at the current time step  $t_n$   $x$  is sensing a free channel and not freezing or waiting, that is,  $x$  is in back off state  $B$  (or equivalently, idle state  $I$ , if its queue is empty), and the parameters  $i', k', y', l'$  are fixed:  $\mathcal{H}_x(t_n) = (i', k', B, 0, \langle y', l' \rangle)$ . Referring to Table 4.1 the channel must be quiet, hence all the neighboring nodes of  $x$  are not sending and not receiving from  $x$  or common neighbors with  $x$  (as  $x$  is known to be in the back-off state). Using the notation of cartesian product, we then have

$$\begin{aligned} \Omega([B_{i',k',0}^{\langle y',l' \rangle}]_x; x_1, \dots, x_r) &= \Omega([B_{i',k',0}^{\langle y',l' \rangle}]_x; x_1) \times \dots \times \Omega([B_{i',k',0}^{\langle y',l' \rangle}]_x; x_r) \\ &= \times_{x_\alpha \in N_x} \Omega([B_{i',k',0}^{\langle y',l' \rangle}]_x; x_\alpha) \\ &= \times_{x_\alpha \in N_x} \{ \mathcal{H}_{x_\alpha}(t_n) \mid \underbrace{\chi_\alpha \notin \{R_{\rightarrow}, C_{\rightarrow}, A_{\rightarrow}\}}_{\text{not transmitting}} \ \& \ \underbrace{\chi_\alpha \notin \{R_{\leftarrow/z'}, C_{\leftarrow/z'}, A_{\leftarrow/z'}, D_{z'}\}}_{\text{not interacting with } x \text{ and } N_x}, z' \notin N_x \} \end{aligned}$$

such that  $P^{(n)}([B_{i',k',0}^{\langle y',l' \rangle}]_x) = \mathcal{F}_\Omega([B_{i',k',0}^{\langle y',l' \rangle}]_x)$ . At the next time step  $t_{n+1}$ , if no neighbors of  $x$  are ready to send any signals, the channel will remain quiet. Hence we conclude that

$$\textcircled{1a} = \frac{\mathcal{F}_{\Omega_{1a}}([B_{i',k',0}^{\langle y',l' \rangle}]_x)}{\mathcal{F}_\Omega([B_{i',k',0}^{\langle y',l' \rangle}]_x)} = \frac{\sum_{\Omega_{1a}([B_{i',k',0}^{\langle y',l' \rangle}]_x; x_1, \dots, x_r)} P^{(n)}([B_{i',k',0}^{\langle y',l' \rangle}]_x, [\chi_{i,k,j}^{\langle y,l \rangle}]_{x_1}, \dots, [\chi_{i,k,j}^{\langle y,l \rangle}]_{x_r})}{\sum_{\Omega([B_{i',k',0}^{\langle y',l' \rangle}]_x; x_1, \dots, x_r)} P^{(n)}([B_{i',k',0}^{\langle y',l' \rangle}]_x, [\chi_{i,k,j}^{\langle y,l \rangle}]_{x_1}, \dots, [\chi_{i,k,j}^{\langle y,l \rangle}]_{x_r})}$$

Here,  $\Omega_{1a}([B_{i',k',0}^{\langle y',l' \rangle}]_x; x_1, \dots, x_r) \subseteq \Omega([B_{i',k',0}^{\langle y',l' \rangle}]_x; x_1, \dots, x_r)$  and includes an extra restriction:

$$\begin{aligned} \Omega_{1a}([B_{i',k',0}^{\langle y',l' \rangle}]_x; x_1, \dots, x_r) &= \times_{x_\alpha \in N_x} \Omega_{1a}([B_{i',k',0}^{\langle y',l' \rangle}]_x; x_\alpha) \\ &= \times_{x_\alpha \in N_x} \{ \mathcal{H}_{x_\alpha}(t_n) \in \Omega([B_{i',k',0}^{\langle y',l' \rangle}]_x; x_\alpha) \mid \underbrace{(\chi, k, j)_{x_\alpha} \notin \{(B, 0, 0), (R_{\leftarrow}, k, 0), (C_{\leftarrow}, 0, 0)\}}}_{\text{not begin to send RTS/CTS/DATA}} \}. \end{aligned}$$

For transition  $\textcircled{1b}$ , it accounts for the fact that one neighbor of  $x$ , for example,  $x'$ , begins to send a RTS packet to  $x$ , while the rest neighbors do not begin to send. We thus have

$$\begin{aligned} \Omega_{1b}([B_{i',k',0}^{(y',l')}]_x; x', \dots, x_r) &= \Omega_{1b}([B_{i',k',0}^{(y',l')}]_x; x') \times_{x_\alpha \in N_x \setminus x'} \Omega_{1a}([B_{i',k',0}^{(y',l')}]_x; x_\alpha) \\ &= \{\mathcal{H}_{x'}(t_n) \mid \underbrace{(\chi, k, y)_{x'} = (B, 0, x)}_{\text{begins to sent a RTS to } x}\} \times_{x_\alpha \in N_x \setminus x'} \Omega_{1a}([B_{i',k',0}^{(y',l')}]_x; x_\alpha) \end{aligned}$$

such that

$$\textcircled{1b} = \frac{\mathcal{F}_{\Omega_{1b}, x'}([B_{i',k',0}^{(y',l')}]_x)}{\mathcal{F}_\Omega([B_{i',k',0}^{(y',l')}]_x)}.$$

On the other hand, if  $x'$  begins to send a RTS not to  $x$  while all other neighbors remain quiet and do not start to transmit any packet,  $x$  will start to overhear the RTS. The probability  $\textcircled{1c}$  is given by

$$\textcircled{1c} = \frac{\mathcal{F}_{\Omega_{1c}, x'}([B_{i',k',0}^{(y',l')}]_x, x')}{\mathcal{F}_\Omega([B_{i',k',0}^{(y',l')}]_x)}$$

where  $\Omega_{1c}([B_{i',k',0}^{(y',l')}]_x; x', \dots, x_r)$  is similarly defined by

$$\begin{aligned} \Omega_{1c}([B_{i',k',0}^{(y',l')}]_x; x', \dots, x_r) \\ = \{\mathcal{H}_{x'}(t_n) \mid \underbrace{(\chi, k)_{x'} = (B, 0) \ \& \ y_{x'} \neq x}_{\text{begins to sent a RTS not to } x}\} \times_{x_\alpha \in N_x \setminus x'} \Omega_{1a}([B_{i',k',0}^{(y',l')}]_x; x_\alpha) \end{aligned}$$

Likewise, if  $x'$  starts to sent a CTS not to  $x$  while the remaining neighbors stay quiet and do not initiate a transmission, we get

$$\begin{aligned} \Omega_{1d}([B_{i',k',0}^{(y',l')}]_x; x', \dots, x_r) \\ = \{\mathcal{H}_{x'}(t_n) \mid \underbrace{(\chi, k)_{x'} = (R_{\bar{z}}, 0), z \notin N_x}_{\text{begins to sent a CTS not to } x \text{ (or } N_x)}\} \times_{x_\alpha \in N_x \setminus x'} \Omega_{1a}([B_{i',k',0}^{(y',l')}]_x; x_\alpha) \end{aligned}$$

so that

$$\textcircled{1d} = \frac{\mathcal{F}_{\Omega_{1d}, x'}([B_{i',k',0}^{(y',l')}]_x)}{\mathcal{F}_\Omega([B_{i',k',0}^{(y',l')}]_x)}$$

Otherwise,  $x$  detects an unidentified busy channel. The corresponding transition has probability computed by

$$\textcircled{1}_e = 1 - \frac{\mathcal{F}_{\Omega_{1a}}([B_{i',k',0}^{\langle y',l' \rangle}]_x)}{\mathcal{F}_{\Omega}([B_{i',k',0}^{\langle y',l' \rangle}]_x)} - \sum_{x' \in N_x} \left( \frac{\mathcal{F}_{\Omega_{1b},x'}([B_{i',k',0}^{\langle y',l' \rangle}]_x)}{\mathcal{F}_{\Omega}([B_{i',k',0}^{\langle y',l' \rangle}]_x)} + \frac{\mathcal{F}_{\Omega_{1c},x'}([B_{i',k',0}^{\langle y',l' \rangle}]_x)}{\mathcal{F}_{\Omega}([B_{i',k',0}^{\langle y',l' \rangle}]_x)} \right. \\ \left. + \frac{\mathcal{F}_{\Omega_{1d},x'}([B_{i',k',0}^{\langle y',l' \rangle}]_x)}{\mathcal{F}_{\Omega}([B_{i',k',0}^{\langle y',l' \rangle}]_x)} \right)$$

#### 4.2.3.2 Receiving/overhearing Packets

Next suppose at  $t_n$   $x$  is receiving or overhearing a packet from a neighbor  $x'$  without interference by the others that are hidden from  $x'$ :  $\mathcal{H}_x(t_n) = (i', k', \tilde{\chi}, j', \langle y', l' \rangle)$ ,  $\tilde{\chi} \in \{R_{\tilde{x}'}^{\leftarrow}, R_{\tilde{x}'}^{\rightarrow}, C_{\tilde{x}'}^{\leftarrow}, C_{\tilde{x}'}^{\rightarrow}, A_{\tilde{x}'}^{\leftarrow}\}$ ,  $j' \neq 0$ . We observe that  $x'$  is at the  $j'$ -th step of transmitting the same packet, and all the other neighbors of  $x$  that are hidden from  $x'$  are quiet and do not interact with  $x$ . The common neighbors of  $x$  and  $x'$  are ignored because they share the same channel and will not intervene. Now let  $N_{xx'}$  represent the neighbors of  $x$  that hidden from  $x'$ , we can write

$$\Omega([\tilde{\chi}_{i',k',j'}^{\langle y',l' \rangle}]_x; x', \dots, x_r) = \Omega([\tilde{\chi}_{i',k',j'}^{\langle y',l' \rangle}]_x; x') \times_{x_\alpha \in N_{xx'}} \Omega([\tilde{\chi}_{i',k',j'}^{\langle y',l' \rangle}]_x; x'; x_\alpha),$$

such that

$$\left\{ \begin{array}{l} \Omega([R_{\tilde{x}'/i',k',j'}^{\langle y',l' \rangle}]_x; x') = \{ \mathcal{H}_{x'}(t_n) \mid \underbrace{(\chi, j)_{x'} = (R_{\tilde{x}'}^{\rightarrow}, j')}_{j' \text{-th step of sending RTS to } x} \} \\ \Omega([R_{\tilde{x}'/i',k',j'}^{\langle y',l' \rangle}]_x; x') = \{ \mathcal{H}_{x'}(t_n) \mid \underbrace{(\chi, j)_{x'} = (R_{\tilde{z}'}^{\rightarrow}, j'), z \neq x}_{j' \text{-th step of sending RTS not to } x} \} \\ \Omega([C_{\tilde{x}'/i',k',j'}^{\langle y',l' \rangle}]_x; x') = \{ \mathcal{H}_{x'}(t_n) \mid \underbrace{(\chi, j)_{x'} = (C_{\tilde{z}'}^{\rightarrow}, j'), z \notin N_x}_{j' \text{-th step of sending CTS not to } x \text{ and } N_x} \} \\ \Omega([C_{\tilde{x}'/i',k',j'}^{\langle y',l' \rangle}]_x; x') = \{ \mathcal{H}_{x'}(t_n) \mid \underbrace{(\chi, j)_{x'} = (C_{\tilde{x}'}^{\rightarrow}, j')}_{j' \text{-th step of sending CTS to } x} \} \\ \Omega([A_{\tilde{x}'/i',k',j'}^{\langle y',l' \rangle}]_x; x') = \{ \mathcal{H}_{x'}(t_n) \mid \underbrace{(\chi, j)_{x'} = (A_{\tilde{x}'}^{\rightarrow}, j')}_{j' \text{-th step of sending DATA to } x} \} \end{array} \right.$$

where  $\Omega([\tilde{\chi}_{i',k',j'}^{\langle y',l' \rangle}]_x; x'; x_\alpha)$  contains all the possible states of neighboring node  $x_\alpha$  in  $N_{xx'}$  given ongoing communication between  $x$  and  $x'$ . If  $x$  is receiving a RTS or overhearing

a RTS/CTS from  $x'$  ( $\tilde{\chi} \in \{R_{x'}^{\leftarrow}, R_{x'}^{\rightarrow}, C_{x'}^{\rightarrow}\}$ ), then for the hidden nodes  $x_\alpha$ ,  $x$  should appear to be in a back-off or idle state since the conversation between  $x$  and  $x'$  are concealed:

$$\Omega([\tilde{\chi}_{i',k',j'}^{\langle y',l' \rangle}]_x; x'; x_\alpha) = \Omega([B_{i',k',0}^{\langle y',l' \rangle}]_x; x_\alpha), \quad \tilde{\chi} \in \{R_{x'}^{\leftarrow}, R_{x'}^{\rightarrow}, C_{x'}^{\rightarrow}\}.$$

On the other hand, if  $x$  is receiving a CTS or DATA from  $x'$ , then  $x_\alpha$  should be informed because of the network allocation vector (NAV) incorporated inside the previous RTS/CTS packets sent from  $x$ . As a result,  $x_\alpha$  should be in corresponding step of NAV delay. If not, it is also impossible for  $x_\alpha$  to receive any CTS/DATA packets because its own RTS/CTS handshakes should have failed. To summarize, we have the following:

$$\begin{aligned} \Omega([C_{x'/i',k',j'}^{\langle y',l' \rangle}]_x; x'; x_\alpha) &= \Omega([B_{i',k',0}^{\langle y',l' \rangle}]_x; x_\alpha) \bigcup \{\mathcal{H}_{x'}(t_n) | \\ &\underbrace{(\chi, j)_{x_\alpha} = (D_x, t_{NAVc} + 1 + j')}_{t_{NAVc} + 1 + j'\text{-th step of NAV delay}} \& \underbrace{\chi_{x_\alpha} \notin \{C_{x'}^{\leftarrow}, A_{x'}^{\leftarrow}\}}_{\text{not receiving CTS/DATA}} \& \underbrace{(\chi, j)_{x_\alpha} \neq (R_{x'}^{\leftarrow}, 0)}_{\text{not begin to send CTS}} \} \end{aligned}$$

$$\begin{aligned} \Omega([A_{x'/i',k',j'}^{\langle y',l' \rangle}]_x; x'; x_\alpha) &= \Omega([B_{i',k',0}^{\langle y',l' \rangle}]_x; x_\alpha) \bigcup \{\mathcal{H}_{x'}(t_n) | \\ &\underbrace{(\chi, j)_{x_\alpha} = (D_x, j')}_{j'\text{-th step of NAV delay}} \& \underbrace{\chi_{x_\alpha} \notin \{C_{x'}^{\leftarrow}, A_{x'}^{\leftarrow}\}}_{\text{not receiving CTS/DATA}} \}. \end{aligned}$$

Note that in general  $t_{DATA} \gg t_{RTS}(t_{CTS})$ , thus it is possible that  $x_\alpha$  finishes receiving a RTS and starts to broadcast a CTS during the period of DATA reception at  $x$ .

At the next time step  $t_{n+1}$ ,  $x$  will continue to receive from  $x'$  unless some neighbors starts to broadcast, thus

$$\begin{aligned} \Omega_2([R_{x'/i',k',j'}^{\langle y',l' \rangle}]_x; x', \dots, x_r) &= \Omega([R_{x'/i',k',j'}^{\langle y',l' \rangle}]_x; x') \times_{x_\alpha \in N_{xx'}} \\ &\{\mathcal{H}_{x_\alpha}(t_n) \in \Omega([R_{x'/i',k',j'}^{\langle y',l' \rangle}]_x; x'; x_\alpha) | \underbrace{(\chi, k, j)_{x_\alpha} \notin \{(B, 0, 0), (R_{x'}^{\leftarrow}, k, 0), (C_{x'}^{\leftarrow}, 0, 0)\}}_{\text{not begin to send RTS/CTS/DATA}} \} \end{aligned}$$

$$\begin{aligned} \Omega_3([R_{x'/i',k',j'}^{\langle y',l' \rangle}]_x; x', \dots, x_r) &= \Omega([R_{x'/i',k',j'}^{\langle y',l' \rangle}]_x; x') \times_{x_\alpha \in N_{xx'}} \\ &\{\mathcal{H}_{x_\alpha}(t_n) \in \Omega([R_{x'/i',k',j'}^{\langle y',l' \rangle}]_x; x'; x_\alpha) | \underbrace{(\chi, k, j)_{x_\alpha} \notin \{(B, 0, 0), (R_{x'}^{\leftarrow}, k, 0), (C_{x'}^{\leftarrow}, 0, 0)\}}_{\text{not begin to send RTS/CTS/DATA}} \} \end{aligned}$$

$$\Omega_4([C_{x'/i',k',j'}^{\langle y',l' \rangle}]_x; x', \dots, x_r) = \Omega([C_{x'/i',k',j'}^{\langle y',l' \rangle}]_x; x') \times_{x_\alpha \in N_{xx'}} \\ \{\mathcal{H}_{x_\alpha}(t_n) \in \Omega([C_{x'/i',k',j'}^{\langle y',l' \rangle}]_x; x'; x_\alpha) \mid \underbrace{(\chi, k, j)_{x_\alpha} \notin \{(B, 0, 0), (R_{\tilde{z}}, k, 0), (C_{\tilde{z}}, 0, 0)\}}_{\text{not begin to send RTS/CTS/DATA}}\}$$

$$\Omega_6([A_{x'/i',k',j'}^{\langle y',l' \rangle}]_x; x', \dots, x_r) = \Omega([A_{x'/i',k',j'}^{\langle y',l' \rangle}]_x; x') \times_{x_\alpha \in N_{xx'}} \\ \{\mathcal{H}_{x_\alpha}(t_n) \in \Omega([A_{x'/i',k',j'}^{\langle y',l' \rangle}]_x; x'; x_\alpha) \mid \underbrace{(\chi, k, j)_{x_\alpha} \notin \{(B, 0, 0), (R_{\tilde{z}}, k, 0)\}}_{\text{not begin to send RTS/CTS}}\}$$

$$\Omega_{10}([C_{x'/i',k',j'}^{\langle y',l' \rangle}]_x; x', \dots, x_r) = \Omega([C_{x'/i',k',j'}^{\langle y',l' \rangle}]_x; x') \times_{x_\alpha \in N_{xx'}} \\ \{\mathcal{H}_{x_\alpha}(t_n) \in \Omega([C_{x'/i',k',j'}^{\langle y',l' \rangle}]_x; x'; x_\alpha) \mid \underbrace{(\chi, k, j)_{x_\alpha} \neq (B, 0, 0)}_{\text{not begin to send RTS}}\}$$

and the transition probability functions during receiving are given by

$$\begin{aligned} \textcircled{2}_a &= \frac{\mathcal{F}_{\Omega_2}([R_{x'/i',k',j'}^{\langle y',l' \rangle}]_x)}{\mathcal{F}_\Omega([R_{x'/i',k',j'}^{\langle y',l' \rangle}]_x)}, & \textcircled{3}_a &= \frac{\mathcal{F}_{\Omega_3}([R_{x'/i',k',j'}^{\langle y',l' \rangle}]_x)}{\mathcal{F}_\Omega([R_{x'/i',k',j'}^{\langle y',l' \rangle}]_x)}, & \textcircled{4}_a &= \frac{\mathcal{F}_{\Omega_4}([C_{x'/i',k',j'}^{\langle y',l' \rangle}]_x)}{\mathcal{F}_\Omega([C_{x'/i',k',j'}^{\langle y',l' \rangle}]_x)}, \\ \textcircled{6}_a &= \frac{\mathcal{F}_{\Omega_6}([A_{x'/i',k',j'}^{\langle y',l' \rangle}]_x)}{\mathcal{F}_\Omega([A_{x'/i',k',j'}^{\langle y',l' \rangle}]_x)}, & \textcircled{10}_a &= \frac{\mathcal{F}_{\Omega_{10}}([C_{x'/i',k',j'}^{\langle y',l' \rangle}]_x)}{\mathcal{F}_\Omega([C_{x'/i',k',j'}^{\langle y',l' \rangle}]_x)}. \end{aligned}$$

#### 4.2.3.3 End of Sending

At the last step of transmissions from  $x$  to  $x'$ ,  $\mathcal{H}_x(t_n) = (i', k', \tilde{\chi}, 0, \langle y', l' \rangle)$ ,  $\tilde{\chi} \in \{R_{x \rightarrow}, C_{x \rightarrow}\}$ , we know the communications are successful only if  $x'$  also reaches the last step of receiving. Thus we only consider the joint state probability functions between  $x$  and  $x'$  in this case:

$$\begin{aligned} \textcircled{9}_a &= \sum_{\Omega_9([R_{x \rightarrow}^{\langle x', l' \rangle}]_x; x')} P^{(n)}([R_{x \rightarrow}^{\langle x', l' \rangle}]_x, [\chi_{i,k,j}^{\langle y, l \rangle}]_{x'}) \frac{1}{P^{(n)}([R_{x \rightarrow}^{\langle x', l' \rangle}]_x)}, \\ \textcircled{5}_a &= \sum_{\Omega_5([C_{x \rightarrow}^{\langle y', l' \rangle}]_x; x')} P^{(n)}([C_{x \rightarrow}^{\langle y', l' \rangle}]_x, [\chi_{i,k,j}^{\langle y, l \rangle}]_{x'}) \frac{1}{P^{(n)}([C_{x \rightarrow}^{\langle y', l' \rangle}]_x)}, \end{aligned}$$

where

$$\begin{aligned}\Omega_9([R_{\vec{x}/i',0,0}^{\langle x',l' \rangle}]_x; x') &= \{\mathcal{H}_{x'}(t_n) \mid \underbrace{(\chi, j)_{x'} = (R_{\vec{x}}, 0)}_{\text{last step of receiving RTS from } x}\}, \\ \Omega_5([C_{\vec{x}/i',k',0}^{\langle y',l' \rangle}]_x; x') &= \{\mathcal{H}_{x'}(t_n) \mid \underbrace{(\chi, j)_{x'} = (C_{\vec{x}}, 0)}_{\text{last step of receiving CTS from } x}\}.\end{aligned}$$

Furthermore, since the RTS/CTS  $x'$  received must be sent from  $x$ , we have

$$\begin{aligned}P^{(n)}([R_{\vec{x}/i,k,0}^{\langle y,l \rangle}]_{x'}) &= \mathcal{F}_\Omega([R_{\vec{x}/i,k,0}^{\langle y,l \rangle}]_{x'}) = \sum_{\Omega([R_{\vec{x}/i,k,0}^{\langle y,l \rangle}]_{x'}; x)} P^{(n)}([R_{\vec{x}/i,k,0}^{\langle y,l \rangle}]_{x'}, [\chi_{i,k,j}^{\langle y,l \rangle}]_x), \\ P^{(n)}([C_{\vec{x}/i,0,0}^{\langle x,l \rangle}]_{x'}) &= \mathcal{F}_\Omega([C_{\vec{x}/i,0,0}^{\langle x,l \rangle}]_{x'}) = \sum_{\Omega([C_{\vec{x}/i,0,0}^{\langle x,l \rangle}]_{x'}; x)} P^{(n)}([C_{\vec{x}/i,0,0}^{\langle x,l \rangle}]_{x'}, [\chi_{i,k,j}^{\langle y,l \rangle}]_x),\end{aligned}$$

where  $i$  and  $l$  are fixed for  $x'$  and

$$\begin{aligned}\Omega([R_{\vec{x}/i,k,0}^{\langle y,l \rangle}]_{x'}; x) &= \{\mathcal{H}_x(t_n) \mid \underbrace{(\chi, j)_x = (R_{\vec{x}}, 0)}_{\text{last step of sending RTS to } x'}\}, \\ \Omega([C_{\vec{x}/i',0,0}^{\langle x,l \rangle}]_{x'}; x) &= \{\mathcal{H}_x(t_n) \mid \underbrace{(\chi, j)_x = (C_{\vec{x}}, 0)}_{\text{last step of sending CTS to } x'}\}.\end{aligned}$$

We can now rewrite the transition probability functions as

$$\begin{aligned}\textcircled{9}_a &= \sum_{\Omega_9([R_{\vec{x}/i',0,0}^{\langle x',l' \rangle}]_x; x')} \left( \frac{P^{(n)}([R_{\vec{x}/i',0,0}^{\langle x',l' \rangle}]_x, [\chi_{i,k,j}^{\langle y,l \rangle}]_{x'})}{\mathcal{F}_\Omega([R_{\vec{x}/i,k,0}^{\langle y,l \rangle}]_{x'})} \frac{P^{(n)}([R_{\vec{x}/i,k,0}^{\langle y,l \rangle}]_{x'})}{P^{(n)}([R_{\vec{x}/i',0,0}^{\langle x',l' \rangle}]_x)} \right), \\ \textcircled{5}_a &= \sum_{\Omega_5([C_{\vec{x}/i',k',0}^{\langle y',l' \rangle}]_x; x')} \left( \frac{P^{(n)}([C_{\vec{x}/i',k',0}^{\langle y',l' \rangle}]_x, [\chi_{i,k,j}^{\langle y,l \rangle}]_{x'})}{\mathcal{F}_\Omega([C_{\vec{x}/i,0,0}^{\langle x,l \rangle}]_{x'})} \frac{P^{(n)}([C_{\vec{x}/i,0,0}^{\langle x,l \rangle}]_{x'})}{P^{(n)}([C_{\vec{x}/i',k',0}^{\langle y',l' \rangle}]_x)} \right).\end{aligned}$$

#### 4.2.3.4 End of Waiting

Finally, suppose at time  $t_n$  node  $x$  is waiting (busy channel/NAV/CTS timeout) as well as monitoring the channel:  $\mathcal{H}_x(t_n) = (i', k', \tilde{\chi}, 0, \langle y', l' \rangle)$ ,  $\tilde{\chi} \in \{U, D_z, W\}$ . If a busy channel is sensed by  $x$  during backing-off or idle, then there must be at least one active neighbor accessing the channel at the same time. Moreover, it is impossible for

$x$  to send any packet, or receive a responding CTS (as  $x$  will be a sender in that case).

Thus

$$\begin{aligned}
\Omega([U_{x'/i',k',0}^{(y',l')}]_x; x_1, \dots, x_r) &= \times_{x_\alpha \in N_x} \Omega([U_{x'/i',k',0}^{(y',l')}]_x; x_\alpha; x_1, \dots, x_{\alpha-1}, x_{\alpha+1}, \dots, x_r) \\
&= \bigcup_{x_\alpha \in N_x} \Omega([U_{x'/i',k',0}^{(y',l')}]_x; x_\alpha) \times_{x_\beta \in N_x \setminus x_\alpha} \Omega([U_{x'/i',k',0}^{(y',l')}]_x; x_\alpha; x_\beta) \\
&= \bigcup_{x_\alpha \in N_x} \underbrace{\{\mathcal{H}_{x_\alpha}(t_n) \mid \chi_{x_\alpha} \in \{R_{\vec{z}}, C_{\vec{z}}, A_{\vec{z}}\}, z' \neq x\}}_{\text{transmitting (except CTS to } x)} \\
&\quad \times_{x_\beta \in N_x \setminus x_\alpha} \underbrace{\{\mathcal{H}_{x_\beta}(t_n) \mid \chi_{x_\beta} \notin \{R_{\vec{x}/\bar{x}}, C_{\vec{x}/\bar{x}}, A_{\vec{x}/\bar{x}}\}} \& \underbrace{\chi_{x_\beta} \neq C_{\vec{x}}}_{\text{not sending CTS to } x}}_{\text{not receiving from } x} \}
\end{aligned}$$

At the next time step if at least one neighbor is at the end of transmitting while no neighbors are in the middle of or ready to initiate a broadcasting,  $x$  will sense a free channel again and resume back-off counting (or become idle if the queue is empty) at the next time step. Otherwise,  $x$  will continue waiting. Therefore,

$$\begin{aligned}
&\Omega_8([U_{x'/i',k',0}^{(y',l')}]_x; x_1, \dots, x_r) \\
&= \bigcup_{x_\alpha \in N_x} \underbrace{\{\mathcal{H}_{x_\alpha}(t_n) \mid (\chi, j)_{x_\beta} \in \{(R_{\vec{z}}, 0), (C_{\vec{z}}, 0), (A_{\vec{z}}, 0)\}, z' \neq x\}}_{\text{end of transmitting (except CTS to } x)} \\
&\quad \times_{x_\beta \in N_x \setminus x_\alpha} \{\mathcal{H}_{x_\beta}(t_n) \in \Omega([U_{x'/i',k',0}^{(y',l')}]_x; x_\alpha; x_\beta) \mid \\
&\quad \underbrace{(\chi, j)_{x_\beta} \notin \{(R_{\vec{z}}, j'), (C_{\vec{z}}, j'), (A_{\vec{z}}, j')\}, j' \neq 0}_{\text{not in the middle of sending}} \\
&\quad \& \underbrace{(\chi, k, j)_{x_\beta} \notin \{(B, 0, 0), (R_{\vec{z}}, k, 0), (C_{\vec{z}}, 0, 0)\}}_{\text{not begin to send RTS/CTS/DATA}} \}
\end{aligned}$$

so that

$$\textcircled{8}_a = \frac{\mathcal{F}_{\Omega_8}([U_{i',k',0}^{(y',l')}]_x)}{\mathcal{F}_{\Omega}([U_{i',k',0}^{(y',l')}]_x)}$$

If  $x$  is at the end of NAV waiting period due to RTS or CTS from  $x'$ . Using the facts that  $x$  can not interact with other nodes during waiting and if  $x'$  is sending or receiving

DATA, it must be at the last step, we conclude that

$$\begin{aligned}
& \Omega([D_{x'/i',k',0}^{(y',l')}]_x; x', \dots, x_r) \\
&= \{\mathcal{H}_{x'}(t_n) \mid \underbrace{(\chi, j)_{x'} \notin \{(A_{\bar{z}/\bar{z}}, j')\}, j' \neq 0}_{\text{not in the middle of DATA}} \ \& \ \underbrace{\chi_{x'} \notin \{R_{\bar{x}/\bar{x}}, C_{\bar{x}'/\bar{x}'/\bar{x}}, A_{\bar{x}'/\bar{x}'}, D_x\}}_{\text{not interacting with } x}\} \\
& \quad \times_{x_\alpha \in N_x \setminus x'} \{\mathcal{H}_{x_\alpha}(t_n) \mid \underbrace{\chi_{x_\alpha} \notin \{R_{\bar{x}/\bar{x}}, C_{\bar{x}'/\bar{x}'/\bar{x}}, A_{\bar{x}'/\bar{x}'}, D_x\}}_{\text{not interacting with } x}\}
\end{aligned}$$

At the next time step if all neighbors of  $x$  are not transmitting or begin to send,  $x$  will detect a free channel and consequentially resume back-off counting (or become idle). Otherwise we assume  $x$  will wait until the channel is clear. The corresponding conditions are

$$\begin{aligned}
\Omega_7([D_{x'/i',k',0}^{(y',l')}]_x; x', \dots, x_r) &= \Omega([D_{x'/i',k',0}^{(y',l')}]_x; x', \dots, x_r) \bigcap \times_{x_\alpha \in N_x} \{\mathcal{H}_{x_\alpha}(t_n) \mid \\
& \underbrace{\chi_{x_\alpha} \notin \{R_{\bar{z}}, C_{\bar{z}}, A_{\bar{z}}\}}_{\text{not transmitting}} \ \& \ \underbrace{(\chi, k, j)_{x_\alpha} \notin \{(B, 0, 0), (R_{\bar{z}}, k, 0), (C_{\bar{z}}, 0, 0)\}}_{\text{not begin to send RTS/CTS/DATA}}\}
\end{aligned}$$

such that

$$\textcircled{7}_a = \frac{\mathcal{F}_{\Omega_7}([D_{x'/i',k',0}^{(y',l')}]_x)}{\mathcal{F}_\Omega([D_{x'/i',k',0}^{(y',l')}]_x)}$$

If  $x$  is at the last step of CTS timeout for  $x'$ , the previous RTS/CTS between  $x$  and  $x'$  fails, Based on the timing assumption of CTS timeout in Section 4.1.2, the possible concurrent states of  $x'$  are summarized as

$$\Omega([W_{i',0,0}^{(x',l')}]_x; x') = \{\mathcal{H}_{x'}(t_n) \mid \chi_{x'} \in \{I, B, U, R_{\bar{z}}, R_{\bar{z}'/\bar{z}'}\}, z' \neq x\}$$

For any other neighbor  $x_\alpha \in N_x \setminus x'$ , the previous RTS from  $x$  maybe overheard. Then

$$\Omega([W_{i',0,0}^{(x',l')}]_x; x'; x_\alpha) = \Omega([W_{i',0,0}^{(x',l')}]_x; x_\alpha) \bigcup \underbrace{\{\mathcal{H}_{x_\alpha}(t_n) \mid (\chi, j)_{x_\alpha} = (D_x, t_{NAVc})\}}_{t_{NAVc}\text{-th step of NAV for } x}$$

Thus for all neighboring nodes of  $x$  we have

$$\Omega([W_{i',0,0}^{(x',l')}]_x; x', \dots, x_r) = \Omega([W_{i',0,0}^{(x',l')}]_x; x') \times_{x_\alpha \in N_x \setminus x'} \Omega([W_{i',0,0}^{(x',l')}]_x; x'; x_\alpha)$$

At the next time step, if no neighbors are sending or begin to send RTS:

$$\Omega_{11}([W_{i',0,0}^{\langle x',l' \rangle}]_x; x', \dots, x_r) = \Omega([W_{i',0,0}^{\langle x',l' \rangle}]_x; x', \dots, x_r) \bigcap \\ \times_{x_\alpha \in N_x} \{ \mathcal{H}_{x_\alpha}(t_n) \mid \underbrace{(\chi, k)_{x_\alpha} \neq (B, 0) \ \& \ \chi_{x_\alpha} \neq R_{\vec{z}}}_{\text{not sending or begin to send RTS}} \}$$

$x$  resumes idle or back-off with probability evaluated by

$$\textcircled{11a} = \frac{\mathcal{F}_{\Omega_{11}}([W_{i',0,0}^{\langle x',l' \rangle}]_x)}{\mathcal{F}_{\Omega}([W_{i',0,0}^{\langle x',l' \rangle}]_x)}$$

#### 4.2.4 Equilibrium Distribution

In this section we will set up the global balance equations [36] for solving the stationary distribution,  $\pi[\chi_{i,k,j}^{\langle y,l \rangle}]_x$ , of the discrete time Markov chain as  $n \rightarrow \infty$ . *i.e.*  $\pi[\chi_{i,k,j}^{\langle y,l \rangle}]_x = \lim_{n \rightarrow \infty} P^{(n)}([\chi_{i,k,j}^{\langle y,l \rangle}]_x)$ . For the transition probabilities such as  $\textcircled{1a}$ , we adopt the following notation:

$$p_{1a}^x = \lim_{n \rightarrow \infty} P_{1a}^x(t_n) := \lim_{n \rightarrow \infty} \textcircled{1a}$$

If the transition such as  $\textcircled{2a}$  involves a specific neighboring node  $x'$ , we use

$$p_{2a}^{xx'} = \lim_{n \rightarrow \infty} P_{2a}^{xx'}(t_n) := \lim_{n \rightarrow \infty} \textcircled{2a}$$

##### 4.2.4.1 System Formulation

We start building the system from the base layer where  $l = 0$ :

$$\pi[I_{0,0,0}^{\langle \emptyset, 0 \rangle}]_x = p_{1a}^x \pi[I_{0,0,0}^{\langle \emptyset, 0 \rangle}]_x + p_{8a}^x \pi[U_{0,0,0}^{\langle \emptyset, 0 \rangle}]_x + \sum_{z \in N_x} (p_{5b}^{xz} \pi[C_{\vec{z}/0,0,0}^{\langle \emptyset, 0 \rangle}]_x + p_{7a}^{xz} \pi[D_{z/0,0,0}^{\langle \emptyset, 0 \rangle}]_x) \\ + \begin{cases} \sum_{z \in N_x} (\pi[W_{m,0,0}^{\langle z, 1 \rangle}]_x + \pi[A_{\vec{z}/0,0,0}^{\langle z, 1 \rangle}]_x), & L_x > 0 \\ \sum_{z \in N_x} \pi[A_{\vec{z}/0,0,0}^{\langle \emptyset, 0 \rangle}]_x, & L_x = 0 \end{cases} \quad (4.2.4.1)$$

$L_x = 0$  implies that node  $x$  has an empty queue. Next, suppose the queue is non-empty ( $l > 0$ ) and node  $x$  is backing off for node  $y$  where  $y \in N_x$ . If  $k = 0$ ,  $x$  transmits immediately, thus

$$\pi[B_{i,0,0}^{\langle y, l \rangle}]_x = p_{1a}^x \pi[B_{i,1,0}^{\langle y, l \rangle}]_x \quad (4.2.4.2)$$

Otherwise, depending on the value of  $i$  (back-off stage),  $k$  (back-off counter) and  $l$  (size of queue), we have

$$\begin{aligned}
\pi[B_{i,k,0}^{(y,l)}]_x &= \begin{cases} p_{1a}^x \pi[B_{i,k+1,0}^{(y,l)}]_x + p_{8a}^x \pi[U_{i,k,0}^{(y,l)}]_x \\ \quad + \sum_{z \in N_x} (p_{5b}^{xz} \pi[C_{\bar{z}/i,k,0}^{(y,l)}]_x + p_{7a}^{xz} \pi[D_{z/i,k,0}^{(y,l)}]_x), & 0 < k < 2^i w \\ p_{8a}^x \pi[U_{i,k,0}^{(y,l)}]_x + \sum_{z \in N_x} (p_{5b}^{xz} \pi[C_{\bar{z}/i,k,0}^{(y,l)}]_x + p_{7a}^{xz} \pi[D_{z/i,k,0}^{(y,l)}]_x), & k = 2^i w \end{cases} \\
&+ \begin{cases} \sum_{z \in N_x} \pi[A_{\bar{z}/i,k,0}^{(y,l-1)}]_x, & 1 < l < L_x \\ \sum_{z \in N_x} (\pi[A_{\bar{z}/i,k,0}^{(y,L_x-1)}]_x + \pi[A_{\bar{z}/i,k,0}^{(y,L_x)}]_x), & l = L_x \\ 0, & l = 1 \end{cases} \\
&+ \begin{cases} \frac{1}{2^i w} \pi[W_{i-1,0,0}^{(y,l)}]_x, & i > 0 \\ \sum_{z \in N_x} \frac{P_{xy}}{w} (\pi[W_{m,0,0}^{(z,l+1)}]_x + \pi[A_{\bar{z}/0,0,0}^{(z,l+1)}]_x), & i = 0 \end{cases} \\
&+ \begin{cases} \sum_{z \in N_x} \frac{P_{xy}}{w} \pi[A_{\bar{z}/0,0,0}^{(\emptyset,0)}]_x, & i = 0, l = 1 \\ 0, & \text{otherwise} \end{cases} \tag{4.2.4.3}
\end{aligned}$$

where  $P_{xy}$  denotes the probability of  $x$  sending a data packet to its neighbor  $y$ . Within each CSB and RCB, the steady state distribution of  $x$  should satisfy:

$$\begin{aligned}
\pi[A_{\bar{z}/i,k,0}^{(y,l)}]_x &= \dots = (p_{6a}^{xz})^{t_{DATA}} \pi[A_{\bar{z}/i,k,t_{DATA}}^{(y,l)}]_{zx} = (p_{6a}^x)^{t_{DATA}} \cdot p_{5a}^{xz} \pi[C_{\bar{z}/i,k,0}^{(y,l)}]_x \\
&= \dots = (p_{6a}^{xz})^{t_{DATA}} \cdot p_{5a}^{xz} \cdot (p_{2a}^{xz})^{t_{RTS}} \pi[R_{\bar{z}/i,k,t_{RTS}}^{(y,l)}]_x \\
&= ((p_{6a}^{xz})^{t_{DATA}} \cdot p_{5a}^{xz} \cdot (p_{2a}^{xz})^{t_{RTS}} \cdot p_{1b}^{xz}) \pi[B_{i,k,0}^{(y,l)}]_x \tag{4.2.4.4}
\end{aligned}$$

$$\begin{aligned}
p_{7a}^{xz} \pi[D_{z/i,k,0}^{(y,l)}]_x &= \dots = \pi[D_{z/i,k,t_{NAVc}+1}^{(y,l)}]_x + \pi[C_{\bar{z}/i,k,0}^{(y,l)}]_x \\
&= \dots = (p_{3a}^{xz})^{t_{RTS}} \pi[R_{\bar{z}/i,k,t_{RTS}}^{(y,l)}]_x + (p_{4a}^{xz})^{t_{CTS}} \pi[C_{\bar{z}/i,k,t_{CTS}}^{(y,l)}]_x \\
&= ((p_{3a}^{xz})^{t_{RTS}} \cdot p_{1c}^{xz} + (p_{4a}^{xz})^{t_{CTS}} \cdot p_{1d}^{xz}) \pi[B_{i,k,0}^{(y,l)}]_x \tag{4.2.4.5}
\end{aligned}$$

$$\begin{aligned}
p_{8a}^x \pi[U_{i,k,0}^{(y,l)}]_x &= \sum_{z \in N_x} \left( \sum_{j=1}^{t_{RTS}} p_{2b}^{xz} \pi[R_{\bar{z}/i,k,j}^{(y,l)}]_x + \sum_{j=1}^{t_{DATA}} p_{6b}^{xz} \pi[A_{\bar{z}/i,k,j}^{(y,l)}]_x + \sum_{j=1}^{t_{RTS}} p_{3b}^{xz} \pi[R_{\bar{z}/i,k,j}^{(y,l)}]_x \right. \\
&\quad \left. + \sum_{j=1}^{t_{CTS}} p_{4b}^{xz} \pi[C_{\bar{z}/i,k,j}^{(y,l)}]_x + p_{1e}^x \pi[B_{i,k,0}^{(y,l)}]_x \right) \quad (4.2.4.6)
\end{aligned}$$

$$\begin{aligned}
\pi[A_{\bar{y}/0,0,0}^{(y,l)}]_x &= \dots = \sum_{i=0}^m (p_{10a}^{xy})^{t_{CTS}} \pi[C_{\bar{y}/0,0,t_{CTS}}^{(y,l)}]_x = \sum_{i=0}^m (p_{10a}^{xy})^{t_{CTS}} \cdot p_{9a}^{xy} \pi[R_{\bar{y}/i,0,0}^{(y,l)}]_x \\
&= \dots = \sum_{i=0}^m (p_{10a}^{xy})^{t_{CTS}} \cdot p_{9a}^{xy} \pi[B_{i,0,0}^{(y,l)}]_x \quad (4.2.4.7)
\end{aligned}$$

$$\begin{aligned}
p_{11a}^{xy} \pi[W_{i,0,0}^{(y,l)}]_x &= \dots = \sum_{j=1}^{t_{CTS}} p_{10b}^{xy} \pi[C_{i,0,j}^{(y,l)}]_x + \pi[W_{i,0,t_{out}}^{(y,l)}]_x \\
&= \dots = (1 - (p_{10a}^{xy})^{t_{CTS}} \cdot p_{9a}^{xy}) \pi[B_{i,0,0}^{(y,l)}]_x \quad (4.2.4.8)
\end{aligned}$$

Now using equations (4.2.4.4)–(4.2.4.8), we can rewrite (4.2.4.1) and (4.2.4.3) as:

$$\begin{aligned}
\pi[I_{0,0,0}^{(\emptyset,0)}]_x &= (p_{1a}^x + p_{1e}^x + \sum_{z \in N_x} (p_{1b}^{xz} (1 - P_R^{xz}) + p_{1c}^{xz} + p_{1d}^{xz})) \pi[I_{0,0,0}^{(\emptyset,0)}]_x \\
&\quad + \sum_{z \in N_x} (P_S^{xz} \sum_{i=0}^{m-1} \pi[B_{i,0,0}^{(z,1)}]_x + \pi[B_{m,0,0}^{(z,1)}]_x) \quad (3.4.1a)
\end{aligned}$$

$$\begin{aligned}
\pi[B_{i,k,0}^{(y,l)}]_x = & \begin{cases} p_{1a}^x \pi[B_{i,k+1,0}^{(y,l)}]_x \\ \quad + (p_{1e}^x + \sum_{z \in N_x} (p_{1b}^{xz} (1 - P_R^{xz}) + p_{1c}^{xz} + p_{1d}^{xz})) \pi[B_{i,k,0}^{(y,l)}]_x, & 1 < k < 2^i w \\ (p_{1e}^x + \sum_{z \in N_x} (p_{1b}^{xz} (1 - P_R^{xz}) + p_{1c}^{xz} + p_{1d}^{xz})) \pi[B_{i,k,0}^{(y,l)}]_x, & k = 2^i w \end{cases} \\
& + \begin{cases} \sum_{z \in N_x} p_{1b}^{xz} P_R^{xz} \pi[B_{i,k,0}^{(y,l-1)}]_x, & 1 < l < L_x \\ \sum_{z \in N_x} p_{1b}^{xz} P_R^{xz} (\pi[B_{i,k,0}^{(y,L_x-1)}]_x + \pi[B_{i,k,0}^{(y,L_x)}]_x), & l = L_x \\ 0 & \text{otherwise} \end{cases} \\
& + \begin{cases} \frac{1 - P_S^{xy}}{2^i w} \pi[B_{i-1,0,0}^{(y,l)}]_x, & i > 0 \\ \frac{P_{xy}}{w} \sum_{z \in N_x} (P_S^{xz} \sum_{i=0}^{m-1} \pi[B_{i,0,0}^{(z,l+1)}]_x + \pi[B_{m,0,0}^{(z,l+1)}]_x), & i = 0 \end{cases} \\
& + \begin{cases} \sum_{z \in N_x} \frac{P_{xy}}{w} p_{1b}^{xz} P_R^{xz} \pi[I_{0,0,0}^{(\emptyset,0)}]_x, & i = 0, l = 1 \\ 0, & \text{otherwise} \end{cases} \tag{3.4.3a}
\end{aligned}$$

where  $P_S^{xz} := (P_{10a}^{xz})^{t_{CTS}} \cdot P_{9a}^{xz}$  represents the probability of a successful sending of a data packet at  $x$  to  $z$ , while  $P_R^{xz} := (p_{6a}^{xz})^{t_{DATA}} \cdot p_{5a}^{xz} \cdot (p_{2a}^{xz})^{t_{RTS}}$  denotes the probability of a successful receiving of a data packet at  $x$  from  $z$ .

#### 4.2.4.2 System Closure

Notice that the transition probability functions are still related to unknown joints probability functions. We remain very interested in a treatment to achieve optimal estimates from given marginals, but as a first step to conclude a solution, we complete the nonlinear system by applying naive product approximations [35, 10]:

$$P^{(n)}([\chi_{i,k,j}^{(y,l)}]_{x_1}, [\chi_{i,k,j}^{(y,l)}]_{x_2}, \dots, [\chi_{i,k,j}^{(y,l)}]_{x_r}) \approx \prod_{\alpha=1}^{\alpha=r} P^{(n)}([\chi_{i,k,j}^{(y,l)}]_{x_\alpha})$$

For simplicity we shall write

$$\frac{\sum_{\Omega_\alpha} \prod_{\gamma=1}^{\gamma=r} P^{(n)}([\chi_{i,k,j}^{(y,l)}]_{x_\gamma})}{\sum_{\Omega_\beta} \prod_{\gamma=1}^{\gamma=r} P^{(n)}([\chi_{i,k,j}^{(y,l)}]_{x_\gamma})} = \mathcal{P}_{\frac{x_1 \times \dots \times x_r}{x_1 \times \dots \times x_r}} \left( \frac{\Omega_\alpha}{\Omega_\beta} \right)$$

for any summation conditions  $\Omega_\alpha$  and  $\Omega_\beta$ , and nodes  $x_1, \dots, x_r$ . Furthermore, if  $\Omega_\alpha$  and  $\Omega_\beta$  can be decomposed as  $\prod_{\gamma=1}^{\gamma=r} \Omega_\alpha(x_\gamma)$  and  $\prod_{\gamma=1}^{\gamma=r} \Omega_\beta(x_\gamma)$ , we can interchange the summation and product and denote:

$$\prod_{\gamma=1}^{\gamma=r} \frac{\sum_{\Omega_\alpha} P^{(n)}([\chi_{i,k,j}^{\langle y,l \rangle}]_{x_\gamma})}{\sum_{\Omega_\beta} P^{(n)}([\chi_{i,k,j}^{\langle y,l \rangle}]_{x_\gamma})} = \prod_{\gamma=1}^{\gamma=r} \mathcal{P}_{x_\gamma}^{x_\gamma} \left( \frac{\Omega_\alpha(x_\gamma)}{\Omega_\beta(x_\gamma)} \right)$$

In terms of each types of actions in Section 4.2.3, we summarize the approximations using tables 4.2 to 4.5. Note that if there are no nodes hidden from  $x$  in the network ( $\forall x'' \in N_x, N_{x''x} = \emptyset$ ), we assume  $\textcircled{6}_a \approx 1$  and  $\textcircled{10}_a \approx 1$ . That is, without hidden terminals, the receiving of *CTS* or *DATA* at  $x$  should always succeed since the channel are expected to have been reserved by  $x$  through NAV contained in previous RTS/CTS messages.

**Table 4.2:** Transition probability function approximations - case 1

Transition Probability	Approximations
$P_{1a}^x$	$\prod_{x_\alpha \in N_x} \mathcal{P}_{x_\alpha}^{x_\alpha} \left( \frac{\Omega_{1a}([B_{i',k',0}^{\langle y',l' \rangle}]_{x;x_\alpha})}{\Omega([B_{i',k',0}^{\langle y',l' \rangle}]_{x;x_\alpha})} \right)$
$P_{1b}^{xx'}$	$\mathcal{P}_{x'}^{x'} \left( \frac{\Omega_{1b}([B_{i',k',0}^{\langle y',l' \rangle}]_{x;x'})}{\Omega([B_{i',k',0}^{\langle y',l' \rangle}]_{x;x'})} \right) \prod_{x_\alpha \in N_x \setminus x'} \mathcal{P}_{x_\alpha}^{x_\alpha} \left( \frac{\Omega_{1a}([B_{i',k',0}^{\langle y',l' \rangle}]_{x;x_\alpha})}{\Omega([B_{i',k',0}^{\langle y',l' \rangle}]_{x;x_\alpha})} \right)$
$P_{1c}^{xx'}$	$\mathcal{P}_{x'}^{x'} \left( \frac{\Omega_{1c}([B_{i',k',0}^{\langle y',l' \rangle}]_{x;x'})}{\Omega([B_{i',k',0}^{\langle y',l' \rangle}]_{x;x'})} \right) \prod_{x_\alpha \in N_x \setminus x'} \mathcal{P}_{x_\alpha}^{x_\alpha} \left( \frac{\Omega_{1a}([B_{i',k',0}^{\langle y',l' \rangle}]_{x;x_\alpha})}{\Omega([B_{i',k',0}^{\langle y',l' \rangle}]_{x;x_\alpha})} \right)$
$P_{1d}^{xx'}$	$\mathcal{P}_{x'}^{x'} \left( \frac{\Omega_{1d}([B_{i',k',0}^{\langle y',l' \rangle}]_{x;x'})}{\Omega([B_{i',k',0}^{\langle y',l' \rangle}]_{x;x'})} \right) \prod_{x_\alpha \in N_x \setminus x'} \mathcal{P}_{x_\alpha}^{x_\alpha} \left( \frac{\Omega_{1a}([B_{i',k',0}^{\langle y',l' \rangle}]_{x;x_\alpha})}{\Omega([B_{i',k',0}^{\langle y',l' \rangle}]_{x;x_\alpha})} \right)$
$P_{1e}^x$	$1 - P_{1a}^x - \sum_{x' \in N_x} (P_{1b}^{xx'} + P_{1c}^{xx'} + P_{1d}^{xx'})$

## 4.3 Examples

### 4.3.1 QualNet Simulation

To validate our model, we compare the detailed equilibrium node states of three representative networks with results from realistic simulations of wireless networks in the QualNet simulator. The parameters used are summarized in Table 4.6, and the

**Table 4.3:** Transition probability function approximations - case 2

Transition Probability	Approximations
$P_{2a}^{xx}$	$\prod_{x_\alpha \in N_{xx'}} \mathcal{P}_{x_\alpha}^{x_\alpha} \left( \frac{\Omega_2([R_{x'/i',k',j'}^{(y',l')}]_x; x'; x_\alpha)}{\Omega([B_{x'/i',k',0}^{(y',l')}]_x; x_\alpha)} \right)$
$P_{3a}^{xx'}$	$\prod_{x_\alpha \in N_{xx'}} \mathcal{P}_{x_\alpha}^{x_\alpha} \left( \frac{\Omega_3([R_{x'/i',k',j'}^{(y',l')}]_x; x'; x_\alpha)}{\Omega([B_{x'/i',k',0}^{(y',l')}]_x; x_\alpha)} \right)$
$P_{4a}^{xx'}$	$\prod_{x_\alpha \in N_{xx'}} \mathcal{P}_{x_\alpha}^{x_\alpha} \left( \frac{\Omega_4([C_{x'/i',k',j'}^{(y',l')}]_x; x'; x_\alpha)}{\Omega([B_{x'/i',k',0}^{(y',l')}]_x; x_\alpha)} \right)$
$P_{6a}^{xx'}$	$\begin{cases} \prod_{x_\alpha \in N_{xx'}} \mathcal{P}_{x_\alpha}^{x_\alpha} \left( \frac{\Omega_6([A_{x'/i',k',j'}^{(y',l')}]_x; x'; x_\alpha)}{\Omega([A_{x'/i',k',j'}^{(y',l')}]_x; x'; x_\alpha)} \right), & \exists x'' \in N_x, \text{ s.t. } N_{x''x} \neq \emptyset \\ 1, & \text{otherwise.} \end{cases}$
$P_{10a}^{xx'}$	$\begin{cases} \prod_{x_\alpha \in N_{xx'}} \mathcal{P}_{x_\alpha}^{x_\alpha} \left( \frac{\Omega_{10}([C_{x'/i',k',j'}^{(y',l')}]_x; x'; x_\alpha)}{\Omega([C_{x'/i',k',j'}^{(y',l')}]_x; x'; x_\alpha)} \right), & \exists x'' \in N_x, \text{ s.t. } N_{x''x} \neq \emptyset \\ 1, & \text{otherwise.} \end{cases}$

**Table 4.4:** Transition probability function approximations - case 3

Transition Probability	Approximations
$P_{5a}^{xx'}$	$\mathcal{P}_{\frac{x'}{x}}^{x'} \left( \frac{\Omega_5([C_{x'/i',k',0}^{(y',l')}]_x; x')}{\Omega([C_{x'/i,0,0}^{(x,l)}]_{x'}; x)} \right)$
$P_{9a}^{xx'}$	$\mathcal{P}_{\frac{x'}{x}}^{x'} \left( \frac{\Omega_9([R_{x'/i',0,0}^{(x,l')}]_x; x')}{\Omega([R_{x'/i,k,0}^{(y,l)}]_{x'}; x)} \right)$

associated model parameters are concluded by the following: (i) The RTS retry limit  $m$  varies from 0 to  $\sqrt{\frac{CW_{\max}}{CW_{\min}}} = 2$ , that is, we allow RTS to retransmit 0, 1 or 2 times in each example. (ii) The initial window size  $w$  is set as  $CW_{\min} = 3$ . (iii) The transmission time of RTS/CTS are discretized as  $t_{RTS} = t_{CTS} = \lceil \frac{T_{RTS}}{\sigma} \rceil - 1 = 1$ , similarly  $t_{DATA} = 5$  and  $t_{out} = 2$ . Note that  $t_{DATA}$  combines the transmission time of both data payload and ACK frame. (iv) The NAV contained in RTS frame should include the remaining time of a complete RTS/CTS/DATA/ACK handshakes thus

**Table 4.5:** Transition probability function approximations - case 4

Transition Probability	Approximations
$P_{7a}^{xx'}$	$\mathcal{P}_{\frac{x' \times \dots \times x_r}{x' \times \dots \times x_r}} \left( \frac{\Omega_7([D_{x'/i',k',j'}^{(y',l')}]_x; x', \dots, x_r)}{\Omega([D_{x'/i',k',j'}^{(y',l')}]_x; x', \dots, x_r)} \right)$
$P_{8a}^x$	$\mathcal{P}_{\frac{x_1 \times \dots \times x_r}{x_1 \times \dots \times x_r}} \left( \frac{\Omega_8([U_{i',k',j'}^{(y',l')}]_x; x_1, \dots, x_r)}{\Omega([U_{i',k',j'}^{(y',l')}]_x; x_1, \dots, x_r)} \right)$
$P_{11a}^{xx'}$	$\mathcal{P}_{\frac{x' \times \dots \times x_r}{x' \times \dots \times x_r}} \left( \frac{\Omega_{11}([W_{i',0,0}^{(x',l')}]_x; x', \dots, x_r)}{\Omega([D_{i',0,0}^{(x',l')}]_x; x', \dots, x_r)} \right)$

$$t_{NAV_r} = \left\lceil \frac{T_{CTS} + T_{DATA} + T_{ACK}}{\sigma} \right\rceil - 1 = 7, \text{ similarly } t_{NAV_c} = 5.$$

### 4.3.2 A 2-node Network.

We first consider the following scenario. The network contains two nodes,  $x_1$  and  $x_2$ . Both nodes have infinite number of packets in their queue and consecutively transmit to each other. Figure 4.6 shows the topology. Due to symmetry, we only

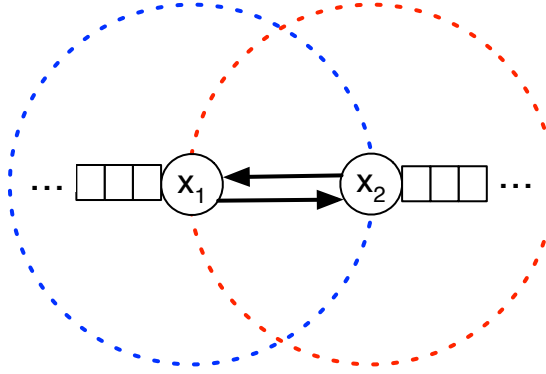


**Figure 4.6:** A 2-node network scenario without hidden terminals.

focus on the behaviors of node  $x_1$ . Since there is no hidden terminal problem in this simple network and channel conditions are assumed to be ideal, all transmissions are

**Table 4.6:** Parameters used in QualNet simulation

Terrain size	1500×1500 m <sup>2</sup>
Mobility	0
Radio range	up to 500 m
PHY protocol	802.11b
Bandwidth	5 Mbps
MAC protocol	MAC 802.11b
Slot time	140 Microsecond
SIFS	0 Microsecond
DIFS	140 Microsecond
RTS/CTS/ACK Tx time	280 Microsecond
CTS Timeout time	420 Microsecond
Data Tx time	562 Microsecond
CWmin	3
CWmax	12

guaranteed against collision and interference unless both nodes reach out at the same moment.

In this case only four non-trivial transition probabilities exists at any time step  $t_n$ , which are described in Table 4.7.

**Table 4.7:** Non-Trivial Transition Probabilities

$\textcircled{1}_a$	$x_1$ detects a quiet channel while back-off
$\textcircled{1}_b$	$x_1$ detects a RTS while back-off
$\textcircled{9}_a$	RTS from $x_1$ succeeds
$\textcircled{9}_b$	RTS from $x_1$ fails

Using product approximations summarized in Table 4.2 and 4.4, we evaluate the above transition probabilities as follows in terms of the marginal densities of  $x_2$

only.

$$P_{1a}^{x_1}(t_n) = \mathcal{P}_{\frac{x_2}{x_2}} \left( \frac{\sum_{\chi=B, k \neq 0} + \sum_{\chi=W}}{\sum_{\chi \in \{B, W\}}} \right) \quad (4.3.2.1)$$

$$P_{1b}^{x_1 x_2}(t_n) = \mathcal{P}_{\frac{x_2}{x_2}} \left( \frac{\sum_{\chi=B, k=0}}{\sum_{\chi \in \{B, W\}}} \right) \quad (4.3.2.2)$$

$$P_{9a}^{x_1 x_2}(t_n) = \mathcal{P}_{\frac{x_2}{x_1}} \left( \frac{\sum_{\chi=R_{\frac{x_1}{x_1}}, j=0}}{\sum_{\chi=R_{\frac{x_2}{x_2}}, j=0}} \right) \quad (4.3.2.3)$$

$$P_{9b}^{x_1 x_2}(t_n) = 1 - P_{9a}^{x_1 x_2}(t_n) \quad (4.3.2.4)$$

For the next step, let  $t_n \rightarrow \infty$  and employing the equilibrium equations (4.2.4.2), (3.4.3a), (4.2.4.4), (4.2.4.7) and (4.2.4.8), we have:

$$\pi[B_{i,0,0}^{(x_2, \infty)}]_{x_1} = p_{1a}^{x_1} \pi[B_{i,1,0}^{(x_2, \infty)}]_{x_1} \quad (4.3.2.5)$$

$$\pi[B_{i,k,0}^{(x_2, \infty)}]_{x_1} = \begin{cases} p_{1a}^{x_1} \pi[B_{i,k+1,0}^{(x_2, \infty)}]_{x_1} + p_{1b}^{x_1 x_2} \pi[B_{i,k,0}^{(x_2, \infty)}]_{x_1}, & 0 < k < 2^i * 3 \\ p_{1b}^{x_1 x_2} \pi[B_{i,2^i w, 0}^{(x_2, \infty)}]_{x_1}, & k = 2^i * 3 \end{cases} \quad (4.3.2.6)$$

$$+ \begin{cases} \frac{1}{2^i * 3} p_{9b}^{x_1 x_2} \pi[B_{i-1,0,0}^{(x_2, \infty)}]_{x_1}, & i > 0, k \neq 0 \\ \frac{1}{3} (p_{9a}^{x_1 x_2} \sum_{i=0}^{m-1} \pi[B_{i,0,0}^{(x_2, \infty)}]_{x_1} + \pi[B_{m,0,0}^{(x_2, \infty)}]_{x_1}), & i = 0, k \neq 0 \end{cases} \quad (4.3.2.7)$$

$$\pi[A_{\frac{x_2}{x_2/i, k, 0}^{(x_2, \infty)}}]_{x_1} = \dots = \pi[A_{\frac{x_2}{x_2/i, k, 5}^{(x_2, \infty)}}]_{x_1} = \pi[C_{\frac{x_2}{x_2/i, k, 0}^{(x_2, \infty)}}]_{x_1} = \dots = \pi[R_{\frac{x_2}{x_2/i, k, 1}^{(x_2, \infty)}}]_{x_1} = p_{1b}^{x_1 x_2} \pi[B_{i,k,0}^{(x_2, \infty)}]_{x_1} \quad (4.3.2.8)$$

$$\pi[A_{\frac{x_2}{x_2/0, 0, 0}^{(x_2, \infty)}}]_{x_1} = \dots = \sum_{i=0}^m \pi[C_{\frac{x_2}{x_2/i, 0, 1}^{(x_2, \infty)}}]_{x_1} = \sum_{i=0}^m p_{9a}^{x_1 x_2} \pi[R_{\frac{x_2}{x_2/i, 0, 0}^{(x_2, \infty)}}]_{x_1} = \dots = \sum_{i=0}^m p_{9a}^{x_1 x_2} \pi[B_{i,0,0}^{(x_2, \infty)}]_{x_1} \quad (4.3.2.9)$$

$$\pi[W_{i,0,0}^{(x_2, \infty)}]_{x_1} = \dots = \pi[W_{i,0,2}^{(x_2, \infty)}]_{x_1} = p_{9b}^{x_1 x_2} \pi[R_{\frac{x_2}{x_2/i, 0, 0}^{(x_2, \infty)}}]_{x_1} = \dots = p_{9b}^{x_1 x_2} \pi[B_{i,0,0}^{(x_2, \infty)}]_{x_1} \quad (4.3.2.10)$$

Given the transition probability functions from (4.3.2.1) to (4.3.2.4), together with the symmetry conditions:

$$\pi[\chi_{i,k,j}^{(x_2, \infty)}]_{x_1} = \pi[\chi_{i,k,j}^{(x_1, \infty)}]_{x_2} \quad (4.3.2.11)$$

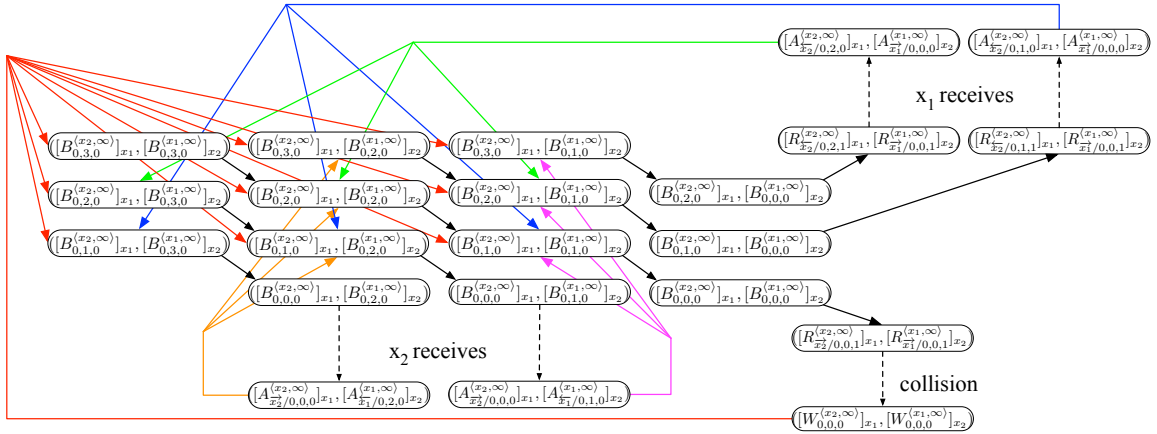
for any  $i, k, \chi, j$ , and the normalization constraints

$$\sum_{i,k,\chi,j} \pi[\chi_{i,k,j}^{\langle x_2, \infty \rangle}]_{x_1} = \sum_{i,k,\chi,j} \pi[\chi_{i,k,j}^{\langle x_1, \infty \rangle}]_{x_2} = 1, \quad (4.3.2.12)$$

the resulting non-linear system can be solved for stationary distribution at  $x_1$  by Matlab's `fsolve` subroutine. The initial conditions of the system are

$$P^{(0)}[\chi_{i,k,j}^{\langle x_2, \infty \rangle}]_{x_1} = \begin{cases} \frac{1}{3}, & \chi = B, i = 0, j = 0, k > 0 \\ 0, & \text{otherwise} \end{cases}$$

and  $P_{1a}^{x_1}(0) = 1, P_{1b}^{x_1}(0) = 0, P_{9a}^{x_1}(0) = 1, P_{9b}^{x_1}(0) = 0$ .



Notation:  $([\chi_{i,k,j}^{\langle y,l \rangle}]_x, [\bar{\chi}_{i',k',j'}^{\langle y',l' \rangle}]_y) = (\mathcal{H}_x(t) = (i, k, \chi, j, \langle y, l \rangle), \mathcal{H}_y(t) = (i', k', \bar{\chi}, j', \langle y', l' \rangle))$

**Figure 4.7:** 2-node joint state model ( $m = 0$ )

Figure 4.7 illustrates the dynamic among all the possible joint states of  $x_1$  and  $x_2$  when no RTS retry is allowed ( $m = 0$ ). The stationary joint state distribution can be solved from the linear system B.0.0.1 - B.0.0.29 given in Appendix B. In the first plot in Figure 4.8, we compare the steady state distributions attained separately by solving the non-linear system using the product approximation (blue bars), exploring the joint state diagram (red bars) and implementing QualNet simulation (green bars). Overall, the joint state diagram accurately catch the nodes' behaviors and interactions under

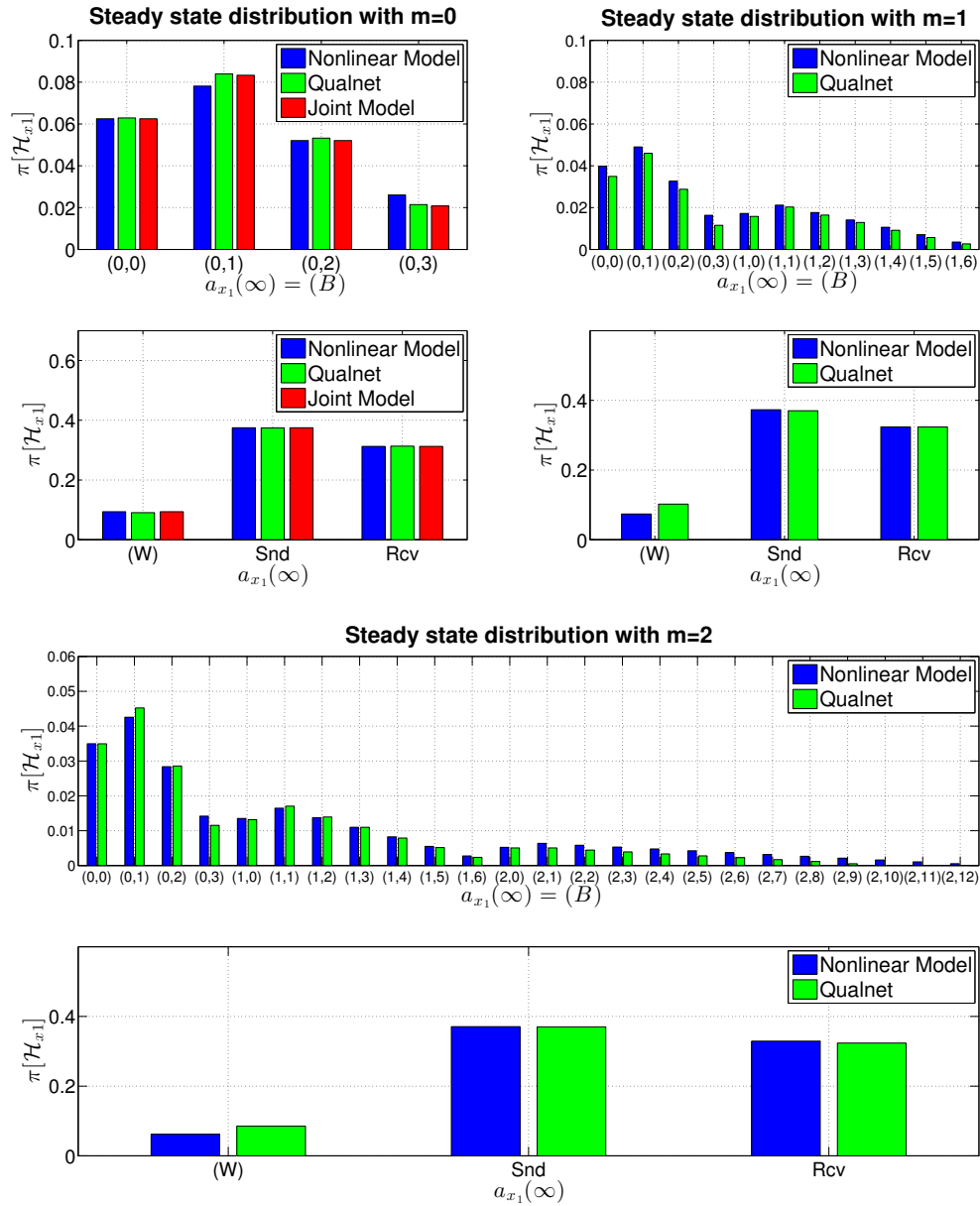


**Figure 4.8:** Comparison of steady state probabilities at  $x_1$ : the tuples represent (back-off stage, back-off counter); 'W' represents the status of CTS timeout; 'Snt' combines states of sending RTS/ receiving CTS/ sending DATA; 'Rcv' combines states of receiving RTS/ sending CTS/ receiving DATA

802.11 DCF, and more importantly, so does the nonlinear system representing our model. The following two graphs in 4.8 show the results when we allow RTS retransmits 1 or 2 times. The joint state model between  $x_1$  and  $x_2$  contains highly irregular structure and therefore is difficult to solve directly. Nevertheless, our non-linear model closely reproduces the network behavior captured by the QualNet simulation.

### 4.3.3 A Triangle Network

As an interesting extension of the simple two-node system, we now consider an equilateral triangle network where three nodes  $x_1$ ,  $x_2$  and  $x_3$  share the medium. Again, we assume each node has infinite packets in the queue and randomly chooses a receiver. Figure 4.9 demonstrates the topology. Due to symmetry, only the transitions

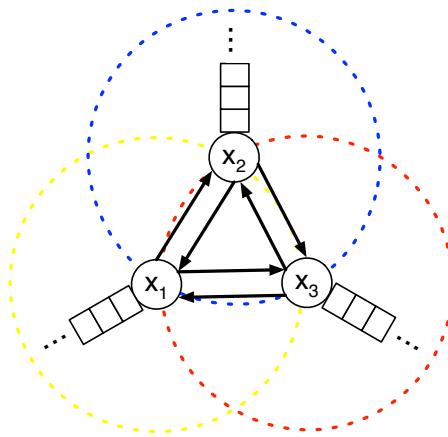


**Figure 4.9:** A 3-node network scenario without hidden terminals.

associated with  $x_1$  will be discussed.

Since there are no hidden nodes, transmissions always succeed unless two or three nodes start to send simultaneously. As a consequence, only 8 transition probability functions at time  $t_n$  are non-trivial, summarized by the following table. Notice in this example,  $x_1$  may detect a busy channel during back-off if  $x_2$  and  $x_3$  send a RTS at

the same moment, resulting in a collision at  $x_1$ . By applying product approximation,

**Table 4.8:** Non-Trivial Transition Probabilities

① <sub>a</sub>	$x_1$ detects a quiet channel while back-off	⑧ <sub>a</sub>	$x_1$ detects the channel is clear
① <sub>b</sub>	$x_1$ detects a RTS while back-off	⑧ <sub>b</sub>	$x_1$ detects the channel is still busy
① <sub>c</sub>	$x_1$ overhears a RTS while back-off	⑨ <sub>a</sub>	RTS sent from $x_1$ succeeds
① <sub>e</sub>	$x_1$ detects an busy channel	⑨ <sub>b</sub>	RTS sent from $x_1$ fails

we can evaluate the above probabilities in terms of the marginal densities of  $x_2$  and  $x_3$  as the following.

$$P_{1a}^{x_1}(t_n) = \prod_{x_\alpha \in \{x_2, x_3\}} \mathcal{P}_{x_\alpha}^{x_\alpha} \left( \frac{\sum_{\chi=B, k \neq 0} + \sum_{\chi \in \{W, U\}}}{\sum_{\chi \in \{B, W, U\}}} \right) \quad (4.3.3.1)$$

$$P_{1b}^{x_1 x_2}(t_n) = \mathcal{P}_{x_2}^{x_2} \left( \frac{\sum_{\chi=B, k=0, y=x_1}}{\sum_{\chi \in \{B, W, U\}}} \right) \mathcal{P}_{x_3}^{x_3} \left( \frac{\sum_{\chi=B, k \neq 0} + \sum_{\chi \in \{W, U\}}}{\sum_{\chi \in \{B, W, U\}}} \right) \quad (4.3.3.2)$$

$$P_{1b}^{x_1 x_3}(t_n) = \mathcal{P}_{x_3}^{x_3} \left( \frac{\sum_{\chi=B, k=0, y=x_1}}{\sum_{\chi \in \{B, W, U\}}} \right) \mathcal{P}_{x_2}^{x_2} \left( \frac{\sum_{\chi=B, k \neq 0} + \sum_{\chi \in \{W, U\}}}{\sum_{\chi \in \{B, W, U\}}} \right) \quad (4.3.3.3)$$

$$P_{1c}^{x_1 x_2}(t_n) = \mathcal{P}_{x_2}^{x_2} \left( \frac{\sum_{\chi=B, k=0, y=x_3}}{\sum_{\chi \in \{B, W, U\}}} \right) \mathcal{P}_{x_3}^{x_3} \left( \frac{\sum_{\chi=B, k \neq 0} + \sum_{\chi \in \{W, U\}}}{\sum_{\chi \in \{B, W, U\}}} \right) \quad (4.3.3.4)$$

$$P_{1c}^{x_1 x_3}(t_n) = \mathcal{P}_{x_3}^{x_3} \left( \frac{\sum_{\chi=B, k=0, y=x_2}}{\sum_{\chi \in \{B, W, U\}}} \right) \mathcal{P}_{x_2}^{x_2} \left( \frac{\sum_{\chi=B, k \neq 0} + \sum_{\chi \in \{W, U\}}}{\sum_{\chi \in \{B, W, U\}}} \right) \quad (4.3.3.5)$$

$$P_{1e}^{x_1}(t_n) = 1 - P_{1a}^{x_1}(t_n) - P_{1b}^{x_1 x_2}(t_n) - P_{1b}^{x_1 x_3}(t_n) - P_{1c}^{x_1 x_2}(t_n) - P_{1c}^{x_1 x_3}(t_n) \quad (4.3.3.6)$$

$$P_{8a}^{x_1}(t_n) = \mathcal{P}_{x_2 \times x_3}^{x_2 \times x_3} \left( \frac{\sum_{\Omega_{8a}([U_{i,k,0}^{(y,\infty)}]_{x_1}; x_2, x_3)}}{\sum_{\Omega([U_{i,k,0}^{(y,\infty)}]_{x_1}; x_2, x_3)}} \right) \quad (4.3.3.7)$$

$$P_{8b}^{x_1}(t_n) = 1 - P_{8a}^{x_1}(t_n) \quad (4.3.3.8)$$

$$P_{9a}^{x_1 x_2}(t_n) = \mathcal{P}_{x_1}^{x_2} \left( \frac{\sum_{\chi=R_{x_1}^{-}, j=0}}{\sum_{\chi=R_{x_2}^{-}, j=0}} \right) \quad (4.3.3.9)$$

$$P_{9b}^{x_1 x_2}(t_n) = 1 - P_{9a}^{x_1 x_2}(t_n) \quad (4.3.3.10)$$

$$P_{9a}^{x_1 x_3}(t_n) = \mathcal{P}_{x_1}^{x_3} \left( \frac{\sum_{\chi=R_{\hat{x}_1}, j=0}}{\sum_{\chi=R_{\hat{x}_3}, j=0}} \right) \quad (4.3.3.11)$$

$$P_{9b}^{x_1 x_3}(t_n) = 1 - P_{9a}^{x_1 x_3}(t_n) \quad (4.3.3.12)$$

where  $\Omega([U_{i,k,0}^{(y,\infty)}]_{x_1}; x_2, x_3)$  represents

$$\begin{aligned} & \{\mathcal{H}_{x_2}(t_n) | \chi_{x_2} \in \{(R/A)_{\vec{x}_1/\vec{x}_3}, C_{\vec{x}_3}\}\} \times \{\mathcal{H}_{x_3}(t_n) | \chi_{x_3} \notin \{R_{\hat{x}_1/\bar{x}_1}, C_{\vec{x}_1/\hat{x}_1/\bar{x}_1}, A_{\hat{x}_1}\}\} \\ & \cup \{\mathcal{H}_{x_3}(t_n) | \chi_{x_3} \in \{(R/A)_{\vec{x}_1/\vec{x}_2}, C_{\vec{x}_2}\}\} \times \{\mathcal{H}_{x_2}(t_n) | \chi_{x_2} \notin \{R_{\hat{x}_1/\bar{x}_1}, C_{\vec{x}_1/\hat{x}_1/\bar{x}_1}, A_{\hat{x}_1}\}\} \end{aligned}$$

and  $\Omega_{8a}([U_{i,k,0}^{(y,\infty)}]_{x_1}; x_2, x_3)$  stands for

$$\begin{aligned} & \{\mathcal{H}_{x_2}(t_n) \in \Omega([U_{i,k,0}^{(y,\infty)}]_{x_1}; x_2) | j_{x_2} = 0\} \times \{\mathcal{H}_{x_3}(t_n) \in \Omega([U_{i,k,0}^{(y,\infty)}]_{x_1}; x_2; x_3) | \\ & \quad (\chi_{x_3}, j_{x_3}) \notin \{((R/C/A)_{\vec{x}_1/\vec{x}_2}, j), j \neq 0, (\chi_{x_3}, k_{x_3}) \neq (B, 0)\}\} \\ & \cup \{\mathcal{H}_{x_3}(t_n) \in \Omega([U_{i,k,0}^{(y,\infty)}]_{x_1}; x_3) | j_{x_3} = 0\} \times \{\mathcal{H}_{x_2}(t_n) \in \Omega([U_{i,k,0}^{(y,\infty)}]_{x_1}; x_3; x_2) | \\ & \quad (\chi_{x_2}, j_{x_2}) \notin \{((R/C/A)_{\vec{x}_1/\vec{x}_3}, j), j \neq 0, (\chi_{x_2}, k_{x_2}) \neq (B, 0)\}\} \end{aligned}$$

The stationary distribution of back-off states as  $t_n \rightarrow \infty$  satisfy:

$$\pi[B_{i,0,0}^{(y,\infty)}]_{x_1} = p_{1a}^{x_1} \pi[B_{i,1,0}^{(y,\infty)}]_{x_1} \quad (4.3.3.13)$$

$$\begin{aligned} \pi[B_{i,k,0}^{(y,\infty)}]_{x_1} &= \begin{cases} p_{1a}^{x_1} \pi[B_{i,k+1,0}^{(y,\infty)}]_{x_1} + (1 - p_{1a}^{x_1}) \pi[B_{i,k,0}^{(y,\infty)}]_{x_1}, & 0 < k < 2^i * 3 \\ (1 - p_{1a}^{x_1}) \pi[B_{i,2^i w, 0}^{(y,\infty)}]_{x_1}, & k = 2^i * 3 \end{cases} \\ &+ \begin{cases} \frac{P_{x_1 y}}{2^i * 3} (p_{9b}^{x_1 x_2} \pi[B_{i-1,0,0}^{(x_2,\infty)}]_{x_1} + p_{9b}^{x_1 x_3} \pi[B_{i-1,0,0}^{(x_3,\infty)}]_{x_1}), & i > 0, k \neq 0 \\ \frac{P_{x_1 y}}{3} (p_{9a}^{x_1 x_2} \sum_{i=0}^{m-1} \pi[B_{i,0,0}^{(x_2,\infty)}]_{x_1} + \pi[B_{m,0,0}^{(x_2,\infty)}]_{x_1} \\ \quad + p_{9a}^{x_1 x_3} \sum_{i=0}^{m-1} \pi[B_{i,0,0}^{(x_3,\infty)}]_{x_1} + \pi[B_{m,0,0}^{(x_3,\infty)}]_{x_1}), & i = 0, k \neq 0 \end{cases} \end{aligned} \quad (4.3.3.14)$$

for any  $y \in \{x_2, x_3\}$ . Note we assume at the beginning of each new DATA session, the sender chooses its receiver randomly, thus  $P_{x_1 y} = \frac{1}{|N_{x_1}|} = \frac{1}{2}$ . In general, this will be set as a parameter that is determined by the routing algorithm or experimental settings.

For the remaining part of the distribution, one can conclude that

$$\begin{aligned}\pi[A_{\vec{x}_2/i,k,0}^{(y,\infty)}]_{x_1} &= \cdots = \pi[A_{\vec{x}_2/i,k,5}^{(y,\infty)}]_{x_1} = \pi[C_{\vec{x}_2/i,k,0}^{(y,\infty)}]_{x_1} = \cdots = \pi[R_{\vec{x}_2/i,k,1}^{(y,\infty)}]_{x_1} = p_{1b}^{x_1 x_2} \pi[B_{i,k,0}^{(y,\infty)}]_{x_1} \\ \pi[A_{\vec{x}_3/i,k,0}^{(y,\infty)}]_{x_1} &= \cdots = \pi[A_{\vec{x}_3/i,k,5}^{(y,\infty)}]_{x_1} = \pi[C_{\vec{x}_3/i,k,0}^{(y,\infty)}]_{x_1} = \cdots = \pi[R_{\vec{x}_3/i,k,1}^{(y,\infty)}]_{x_1} = p_{1b}^{x_1 x_3} \pi[B_{i,k,0}^{(y,\infty)}]_{x_1}\end{aligned}\quad (4.3.3.15)$$

$$\begin{aligned}\pi[D_{\vec{x}_2/i,k,0}^{(y,\infty)}]_{x_1} &= \cdots = \pi[D_{\vec{x}_2/i,k,7}^{(y,\infty)}]_{x_1} = \pi[R_{\vec{x}_2/i,k,0}^{(y,\infty)}]_{x_1} = \pi[R_{\vec{x}_2/i,k,1}^{(y,\infty)}]_{x_1} = p_{1c}^{x_1 x_2} \pi[B_{i,k,0}^{(y,\infty)}]_{x_1} \\ \pi[D_{\vec{x}_3/i,k,0}^{(y,\infty)}]_{x_1} &= \cdots = \pi[D_{\vec{x}_3/i,k,7}^{(y,\infty)}]_{x_1} = \pi[R_{\vec{x}_3/i,k,0}^{(y,\infty)}]_{x_1} = \pi[R_{\vec{x}_3/i,k,1}^{(y,\infty)}]_{x_1} = p_{1c}^{x_1 x_3} \pi[B_{i,k,0}^{(y,\infty)}]_{x_1}\end{aligned}\quad (4.3.3.16)$$

$$\pi[U_{i,k,0}^{(y,\infty)}]_{x_1} = \frac{p_{1e}^{x_1}}{p_{8a}^{x_1}} \pi[B_{i,k,0}^{(y,\infty)}]_{x_1} \quad (4.3.3.17)$$

$$\begin{aligned}\pi[A_{\vec{x}_2/0,0,0}^{(y,\infty)}]_{x_1} &= \cdots = \sum_{i=0}^m \pi[C_{\vec{x}_2/i,0,1}^{(y,\infty)}]_{x_1} = \sum_{i=0}^m p_{9a}^{x_1 x_2} \pi[R_{\vec{x}_2/i,0,0}^{(y,\infty)}]_{x_1} = \cdots = \sum_{i=0}^m p_{9a}^{x_1 x_2} \pi[B_{i,0,0}^{(y,\infty)}]_{x_1} \\ \pi[A_{\vec{x}_3/0,0,0}^{(y,\infty)}]_{x_1} &= \cdots = \sum_{i=0}^m \pi[C_{\vec{x}_3/i,0,1}^{(y,\infty)}]_{x_1} = \sum_{i=0}^m p_{9a}^{x_1 x_3} \pi[R_{\vec{x}_3/i,0,0}^{(y,\infty)}]_{x_1} = \cdots = \sum_{i=0}^m p_{9a}^{x_1 x_3} \pi[B_{i,0,0}^{(y,\infty)}]_{x_1}\end{aligned}\quad (4.3.3.18)$$

$$\pi[W_{i,0,0}^{(y,\infty)}]_{x_1} = \cdots = \pi[W_{i,0,2}^{(y,\infty)}]_{x_1} = p_{9b}^{x_1 y} \pi[R_{\vec{y}/i,0,0}^{(y,\infty)}]_{x_1} = \cdots = p_{9b}^{x_1 y} \pi[B_{i,0,0}^{(y,\infty)}]_{x_1} \quad (4.3.3.19)$$

Given the transition probability functions from (4.3.3.1) to (4.3.3.12), together with the condition of symmetric topology:

$$\pi[\chi_{i,k,j}^{(y,\infty)}]_{x_1} = \pi[\chi_{i,k,j}^{(y,\infty)}]_{x_2} = \pi[\chi_{i,k,j}^{(y,\infty)}]_{x_3} \quad (4.3.3.20)$$

for any  $i, k, \chi, j, y$ , and the normalization conditions

$$\sum_{i,k,\chi,j,y} \pi[\chi_{i,k,j}^{(y,\infty)}]_{x_1} = \sum_{i,k,\chi,j,y} \pi[\chi_{i,k,j}^{(y,\infty)}]_{x_2} = \sum_{i,k,\chi,j,y} \pi[\chi_{i,k,j}^{(y,\infty)}]_{x_3} = 1 \quad (4.3.3.21)$$

we form a non-linear system which can be solved again by Matlab with initial conditions:

$$P^{(0)}[\chi_{i,k,j}^{(y,\infty)}]_{x_1} = \begin{cases} \frac{1}{6}, & \chi = B, i = 0, j = 0, k > 0 \\ 0, & \text{otherwise} \end{cases}$$

and  $P_{1a}^{x_1}(0) = P_{8a}^{x_1}(0) = P_{9a}^{x_1 x_2}(0) = P_{9a}^{x_1 x_3}(0) = 1$ . The remaining significant transition probabilities are initialized as 0.

The plots in Figure 4.10 compare the steady state distributions with analytical results from the above system and QualNet simulations where the RTS retransmission limit ( $m$ ) is set to be 0, 1, 2 respectively.

#### 4.3.4 2 Senders and 1 Receiver

Finally we examine the following topology shown by Figure 4.11, where three nodes,  $x_1$ ,  $x_2$  and  $x_3$ , are presented in the network. Both  $x_1$  and  $x_3$  have infinite data packets destined to node  $x_2$  in their queues. This case includes hidden terminals because node  $x_3$  is not within range of  $x_1$  and vice versa. Node  $x_2$  has no queue and absorbs data packet from  $x_1$  and  $x_3$ . Due to symmetry, only  $x_1$  and  $x_2$  will be considered.

Unlike the previous example,  $x_1$  and  $x_3$  are hidden to each other thus the receiving procedure of RTS at  $x_2$  may be interrupted by collision. On the other hand the receiving of CTS packets at  $x_1$  always succeeds since  $x_1$  has no other neighbors (beside  $x_2$ ) to interfere. Notice this fact indicates all the subsequent data packets (in this case, from  $x_3$  to  $x_2$ ) will be protected by NAV hence probability  $\textcircled{6}_a \equiv 1$ .

The only possible non-trivial transition probability functions at time  $t_n$  are summarized by Table 4.9 and 4.10. For node  $x_1$  we have

$$P_{1a}^{x_1}(t_n) = \mathcal{P}_{x_2}^{x_2} \left( \frac{\sum_{\chi=R_{x_3}, j \neq 0} + \sum_{\chi \in \{I, U\}}}{\sum_{\chi \in \{I, R_{x_3}, U\}}} \right) \quad (4.3.4.1)$$

$$P_{1d}^{x_1 x_2}(t_n) = \mathcal{P}_{x_2}^{x_2} \left( \frac{\sum_{\chi=R_{x_3}, j=0}}{\sum_{\chi \in \{I, R_{x_3}, U\}}} \right) \quad (4.3.4.2)$$

$$P_{9a}^{x_1 x_2}(t_n) = \mathcal{P}_{x_1}^{x_2} \left( \frac{\sum_{\chi=R_{x_1}, j=0}}{\sum_{\chi=R_{x_3}, j=0}} \right) \quad (4.3.4.3)$$

$$P_{9b}^{x_1 x_2}(t_n) = 1 - P_{9a}^{x_1 x_2}(t_n) \quad (4.3.4.4)$$

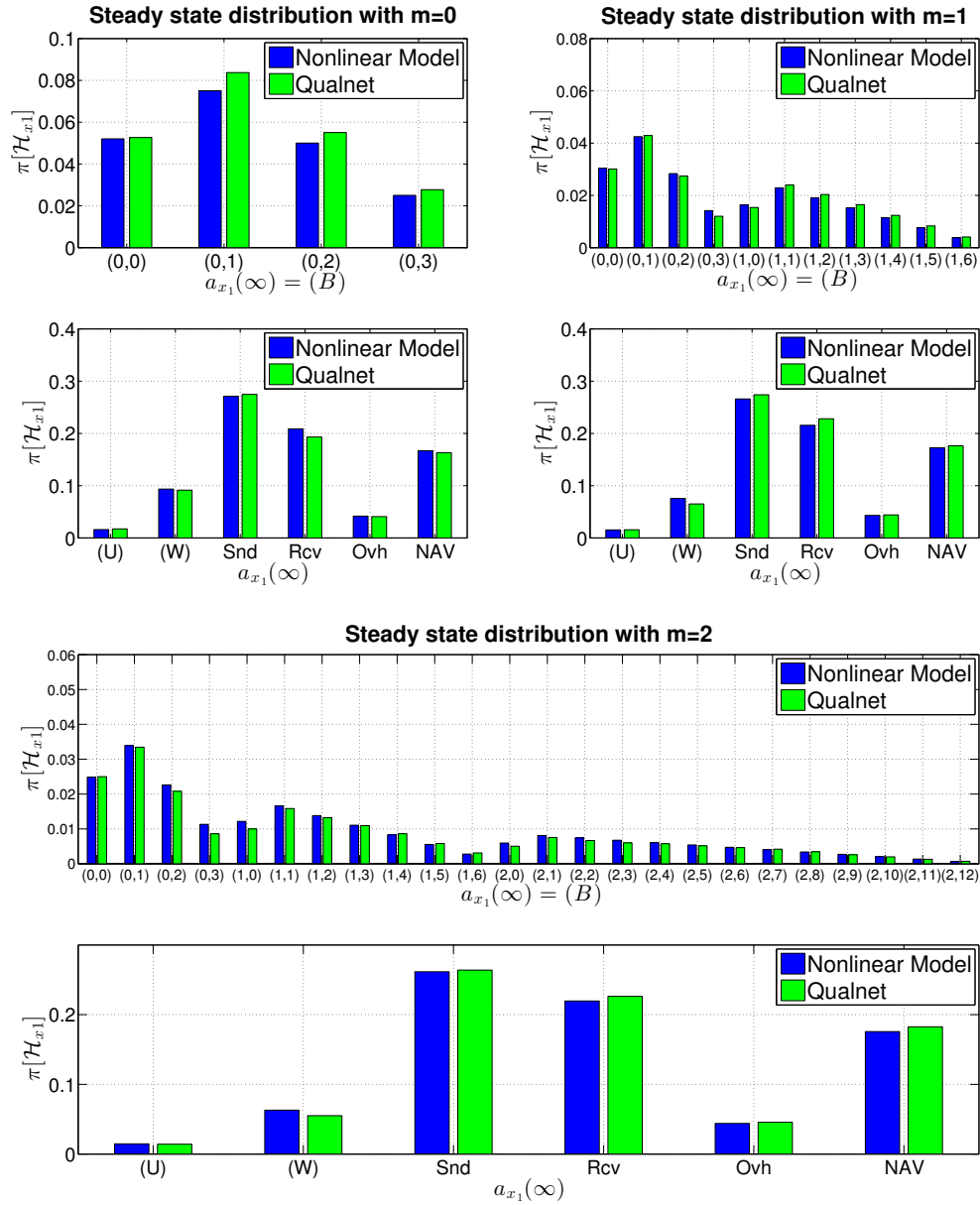


**Figure 4.10:** Comparison of steady state probabilities at  $x_1$ : the tuples represent (back-off stage, back-off counter); 'W' represents the status of CTS timeout; 'U' represents the freezing status due to busy channel; 'Snt' combines states of sending RTS/ receiving CTS/ sending DATA; 'Rcv' combines states of receiving RTS/ sending CTS/ receiving DATA; 'Ovh' denotes overhearing RTS; 'NAV' represents the freezing status due to NAV

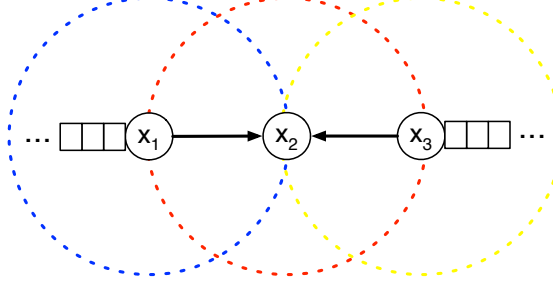


**Figure 4.11:** A 3-node network scenario with hidden terminal.

**Table 4.9:** Non-Trivial Transition Probabilities for  $x_1$

$\textcircled{1}_a$	$x_1$ detects a quiet channel while back-off
$\textcircled{1}_d$	$x_1$ overhears a CTS while back-off
$\textcircled{9}_a$	RTS sent from $x_1$ succeeds
$\textcircled{9}_b$	RTS sent from $x_1$ fails

**Table 4.10:** Non-Trivial Transition Probabilities for  $x_2$

$\textcircled{1}_a$	$x_2$ detects a quiet channel while idle
$\textcircled{1}_b$	$x_2$ detects a RTS while idle
$\textcircled{1}_e$	$x_2$ detects a busy channel while idle
$\textcircled{2}_a$	$x_2$ receives RTS correctly
$\textcircled{2}_b$	$x_2$ detects a collision while receiving RTS
$\textcircled{8}_a$	$x_2$ detects the channel is clear
$\textcircled{8}_b$	$x_2$ detects the channel is still busy

For node  $x_2$ , we have

$$P_{1a}^{x_2}(t_n) = \prod_{x_\alpha \in \{x_1, x_3\}} \mathcal{P}_{x_\alpha}^{x_\alpha} \left( \frac{\sum_{\chi=B, k \neq 0} + \sum_{\chi=W}}{\sum_{\chi \in \{B, W\}}} \right) \quad (4.3.4.5)$$

$$P_{1b}^{x_2 x_1}(t_n) = \mathcal{P}_{x_1}^{x_1} \left( \frac{\sum_{\chi=B, k=0, y=x_2}}{\sum_{\chi \in \{B, W\}}} \right) \mathcal{P}_{x_3}^{x_3} \left( \frac{\sum_{\chi=B, k \neq 0} + \sum_{\chi=W}}{\sum_{\chi \in \{B, W\}}} \right) \quad (4.3.4.6)$$

$$P_{1b}^{x_2x_3}(t_n) = \mathcal{P}_{\frac{x_3}{x_3}} \left( \frac{\sum_{\chi=B, k=0, y=x_2}}{\sum_{\chi \in \{B, W\}}} \right) \mathcal{P}_{\frac{x_1}{x_1}} \left( \frac{\sum_{\chi=B, k \neq 0} + \sum_{\chi=W}}{\sum_{\chi \in \{B, W\}}} \right) \quad (4.3.4.7)$$

$$P_{1e}^{x_2}(t_n) = 1 - P_{1a}^{x_2}(t_n) - P_{1b}^{x_2x_1}(t_n) - P_{1b}^{x_2x_3}(t_n) \quad (4.3.4.8)$$

$$P_{2a}^{x_2x_1}(t_n) = \mathcal{P}_{\frac{x_3}{x_3}} \left( \frac{\sum_{\chi=B, k \neq 0} + \sum_{\chi=W}}{\sum_{\chi \in \{B, W\}}} \right) \quad (4.3.4.9)$$

$$P_{2b}^{x_2x_1}(t_n) = 1 - P_{2a}^{x_2x_1}(t_n) \quad (4.3.4.10)$$

$$P_{2a}^{x_2x_3}(t_n) = \mathcal{P}_{\frac{x_1}{x_1}} \left( \frac{\sum_{\chi=B, k \neq 0} + \sum_{\chi=W}}{\sum_{\chi \in \{B, W\}}} \right) \quad (4.3.4.11)$$

$$P_{2b}^{x_2x_3}(t_n) = 1 - P_{2a}^{x_2x_3}(t_n) \quad (4.3.4.12)$$

$$P_{8a}^{x_2}(t_n) = \mathcal{P}_{\frac{x_1 \times x_3}{x_1 \times x_3}} \left( \frac{\sum_{\Omega_{8a}([U_{0,0,0}^{(\emptyset,0)}]_{x_2}; x_1, x_3)}}{\sum_{\Omega([U_{0,0,0}^{(\emptyset,0)}]_{x_2}; x_1, x_3)}} \right) \quad (4.3.4.13)$$

$$P_{8b}^{x_2}(t_n) = 1 - P_{8a}^{x_2}(t_n) \quad (4.3.4.14)$$

where  $\Omega([U_{0,0,0}^{(\emptyset,0)}]_{x_2}; x_1, x_3)$  represents

$$\begin{aligned} & \{\mathcal{H}_{x_1}(t_n) | \chi_{x_1} \in \{R_{\vec{x}_2}, A_{\vec{x}_2}\}\} \times \{\mathcal{H}_{x_3}(t_n) | \chi_{x_3} \notin \{C_{\vec{x}_2}, C_{\overline{x}_2}\}\} \\ & \cup \{\mathcal{H}_{x_3}(t_n) | \chi_{x_3} \in \{R_{\vec{x}_2}, A_{\vec{x}_2}\}\} \times \{\mathcal{H}_{x_1}(t_n) | \chi_{x_1} \notin \{C_{\vec{x}_2}, C_{\overline{x}_2}\}\} \end{aligned}$$

and  $\Omega_{8a}([U_{0,0,0}^{(\emptyset,0)}]_{x_2}; x_1, x_3)$  stands for

$$\begin{aligned} & \{\mathcal{H}_{x_1}(t_n) \in \Omega([U_{0,0,0}^{(\emptyset,0)}]_{x_2}; x_1) | j_{x_1} = 0\} \times \{\mathcal{H}_{x_3}(t_n) \in \Omega([U_{0,0,0}^{(\emptyset,0)}]_{x_2}; x_1, x_3) | \\ & \quad (\chi_{x_3}, j_{x_3}) \notin \{(R_{\vec{x}_2}, 1), (A_{\vec{x}_2}, j)\}, j \neq 0, (\chi_{x_3}, k_{x_3}) \neq (B, 0)\} \\ & \cup \{\mathcal{H}_{x_3}(t_n) \in \Omega([U_{0,0,0}^{(\emptyset,0)}]_{x_2}; x_3) | j_{x_3} = 0\} \times \{\mathcal{H}_{x_1}(t_n) \in \Omega([U_{0,0,0}^{(\emptyset,0)}]_{x_2}; x_3, x_1) | \\ & \quad (\chi_{x_1}, j_{x_1}) \notin \{(R_{\vec{x}_2}, 1), (A_{\vec{x}_2}, j)\}, j \neq 0, (\chi_{x_1}, k_{x_1}) \neq (B, 0)\} \end{aligned}$$

The equilibrium equations for  $x_1$  as  $t_n \rightarrow \infty$  are

$$\pi[B_{i,0,0}^{(x_2,\infty)}]_{x_1} = p_{1a}^{x_1} \pi[B_{i,1,0}^{(x_2,\infty)}]_{x_1} \quad (4.3.4.15)$$

$$\pi[B_{i,k,0}^{(x_2,\infty)}]_{x_1} = \begin{cases} p_{1a}^{x_1} \pi[B_{i,k+1,0}^{(x_2,\infty)}]_{x_1} + (1 - p_{1a}^{x_1}) \pi[B_{i,k,0}^{(x_2,\infty)}]_{x_1}, & 0 < k < 2^i * 3 \\ (1 - p_{1a}^{x_1}) \pi[B_{i,2^i w,0}^{(x_2,\infty)}]_{x_1}, & k = 2^i * 3 \end{cases}$$

$$+ \begin{cases} \frac{1}{2^i * 3} p_{9b}^{x_1 x_2} \pi[B_{i-1,0,0}^{(x_2,\infty)}]_{x_1}, & i > 0, k \neq 0 \\ \frac{1}{3} (p_{9a}^{x_1 x_2} \sum_{i=0}^{m-1} \pi[B_{i,0,0}^{(x_2,\infty)}]_{x_1} + \pi[B_{m,0,0}^{(x_2,\infty)}]_{x_1}), & i = 0, k \neq 0 \end{cases} \quad (4.3.4.16)$$

$$\pi[D_{x_2/i,k,0}^{(x_2,\infty)}]_{x_1} = \dots = \pi[D_{x_2/i,k,7}^{(x_2,\infty)}]_{x_1} = \pi[C_{x_2/i,k,0}^{(x_2,\infty)}]_{x_1} = \pi[C_{x_2/i,k,1}^{(x_2,\infty)}]_{x_1} = p_{1d}^{x_1 x_2} \pi[B_{i,k,0}^{(x_2,\infty)}]_{x_1} \quad (4.3.4.17)$$

$$\pi[A_{x_2^2/0,0,0}^{(x_2,\infty)}]_{x_1} = \dots = \sum_{i=0}^m \pi[C_{x_2^2/i,0,1}^{(x_2,\infty)}]_{x_1} = \sum_{i=0}^m p_{9a}^{x_1 x_2} \pi[R_{x_2^2/i,0,0}^{(x_2,\infty)}]_{x_1} = \dots = \sum_{i=0}^m p_{9a}^{x_1 x_2} \pi[B_{i,0,0}^{(x_2,\infty)}]_{x_1} \quad (4.3.4.18)$$

$$\pi[W_{i,0,0}^{(x_2,\infty)}]_{x_1} = \dots = \pi[W_{i,0,2}^{(x_2,\infty)}]_{x_1} = p_{9b}^{x_1 x_2} \pi[R_{x_2^2/i,0,0}^{(x_2,\infty)}]_{x_1} = \dots = p_{9b}^{x_1 x_2} \pi[B_{i,0,0}^{(x_2,\infty)}]_{x_1} \quad (4.3.4.19)$$

The equilibrium equations for the receiver  $x_2$  follows (4.2.4.1), (4.2.4.6), (4.2.4.7):

$$\pi[I_{0,0,0}^{(\emptyset,0)}]_{x_2} = \frac{1}{1 - p_{1a}^{x_2}} (p_{8a}^{x_2} \pi[U_{0,0,0}^{(\emptyset,0)}]_{x_2} + \pi[A_{x_1/0,0,0}^{(\emptyset,0)}]_{x_2} + \pi[A_{x_3/0,0,0}^{(\emptyset,0)}]_{x_2}) \quad (4.3.4.20)$$

$$\pi[A_{x_1/0,0,0}^{(\emptyset,0)}]_{x_2} = \dots = \pi[R_{x_1/0,0,0}^{(\emptyset,0)}]_{x_2} = p_{2a}^{x_2 x_1} \pi[R_{x_1/0,0,1}^{(\emptyset,0)}]_{x_2} = p_{2a}^{x_2 x_1} p_{1b}^{x_2 x_1} \pi[I_{0,0,0}^{(\emptyset,0)}]_{x_2}$$

$$\pi[A_{x_3/0,0,0}^{(\emptyset,0)}]_{x_2} = \dots = \pi[R_{x_3/0,0,0}^{(\emptyset,0)}]_{x_2} = p_{2a}^{x_2 x_3} \pi[R_{x_3/0,0,1}^{(\emptyset,0)}]_{x_2} = p_{2a}^{x_2 x_3} p_{1b}^{x_2 x_3} \pi[I_{0,0,0}^{(\emptyset,0)}]_{x_2} \quad (4.3.4.21)$$

$$\pi[U_{i,k,0}^{(y,\infty)}]_{x_1} = \frac{1}{p_{8a}^{x_2}} (p_{1e}^{x_2} \pi[I_{0,0,0}^{(\emptyset,0)}]_{x_2} + p_{8b}^{x_2 x_1} \pi[R_{x_1/0,0,1}^{(\emptyset,0)}]_{x_2} + p_{8b}^{x_2 x_3} \pi[R_{x_3/0,0,1}^{(\emptyset,0)}]_{x_2}) \quad (4.3.4.22)$$

Finally, using the symmetric conditions

$$\pi[\chi_{i,k,j}^{(x_2,\infty)}]_{x_1} = \pi[\chi_{i,k,j}^{(x_2,\infty)}]_{x_3} \quad (4.3.4.23)$$

for any  $i, k, \chi, j$ , and the normalization conditions

$$\sum_{i,k,\chi,j} \pi[\chi_{i,k,j}^{(x_2,\infty)}]_{x_1} = \sum_{i,k,\chi,j} \pi[\chi_{i,k,j}^{(\emptyset,0)}]_{x_2} = \sum_{i,k,\chi,j} \pi[\chi_{i,k,j}^{(x_2,\infty)}]_{x_3} = 1 \quad (4.3.4.24)$$

we form a non-linear system by combining equations (4.3.4.1) - (4.3.4.22). The initial conditions for  $x_1$  are similar to the settings in Section 4.3.2. For  $x_2$ , we have

$$P^{(0)}[\chi_{0,0,j}]_{x_1} = \begin{cases} 1, & \chi = I \\ 0, & \text{otherwise} \end{cases}$$

and  $P_{1a}^{x_2}(0) = P_{2a}^{x_2x_1}(0) = P_{2a}^{x_2x_3}(0) = P_{8a}^{x_2}(0) = 1$  while the remaining non-trivial transition probabilities are initialized as 0.

The plots in Figure 4.12 and 4.13 show the difference between analytical results and QualNet simulations for  $x_1$  and  $x_2$  respectively. When RTS retransmission limit ( $m$ ) is 0, it is possible to construct the stochastic joint state model of  $x_1$ ,  $x_2$  and  $x_3$  similar to the 2-node scenario in Section 4.3.2. We omit the diagram of the model since the structure of transitions is complex, instead, we give the corresponding equilibrium solutions shown by the red bar. As expected, the joint model accurately predicts the behaviors of DCF. For the non-linear system, we observe some significant deviation mainly due to the product approximation approach as we bring closure to the system. In particular, the nonlinear model underestimates the collision rate of RTS. However, as the complexity of the system increases, *i.e.*  $m = 1, 2$ , the results improve.

#### 4.4 Conclusion and Future Work

In this chapter, we have introduced a new Markov model for the IEEE 802.11 Distributed Coordination Function (DCF), a central mechanism of our wireless infrastructure. Our Markov model does not rely upon the assumption that collision probabilities on each node are constant or independent of network topology. Instead, we have developed a detailed model of interconnected node states including multiple back-off stages and binary exponential back-off counters to capture the dominant first order effects of nodes' responses to contention. The model is complex, but it is necessarily so, and it is not so elaborate that it cannot be analyzed. Using the model, we have calculated stationary node states for two and three node networks including a configuration that includes a hidden terminal with varying numbers of back-off stages.

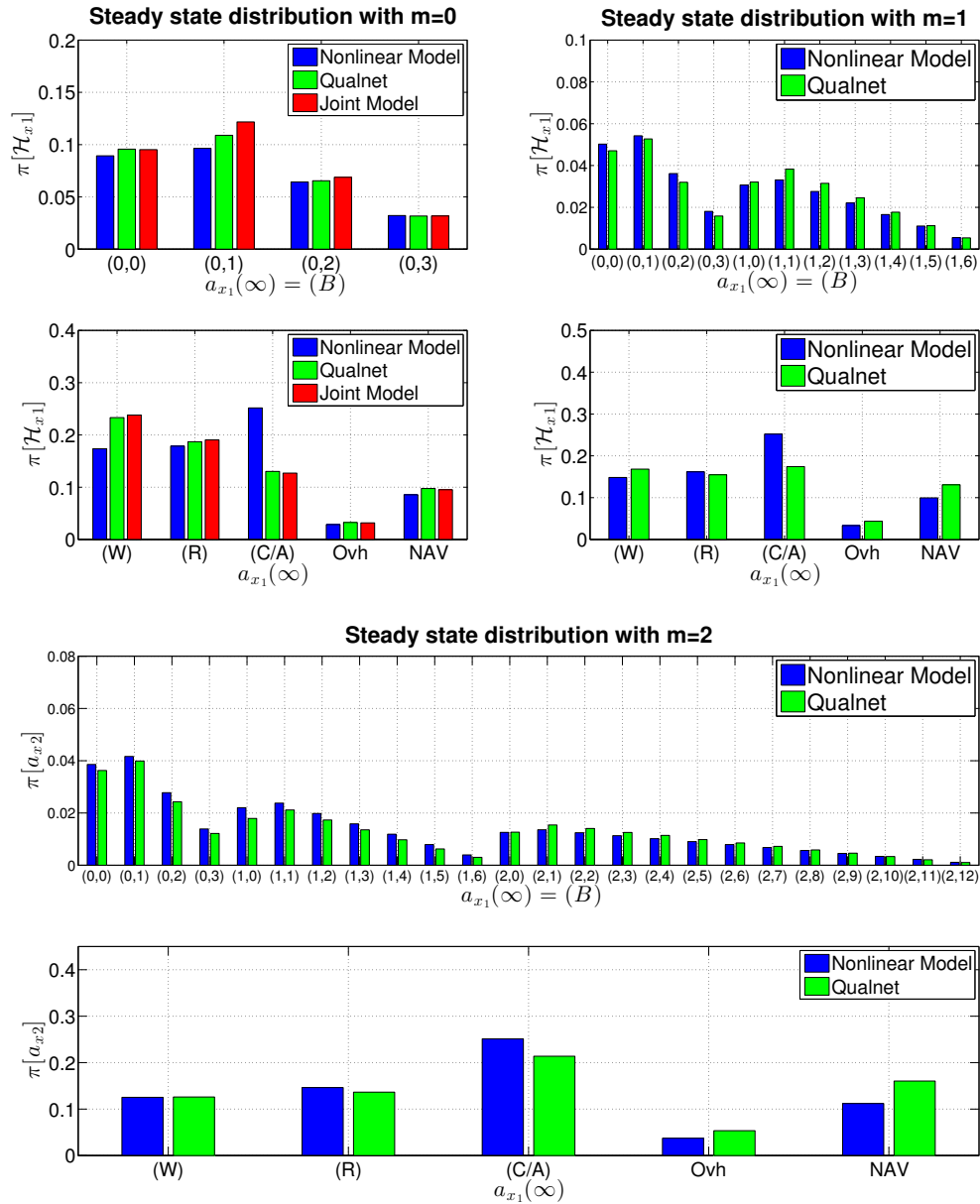


**Figure 4.12:** Comparison of steady state probabilities at  $x_1$ : the tuples denote (back-off stage, back-off counter); 'R' denotes status of sending RTS packets; 'C/A' combines states of sending CTS/ receiving DATA; 'Ovh' denotes overhearing CTS; 'NAV' represents the freezing status due to NAV from CTS

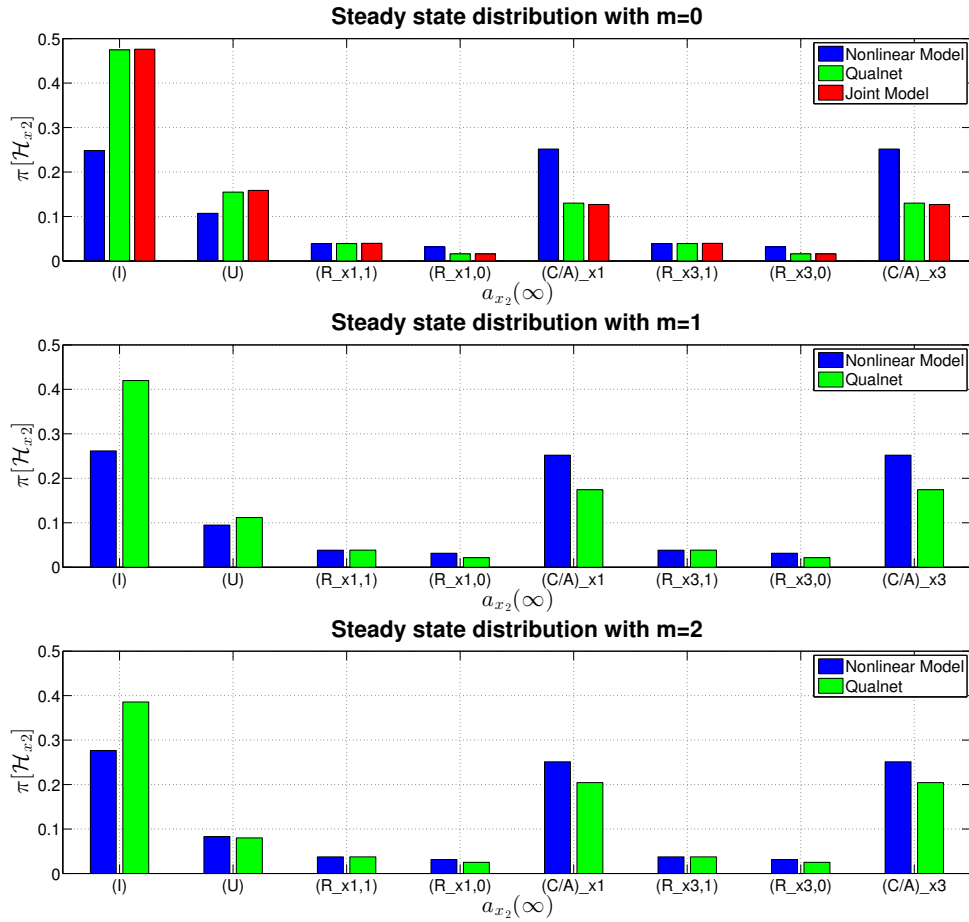


**Figure 4.13:** Comparison of steady state probabilities at  $x_2$ : 'I' represents the idle status; 'U' represents the freezing status due to busy channel; the tuples represent the 1st step or last step of receiving RTS from  $x_1$  or  $x_3$ ; '(C/A)' combines states of receiving CTS/ sending DATA from/to  $x_1$  or  $x_3$

To determine the transition probabilities for steady-state calculations we approximate the joint probability densities with marginal probability densities using a product approximation. While this only uses a small subset of the information available in the network description, we find it sufficient to achieve excellent agreement with realistic simulations of network traffic.

In the future, we will continue to assess the quality of our DCF model through comprehensive analysis on other aspects of the protocol performance such as throughput, delay and packet drop rates. We will also move forward by combining our DCF model and previous BARP model into an unified analytic framework that would rigorously characterize the nonlinear dynamics of ant-based routing algorithms on WLANs given network topology and protocols parameters.

## Chapter 5

### CONCLUSIONS AND FUTURE WORK

In this thesis, we have introduced a dynamic routing exponent strategy to improve ant-based protocols, analyzed the integrated behaviors of ant-based routing with medium access control based on the investigations of MACA protocol in a variety of wireless topologies, and further developed a detailed probabilistic model for IEEE 802.11 Distributed Coordination Functions.

The first chapter has been focused on the mathematical analysis and simulation studies for an analytic framework that was formulated in [59] for ant-based routing protocols. In these protocols, there are a number of key parameters that control the deposition and evaporation of pheromone as well as the exploratory routing of the ants. In particular, the routing exponent  $\beta$  controls the forwarding patterns of the ants, and deposition number  $\Lambda$  balances the evaporation and deposition of pheromone value over the entire network. The previous efforts of a small wired network completely described the nonlinear dynamics of pheromone level over each link. From the description, we observe that  $\beta$  controls the stability of the system, and more importantly, stable multi-route solutions for  $\beta = 0.5$  are dynamically connected to stable single-route solutions for  $\beta = 2$ . These stable single-route solutions correspond to the paths that have the minimum hop count. Based on the observation, we propose a new strategy to improve routing performance of BARP by initially letting  $\beta$  be 0.5 and changing it continuously in time until  $\beta = 2$ . Using simulations in both Matlab and QualNet, we find exactly consistent results to the previous rigorous analysis on the same simple wired network. Then, we leverage these principles to a 50-node network and successfully show the effectiveness of the dynamic  $\beta$  strategy in obtaining optimal or near optimal hop numbers from the source to the destination via Matlab and

QualNet simulations. Specifically, a large series of experiments with random initial pheromone values demonstrates an increase in the frequency of achieving optimal hop count of more than 70% when using dynamic  $\beta$  instead of static  $\beta = 2$ . We also explore the impact of pheromone deposition number  $\Lambda$ . Although large  $\Lambda$  has been shown to impair the performance of the dynamic  $\beta$  algorithm, for moderate  $\Lambda$  our new routing protocol still outperforms the tradition ant-based routing methods in terms of average hop count for stable single-route solution.

In chapter 3, we have examined several basic MAC schemes for wireless networks. We have employed a Markov chain analysis to correctly predict network performance under wireless MAC protocol MACA in a typical 2-node scenario with the present of hidden terminals. We also generalize the proposed Markovian framework to a 3-node wireless topology and implement a Monte Carlo method to approximate transition probabilities when the direct computing becomes difficult. For the second part of this chapter, we have made the first modest effort to rigorously characterize the behaviors of ant-based routing algorithm on wireless LANs. The previous analytic framework of BARP is incorporated with the Markov model of MACA on a simple wireless topology that contains two paths from source to destination. We assess the integration model via comparisons of equilibrium solutions that obtained from numerical solver using Matlab and realistic simulations using QualNet, respectively. Close correspondences are found. In the last section of chapter 3, we have implemented a statistical study using linear regression to evaluate the MACA performance of data delivery ratio on wireless multi-hop ring topologies. Distinct from the Markovian approaches, we avoid the intricate characterization of MACA operations and rely on the regression coefficients to capture all the protocol details. Based on the results derived from the datasets simulated by QualNet, we identify three types of contending transmission pairs that interfere with data delivery the most on a simple 5-node ring. Furthermore, we have shown that the reduced linear model using only significant regressors correctly predicts packet delivery ratio on ring topologies with size 6 and 8.

Finally, in chapter 4, we develop a new discrete time Markov model for the

Distributed Coordination Function (DCF) in IEEE 802.11 standard for WLANs. The model is derived from the detailed descriptions of the DCF where each node behaves as a multi-dimensional stochastic process with intertwined Markov states. The tuples of back-off states including multiple stages and binary exponential counters capture the dominant first order effects of nodes' responses to contention, and the discrete transition events at each node are determined locally by joint behaviors of neighboring nodes. For steady-state computations, we approximate the joint probability densities with marginal probability densities using a product approximation. To validate the model, we have calculated the steady state probability distribution with different back-off stages in three representative scenarios. Comparing with results from realistic simulations, we find very close correspondences in both 2-nodes and 3-nodes examples without hidden terminals. For the configuration that contains a hidden terminal, we observe an underestimation on the packet collision rates since the model only uses a small subset of the information available in the network description. However, the results improve as the complexity of the system increases. We find the model achieves excellent agreement with realistic simulations of network traffic.

## BIBLIOGRAPHY

- [1] IEEE Standards for Local Area Networks: Carrier Sense Multiple Access With Collision Detection (CSMA/CD) Access Method and Physical Layer Specifications. *ANSI/IEEE Std 802.3-1985*, pages 0-1-, 1985.
- [2] QualNet 5.0.2 User's Guide. *Scalable Network Technologies, Inc.*, page 388, March 2010.
- [3] IEEE Standard for Local and metropolitan area networks, Part 11: Wireless LAN Medium Access Control (MAC) and Physical Layer (PHY) Specifications. *IEEE Std 802.11-2012*, 2012.
- [4] Norman Abramson. THE ALOHA SYSTEM: another alternative for computer communications. *Proceedings of the November 17-19, 1970, fall joint . . .*, pages 281–286, 1970.
- [5] Eitan Altman, Pierre Bernhard, and Alonso Silva. The Mathematics of Routing in Massively Dense Ad-Hoc Networks. In David Coudert, David Simplot-Ryl, and Ivan Stojmenovic, editors, *Proceedings of the 7th International Conference on Ad-hoc, Mobile and Wireless Network*, volume 5198 of *Lecture Notes in Computer Science*, pages 122–134, Berlin, Heidelberg, September 2008. Springer Berlin Heidelberg.
- [6] Nigel Bean and Andre Costa. An analytic modelling approach for network routing algorithms that use “ant-like” mobile agents. *Computer Networks*, 49(2):243–268, 2005.
- [7] Giuseppe Bianchi. Performance analysis of the IEEE 802.11 distributed coordination function. *Selected Areas in Communications, IEEE Journal on*, 18(3):535–547, 2000.
- [8] Eric Bonabeau, Marco Dorigo, and Guy Theraulaz. *Swarm Intelligence – From Natural to Artificial Systems*. Oxford University Press, New York, NY, 1999.
- [9] Sandro Bosio, Andreas Eisenbltter, Hans-Florian Geerdes, Iana Siomina, and Di Yuan. Mathematical optimization models for wlan planning. In Arie Koster and Xavier Muñoz, editors, *Graphs and Algorithms in Communication Networks*, Texts in Theoretical Computer Science. An EATCS Series, pages 283–309. Springer Berlin Heidelberg, 2010.

- [10] DT Brown. A note on approximations to discrete probability distributions. *Information and Control*, 392:386–392, 1959.
- [11] G D Caro and M Dorigo. AntNet: A mobile agents approach to adaptive routing, 1997.
- [12] S Corson and J Macker. Mobile Ad hoc Networking (MANET): Routing Protocol Performance Issues and Evaluation Considerations. *Computing Systems*, 54:1–12, 1999.
- [13] Lin Dai and Xinghua Sun. A unified analysis of IEEE 802.11 DCF networks: Stability, throughput, and delay. *Mobile Computing, IEEE Transactions on*, 12(8):1558–1572, 2013.
- [14] F. Daneshgaran, M. Laddomada, F. Mesiti, and M. Mondin. Unsaturated Throughput Analysis of IEEE 802.11 in Presence of Non Ideal Transmission Channel and Capture Effects. *IEEE Transactions on Wireless Communications*, 7(4):1276–1286, April 2008.
- [15] G. Di Caro and M. Dorigo. AntNet: Distributed Stigmergetic Control for Communications Networks. *Journal of Artificial Intelligence Research*, 9:317–365, 1998.
- [16] G. Di Caro, F. Ducatelle, and L.M. Gambardella. AntHocNet: An Adaptive Nature-Inspired Algorithm for Routing in Mobile Ad Hoc Networks. *European Transactions on Telecommunications, Special Issue on Self-organization in Mobile Networking*, 16(5):443–455, October 2005.
- [17] F. Ducatelle, G. Di Caro, and L.M. Gambardella. Principles and applications of swarm intelligence for adaptive routing in telecommunications networks. *Swarm Intelligence*, 4(3):in press, 2010.
- [18] Frederick Ducatelle. *Adaptive routing in ad hoc wireless multi-hop networks*. Ph.d. thesis, Università della Svizzera Italiana (USI), 2007.
- [19] CH Foh and JW Tantra. Comments on IEEE 802. 11 saturation throughput analysis with freezing of backoff counters. *IEEE Communications Letters*, 9(2):130–132, 2005.
- [20] Sergey Foss, Seva Shneer, and Andrey Tyurlikov. Stability of a Markov-modulated Markov chain, with application to a wireless network governed by two protocols. *Stochastic Systems*, 2(1):208–231, 2012.
- [21] CL Fullmer and JJ Garcia-Luna-Aceves. Floor acquisition multiple access (FAMA) for packet-radio networks. In *SIGCOMM '95 Proceedings of the conference on Applications, technologies, architectures, and protocols for computer communication*, pages 262–273, 1995.

- [22] Michele Garetto, Theodoros Salonidis, and Edward W. Knightly. Modeling per-flow throughput and capturing starvation in CSMA multi-hop wireless networks. *IEEE/ACM Transactions on Networking*, 16:864–877, 2008.
- [23] Michele Garetto, Jingpu Shi, and Edward W. Knightly. Modeling media access in embedded two-flow topologies of multi-hop wireless networks. In *Proceedings of the 11th annual international conference on Mobile computing and networking - MobiCom '05*, page 200, New York, New York, USA, August 2005. ACM Press.
- [24] Fabrice Guillemin, Charles Knessl, and Johan S H van Leeuwen. Wireless Multihop Networks with Stealing: Large Buffer Asymptotics via the Ray Method. *SIAM Journal on Applied Mathematics*, 71(4):1220–1240, January 2011.
- [25] M. Gunes, U. Sorges, and I. Bouazizi. ARA-the ant-colony based routing algorithm for MANETs. In *Proceedings. International Conference on Parallel Processing Workshop*, 2002.
- [26] Z. Hadzi-Velkov and B. Spasenovski. Saturation throughput - delay analysis of IEEE 802.11 DCF in fading channel. In *IEEE International Conference on Communications, 2003. ICC '03.*, volume 1, pages 121–126. IEEE, 2003.
- [27] Jaehyuk Choi, Joon Yoo, and Chong-Kwon Kim. A novel performance analysis model for an IEEE 802.11 wireless LAN. *IEEE Communications Letters*, 10(5):335–337, May 2006.
- [28] Beakcheol Jang and Mihail L. Sichitiu. IEEE 802.11 saturation throughput analysis in the presence of hidden terminals. *IEEE/ACM Transactions on Networking*, 20:557–570, 2012.
- [29] David B. Johnson and David A Maltz. Dynamic Source Routing in Ad Hoc Wireless Networks. In *Mobile Computing*, volume 353, pages 153–181. 1996.
- [30] Phil Karn. MACA-a new channel access method for packet radio. In *ARRLCRRL Amateur radio 9th computer networking conference*, volume 140, pages 1–5, 1990.
- [31] HP Keeler and PG Taylor. A STOCHASTIC ANALYSIS OF A GREEDY ROUTING SCHEME IN SENSOR NETWORKS. *SIAM Journal on Applied Mathematics*, 70(7):2214–2238, 2010.
- [32] L Kleinrock and F Tobagi. Packet Switching in Radio Channels: Part I—Carrier Sense Multiple-Access Modes and Their Throughput-Delay Characteristics. *IEEE Transactions on Communications*, 23(12):1400–1416, December 1975.
- [33] Leonard Kleinrock. *Theory, Volume 1, Queueing Systems*. Wiley-Interscience, 1975.

- [34] James F. Kurose and Keith Ross. *Computer Networking: A Top-Down Approach*. Pearson, 6th edition, 2012.
- [35] II Lewis. Approximating probability distributions to reduce storage requirements. *Information and control*, 225:214–225, 1959.
- [36] S.P. Meyn and R.L. Tweedie, editors. *Markov chains and stochastic stability*. Springer-Verlag, London, 1993.
- [37] I Mustapha, JD Jiya, and BU Musa. Modeling and Analysis of Collision Avoidance MAC Protocol in Multi-Hop Wireless Ad-Hoc Network. *International Journal of Communication Networks and Information Security (IJCNIS)*, 3(1):48–56, 2011.
- [38] Roger McHaney Nurul. I. Sarkar. Modeling and Simulation of IEEE 802 . 11 WLANS : A Case Study of a Network Simulator. In *Information Resources Management Association International Conference*, 2006.
- [39] CE Perkins and EM Royer. Ad-hoc on-demand distance vector routing. In *Mobile Computing Systems and Applications, 1999. Proceedings. WMCSA '99. Second IEEE Workshop on*, pages 90–100, 1999.
- [40] Adam Petcher. Qos in wireless data networks, 2006. [http://www.cse.wustl.edu/~jain/cse574-06/ftp/wireless\\_qos](http://www.cse.wustl.edu/~jain/cse574-06/ftp/wireless_qos).
- [41] Neeli Prasad and Anand Prasad, editors. *WLAN Systems and Wireless IP for Next Generation Communications*. Artech House, Inc., Norwood, MA, USA, 2002.
- [42] Punyaslok Purkayastha and John S. Baras. Convergence results for ant routing algorithms via stochastic approximation and optimization. In *Proceedings of the 46th IEEE Conference on Decision and Control*, pages 340–345, Piscataway, NJ, December 12-14 2007. IEEE.
- [43] S. Rajagopalan and C.-C. Shen. ANSI: A Swarm Intelligence-based Unicast Routing Protocol for Hybrid Ad hoc Networks. *Journal of System Architecture, Special issue on Nature Inspired Applied Systems*, 52(8-9):485–504, August-September 2006.
- [44] Theodore Rappaport. *Wireless Communications: Principles and Practice*. Prentice Hall PTR, Upper Saddle River, NJ, USA, 2nd edition, 2001.
- [45] Saikat Ray. On false blocking in RTS/CTS-based multihop wireless networks. *Technology, IEEE Transactions on*, 56(2):849–862, 2007.
- [46] Saikat Ray and JB Carruthers. Evaluation of the masked node problem in ad hoc wireless lans. *Mobile Computing, IEEE*, 4(5):430–442, 2005.
- [47] LG Roberts. ALOHA packet system with and without slots and capture. *ACM SIGCOMM Computer Communication Review*, 1975.

- [48] Martin Roth. The Markovian termite: A soft routing framework. In *Proceedings of the 2007 IEEE Swarm Intelligence Symposium (SIS)*, Piscataway, NJ, April 1-5 2007. IEEE.
- [49] Martin Roth and Stephen Wicker. Asymptotic pheromone behavior in swarm intelligent MANETs. In *Proceedings of the Sixth IFIP/IEEE International Conference on Mobile and Wireless Communication Networks*, pages 335–346, Boston, MA, October 25-27 2004. Springer Boston.
- [50] Muhammad Saleem and Muddassar Farooq. A framework for empirical evaluation of nature inspired routing protocols for wireless sensor networks. In *Proceedings of the IEEE Congress on Evolutionary Computing*, pages 751–758, Piscataway, NJ, September 25-28 2007. IEEE.
- [51] Muhammad Saleem, Syed Khayam, and Muddassar Farooq. Formal modeling of BeeAdHoc: A bio-inspired mobile ad hoc network routing protocol. In *6th international conference on Ant Colony Optimization and Swarm Intelligence*, pages 315–322, Berlin, Germany, 2008. Springer-Verlag.
- [52] Muhammad Saleem, Syed Khayam, and Muddassar Farooq. A formal performance modeling framework for bio-inspired ad hoc routing protocols. In *ACM Genetic and Evolutionary Computation Conference (GECCO)*, pages 103–110, New York, NY, July 2008. ACM.
- [53] Rimli Sengupta Samir R. Das, Robert Castañeda, Jiangtao Yan. Comparative Performance Evaluation of Routing Protocols for Mobile, Ad hoc Networks. In *Mobile Networks and Applications*, pages 153—161, 1998.
- [54] R. Schoonderwoerd, O. E. Holland, J. L. Bruten, and L. J. M. Rothkrantz. Ant-Based Load Balancing in Telecommunications Networks. *Adaptive Behavior*, 5:169–207, 1997.
- [55] Zhefu Shi, Cory Beard, and Ken Mitchell. Analytical models for understanding space, backoff, and flow correlation in CSMA wireless networks. *Wireless Networks*, 19(3):393–409, July 2012.
- [56] J. M. Sobrinho, J. L., De Haan, R., Brázio. Why RTS-CTS is not your ideal wireless LAN multiple access protocol. *IEEE Wireless Communications and Networking Conference, WCNC*, 1:81–87, 2005.
- [57] Ilenia Tinnirello, Giuseppe Bianchi, and Yang Xiao. Refinements on IEEE 802.11 distributed coordination function modeling approaches. *IEEE Transactions on Vehicular Technology*, 59(3):1055–1067, 2010.
- [58] F Tobagi and L Kleinrock. Packet Switching in Radio Channels: Part II—The Hidden Terminal Problem in Carrier Sense Multiple-Access and the Busy-Tone

- Solution. *IEEE Transactions on Communications*, 23(12):1417–1433, December 1975.
- [59] Claudio E. Torres, Louis F. Rossi, Jeremy Keffer, Ke Li, and Chien-Chung Shen. Modeling, analysis and simulation of ant-based network routing protocols. *Swarm Intelligence*, 4(3):221–244, July 2010.
- [60] Athanasia Tsertou and D.I. Laurenson. Revisiting the Hidden Terminal Problem in a CSMA/CA Wireless Network. *IEEE Transactions on Mobile Computing*, 7(7):817–831, July 2008.
- [61] Roberto Dieguez Virgilio J. Martins, Ferreira Filho. A Survey of Computer network Design. *Investigacion Operativa*, 4(3):183–211, 1994.
- [62] Zhigang Wang, Lichuan Liu, and MengChu Zhou. Space and network diversity combination for masked node collision resolution in wireless ad hoc network. *IEEE Transactions on Wireless Communications*, 6:478–485, 2007.
- [63] Haitao Wu, Yong Peng, and Keping Long. Performance of reliable transport protocol over IEEE 802.11 wireless LAN: analysis and enhancement. *Proceedings of the 21st Annual Joint Conference of the IEEE Computer and Communications Societies*, 2:599–607, 2002.
- [64] Haitao Wu, Fan Zhu, Qian Zhang, and Zhisheng Niu. WSN02-1: Analysis of IEEE 802.11 DCF with Hidden Terminals. *IEEE Globecom 2006*, pages 2–6, 2006.
- [65] Joon-Hyuk Yoo, Richard J. La, and Armand M. Makowski. Convergence results for ant routing. In *Conf. Info. Sci. and Systems*, Piscataway, NJ, 2004. IEEE.
- [66] S. Zahid, M. Shahzad, S.U. Ali, and M. Farooq. A comprehensive formal framework for analyzing the behavior of nature-inspired routing protocols. In *Evolutionary Computation, 2007. CEC 2007. IEEE Congress on*, pages 180–187, Piscataway, NJ, September 25-28 2007. IEEE.
- [67] Hongqiang Zhai and Yuguang Fang. Performance of wireless LANs based on IEEE 802.11 MAC protocols. *Personal, Indoor and Mobile Radio Communications, 2003. {PIMRC} 2003.*, 3:2586–2590, 2003.
- [68] Eustathia Ziouva and Theodore Antonakopoulos. CSMA/CA performance under high traffic conditions: throughput and delay analysis. *Computer communications*, 25:313–321, 2002.
- [69] J.M. Zytkow. From Statistical Regularities to Concepts, Hierarchies, Equation Clusters and Rules. In Oliver J.J. Dowe D., Korb K.B., editor, *Information, Statistics and Induction in Science*, pages 269–280, Melbourne, Australia, 1996. World Scientific.

**Appendix A**  
**DERIVATION OF EQUATIONS**

Here, we show the stationary states of  $\tau_{ij}^{(n)}$  satisfy the system 2.2.0.7. First, given Taylor expansion

$$(1 - h_1 \kappa_1)^{(h_2/h_1)} = 1 - h_2 \kappa_1 + \frac{1}{2} \frac{h_2}{h_1} \left( \frac{h_2}{h_1} - 1 \right) (h_1 \kappa_1)^2 + \dots \quad (\text{A.0.0.1})$$

and the assumption for time intervals:  $h_1 < h_2$ , 2.2.0.6 can be expanded as follows:

$$\begin{aligned} \tau_{ij}^{(n+1)} &= (1 - h_1 \kappa_1)^{(h_2/h_1)} \tau_{ij}^{(n)} + h_2 \kappa_2 \sum_{k=1}^{\infty} \frac{1}{k^p} \tilde{p}_{ij}^{sd}(k) \\ &= \left( 1 - h_2 \kappa_1 + \frac{1}{2} \frac{h_2}{h_1} \left( \frac{h_2}{h_1} - 1 \right) (h_1 \kappa_1)^2 + \dots \right) \tau_{ij}^{(n)} + h_2 \kappa_2 \sum_{k=1}^{\infty} \frac{1}{k^p} \tilde{p}_{ij}^{sd}(k) \\ &= \tau_{ij}^{(n)} - h_2 \kappa_1 \tau_{ij}^{(n)} + \mathcal{O}(h_2^2) + h_2 \kappa_2 \sum_{k=1}^{\infty} \frac{1}{k^p} \tilde{p}_{ij}^{sd}(k) \\ &= \tau_{ij}^{(n)} + h_2 \left( \kappa_2 \sum_{k=1}^{\infty} \frac{1}{k^p} \tilde{p}_{ij}^{sd}(k) - \kappa_1 \tau_{ij}^{(n)} \right) + \mathcal{O}(h_2) \end{aligned} \quad (\text{A.0.0.2})$$

Now, move  $\tau_{ij}^{(n)}$  to the left and divide both sides of A.0.0.2 by  $h_2$ , we get

$$\frac{\tau_{ij}^{(n+1)} - \tau_{ij}^{(n)}}{h_2} = \kappa_2 \sum_{k=1}^{\infty} \frac{1}{k^p} \tilde{p}_{ij}^{sd}(k) - \kappa_1 \tau_{ij}^{(n)} + \mathcal{O}(h_2)$$

Taking the limit as  $h_2 \rightarrow 0$  and implementing the definition of derivative with respect to time, we have

$$\begin{aligned} \frac{d\tau_{ij}}{dt} &= \lim_{h_2 \rightarrow 0} \frac{\tau_{ij}^{(n+1)} - \tau_{ij}^{(n)}}{h_2} \\ &= \lim_{h_2 \rightarrow 0} \left( \kappa_2 \sum_{k=1}^{\infty} \frac{1}{k^p} \tilde{p}_{ij}^{sd}(k) - \kappa_1 \tau_{ij}^{(n)} \right) + \mathcal{O}(h_2) \\ &= \kappa_2 \sum_{k=1}^{\infty} \frac{1}{k^p} \tilde{p}_{ij}^{sd}(k) - \kappa_1 \tau_{ij}^{(n)} \end{aligned} \quad (\text{A.0.0.3})$$

If the dynamic system [2.2.0.6](#) is in equilibrium, we will observe  $\frac{d\tau_{ij}}{dt} = 0$ . Therefore, from [A.0.0.3](#) we conclude that the stationary pheromone distribution  $\tau_{ij}^{(n)}$  is governed by

$$\Lambda \tau_{ij}^{(n)} = \sum_{k=1}^{\infty} \frac{1}{k} \tilde{p}_{ij}^{sd}(k)$$

where  $\Lambda = \kappa_1/\kappa_2$ .

## Appendix B

### BALANCE EQUATIONS FOR STATIONARY JOINT STATES

Here we formulate the global balance equations deviated from the joint state diagram 4.7. For simplicity, we adopt the following notations to represent the limiting state probabilities.

$$\begin{aligned}
 B_{k_1 k_2} &= \lim_{n \rightarrow \infty} P^{(n)}([B_{0, k_1, 0}^{\langle x_2, \infty \rangle}]_{x_1}, [B_{0, k_2, 0}^{\langle x_1, \infty \rangle}]_{x_2}) \\
 W_j &= \lim_{n \rightarrow \infty} P^{(n)}([W_{0, 0, j}^{\langle x_2, \infty \rangle}]_{x_1}, [W_{0, 0, j}^{\langle x_1, \infty \rangle}]_{x_2}) \\
 R_j &= \lim_{n \rightarrow \infty} P^{(n)}([R_{\vec{x}_2/0, 0, j}^{\langle x_2, \infty \rangle}]_{x_1}, [R_{\vec{x}_1/0, 0, j}^{\langle x_1, \infty \rangle}]_{x_2}) \\
 \vec{\chi}_{kj} &= \lim_{n \rightarrow \infty} P^{(n)}([\chi_{\vec{x}_2/0, 0, j}^{\langle x_2, \infty \rangle}]_{x_1}, [\chi_{\vec{x}_1/0, k, j}^{\langle x_1, \infty \rangle}]_{x_2}), \quad \chi \in \{R, C, A\} \\
 \overleftarrow{\chi}_{kj} &= \lim_{n \rightarrow \infty} P^{(n)}([\chi_{\vec{x}_2/0, k, j}^{\langle x_2, \infty \rangle}]_{x_1}, [\chi_{\vec{x}_1/0, 0, j}^{\langle x_1, \infty \rangle}]_{x_2}), \quad \chi \in \{R, C, A\}
 \end{aligned}$$

The balance equations, known as *outward flux = inward flux at each state*, are concluded as follows:

$$B_{00} = B_{11} \tag{B.0.0.1}$$

$$B_{01} = B_{12} \tag{B.0.0.2}$$

$$B_{02} = B_{13} \tag{B.0.0.3}$$

$$B_{10} = B_{21} \tag{B.0.0.4}$$

$$B_{11} = B_{22} + \frac{1}{9}W_0 + \frac{1}{3}\vec{A}_{10} + \frac{1}{3}\overleftarrow{A}_{10} \tag{B.0.0.5}$$

$$B_{12} = B_{23} + \frac{1}{9}W_0 + \frac{1}{3}\vec{A}_{20} + \frac{1}{3}\overleftarrow{A}_{10} \tag{B.0.0.6}$$

$$B_{13} = \frac{1}{9}W_{00} + \frac{1}{3}\overleftarrow{A}_{10} \tag{B.0.0.7}$$

$$B_{20} = B_{31} \tag{B.0.0.8}$$

$$B_{21} = B_{32} + \frac{1}{9}W_0 + \frac{1}{3}\vec{A}_{10} + \frac{1}{3}\overleftarrow{A}_{20} \quad (\text{B.0.0.9})$$

$$B_{22} = B_{33} + \frac{1}{9}W_0 + \frac{1}{3}\vec{A}_{20} + \frac{1}{3}\overleftarrow{A}_{20} \quad (\text{B.0.0.10})$$

$$B_{23} = \frac{1}{9}W_0 + \frac{1}{3}\overleftarrow{A}_{20} \quad (\text{B.0.0.11})$$

$$B_{31} = \frac{1}{9}W_0 + \frac{1}{3}\vec{A}_{10} \quad (\text{B.0.0.12})$$

$$B_{32} = \frac{1}{9}W_0 + \frac{1}{3}\vec{A}_{20} \quad (\text{B.0.0.13})$$

$$B_{33} = \frac{1}{9}W_0 \quad (\text{B.0.0.14})$$

$$R_1 = B_{00} \quad (\text{B.0.0.15})$$

$$W_0 = W_1 = W_2 = R_0 = R_1 \quad (\text{B.0.0.16})$$

$$\vec{R}_{10} = \vec{R}_{11} = B_{01} \quad (\text{B.0.0.17})$$

$$\overleftarrow{C}_{10} = \overleftarrow{C}_{11} = \vec{R}_{10} \quad (\text{B.0.0.18})$$

$$\vec{A}_{10} = \vec{A}_{11} = \vec{A}_{12} = \vec{A}_{13} = \vec{A}_{14} = \vec{A}_{15} = \overleftarrow{C}_{10} \quad (\text{B.0.0.19})$$

$$\vec{R}_{20} = \vec{R}_{21} = B_{02} \quad (\text{B.0.0.20})$$

$$\overleftarrow{C}_{20} = \overleftarrow{C}_{21} = \vec{R}_{20} \quad (\text{B.0.0.21})$$

$$\vec{A}_{20} = \vec{A}_{21} = \vec{A}_{22} = \vec{A}_{23} = \vec{A}_{24} = \vec{A}_{25} = \overleftarrow{C}_{20} \quad (\text{B.0.0.22})$$

$$\overleftarrow{R}_{10} = \overleftarrow{R}_{11} = B_{10} \quad (\text{B.0.0.23})$$

$$\overrightarrow{C}_{10} = \overrightarrow{C}_{11} = \overleftarrow{R}_{10} \quad (\text{B.0.0.24})$$

$$\overleftarrow{A}_{10} = \overleftarrow{A}_{11} = \overleftarrow{A}_{12} = \overleftarrow{A}_{13} = \overleftarrow{A}_{14} = \overleftarrow{A}_{15} = \overrightarrow{C}_{10} \quad (\text{B.0.0.25})$$

$$\overleftarrow{R}_{20} = \overleftarrow{R}_{21} = B_{20} \quad (\text{B.0.0.26})$$

$$\overrightarrow{C}_{20} = \overrightarrow{C}_{21} = \overleftarrow{R}_{20} \quad (\text{B.0.0.27})$$

$$\overleftarrow{A}_{20} = \overleftarrow{A}_{21} = \overleftarrow{A}_{22} = \overleftarrow{A}_{23} = \overleftarrow{A}_{24} = \overleftarrow{A}_{25} = \overrightarrow{C}_{20} \quad (\text{B.0.0.28})$$

Here Equations [B.0.0.1](#) - [B.0.0.14](#) correspond to the transitions among backing off states while Equations [B.0.0.15](#) - [B.0.0.16](#) correspond to the state transitions when RTS collides. The successful transmission from  $x_1$  to  $x_2$  accounts for Equations [B.0.0.17](#) - [B.0.0.22](#) and that from  $x_2$  to  $x_1$  explains Equations [B.0.0.23](#) - [B.0.0.28](#). Together with

the conservation law of probabilities:

$$\sum_{k_1} \sum_{k_2} B_{k_1 k_2} + \sum_j W_j + \sum_{j'} R_{j'} + \sum_{\chi} \sum_k \sum_{j''} (\vec{\chi}_{k j''} + \overleftarrow{\chi}_{k j''}) = 1 \quad (\text{B.0.0.29})$$

the above linear system [B.0.0.1](#) - [B.0.0.28](#) can be solved for equilibrium joint states distribution.